

Elucidating the Roles of Conserved Active Site Amino Acids in the *Escherichia coli* Cytochrome *c* Nitrite Reductase

Colin William James Lockwood

PhD thesis, September 2013

University of East Anglia

School of Biological Sciences

Norwich

© Colin William James Lockwood, September 2013

This copy of the thesis has been supplied on condition that anyone who consults it is understood to recognise that its copyright rests with the author and that use of any information derived there from must be in accordance with the current UK Copyright Law. In addition, any quotation or extract must include full attribution.

Abstract

The periplasmic cytochrome *c* nitrite reductase NrfA is a homodimeric protein containing ten *c*-type cytochromes. NrfA catalyses the six electron reduction of nitrite to ammonia which in turn facilitates anaerobic respiration. NrfA also reduces nitric oxide and hydroxylamine to ammonium. The reduction of substrate is carried out at the distal position of a lysine ligated heme and in an active site cavity dominated by a conserved catalytic triad of histidine, tyrosine and arginine residues.

The role of the catalytic triad of *Escherichia coli* NrfA has been explored by generating NrfA variants. Three NrfA variants were studied in which a single active site residue was substituted: arginine to lysine (R106K), tyrosine to phenylalanine (Y216F) and histidine to asparagine (H264N). These NrfA variants were then compared to the wild type enzyme. The comparison of the crystal structures revealed the substituted residues in the NrfA variants adopted similar positions to the native residues. The ability of the NrfA proteins to reduce nitrogenous substrates was characterised by both solution assay and protein film electrochemistry (PFE). The results revealed that R106K and Y216F NrfA maintained the ability to reduce nitrite whereas the H264N NrfA did not. Further characterisation of H264N NrfA using PFE identified that not only was nitrite no longer a substrate, it could instead act as an inhibitor of hydroxylamine reduction.

A fourth variant of *E. coli* NrfA, in which the lysine ligand was substituted for a histidine residue (K126H), attempted to examine the importance of lysine ligation to the active site heme. The crystal structure of the K126H variant revealed the histidine was not ligating the heme iron. However, spectroscopy of the K126H NrfA was unable to confirm the presence of a tetra-coordinated heme.

The substitution of the four key residues resulted in proteins with different characteristics to the wild type enzyme and to each other. This offered an insight into role these residues play in the reaction mechanism of NrfA.

Acknowledgments

I would like to express my gratitude to my three supervisors. Prof. David Richardson, for the opportunity to carry out this Ph.D. and his support and guidance throughout. Dr Tom Clarke, for his help during the purification and crystallisation of NrfA. And finally Prof. Julea Butt, who introduced me to protein electrochemistry and offered me great support towards the end of my PhD and during my write up period. Thank you also to UEA for sponsoring my Ph.D.

Many thanks to Prof. Jeff Cole and his group at the University of Birmingham for providing me with the NrfA variants used in this work. Thank you to Prof. James Durrant and his group at Imperial College for providing me with the SnO₂ electrodes used for the spectroelectrochemistry of NrfA.

I would like to thank Dr Rose-Marie Doyle, for her time spent teaching me protein film electrochemistry and for many helpful discussions on NrfA and TvNir biochemistry. Thank you to Dr Sophie Marritt for guidance on carrying out spectroelectrochemistry of NrfA. Thank you to Dr Marcus Edwards for helping me to collect and analyse numerous crystallography data sets.

I would also like to thank the technical staff at UEA, especially Verity Lyall, her knowledge has been invaluable on too many occasions to mention. I would also like to thank all those members of BIO Lab 2.30 past and present who have shared cake and conversation on numerous coffee breaks, my PhD would not have been the same without you all.

I would like to thank my friends and family. My sisters, Hayley and Lucy, their regular visits never failed to cheer me up, especially when they were joined by the new edition to the family my niece, Isabella. I cannot express the gratitude that I owe to my parents, Diana and Colin for their constant support in all my endeavours. Finally I would like to thank Michael Twigg for his endless support over the last four years, although carrying out our PhDs at the same time may have been occasionally stressful, it has always been fun.

Table of Contents

Abbreviations.....	7
Chapter 1 - Introduction	9
1.1 The Nitrogen Cycle	9
1.2 The physiological role of Cytochrome c Nitrite Reductase, (NrfA)	12
1.3 NrfA Structure.....	15
1.3.1 Overview of the structure of NrfA.....	15
1.3.2 Heme arrangement within NrfA.....	17
1.3.3 Calcium binding sites.....	18
1.4 Heme reduction potentials	21
1.5. Catalytic chemistry of NrfA.....	23
1.5.1 The active site structure of NrfA.....	23
1.5.2 Determination of NrfA activity	24
1.5.3 Reaction mechanism	27
1.6 Mutational studies of NrfA.....	30
1.7 Aim of thesis	32
Chapter 2 – Materials and Methods	34
2.1 Expression of recombinant WT and NrfA variants.....	34
2.1.1 Bacterial strains and plasmids	34
2.1.2 Growth of the recombinant WT and variant NrfA strains	34
2.1.3 NrfA purification.....	36
2.2 Protein visualisation.....	37
2.3 Solution spectroscopy.....	37
2.4 Protein structure determination.....	38
2.4.1 Crystallisation	38
2.4.2 Data collection.....	38
2.4.3 Crystal structure determination	39
2.5 Characterisation of the catalytic and redox activities of NrfA.....	42
2.5.1 Reagent preparation.....	42
2.5.2 Spectroscopic assays.....	43
2.5.3 Protein film electrochemistry using graphite electrodes	44
2.5.4 Spectroelectrochemistry using SnO ₂ electrodes	48
Chapter 3 - The role of the distal pocket residues in the NrfA reaction cycle	53
3.1 Introduction.....	53
3.2 A comparison of WT and H264N NrfA	54
3.2.1 Crystal Structures of rWT and H264N NrfA.....	54

3.2.1.1 The structure of rWT NrfA to a resolution of 2.10 Å	54
3.2.1.2 The crystal structure of H264N NrfA to a resolution of 2.15 Å.....	55
3.2.3 Spectroscopic characterisation of rWT and H264N NrfA.....	59
3.2.4 Spectroelectrochemistry of rWT and H264N NrfA.....	61
3.2.5 Spectrophotometric assays of nitrite and hydroxylamine reduction by rWT and H264N NrfA.....	65
3.2.6 A comparison of the electrocatalytic properties of rWT and H264N NrfA adsorbed on PGE electrodes	68
3.2.6.1 Assessing the activity towards nitrite and hydroxylamine.....	68
3.2.6.2 Assessing the activity towards nitric oxide	73
3.3 Characteristics of R106K NrfA	74
3.3.1 Structural aspects of the arginine to lysine substitution.....	74
3.3.2 The nitrite and hydroxylamine reduction characteristics of R106K NrfA	76
3.4 Characterisation of Y216F NrfA	80
3.4.1 Crystal structure of Y216F to a resolution of 2.11 Å.....	80
3.4.2 A spectroelectrochemical investigation of Y216F NrfA.....	81
3.4.3 Catalytic properties Y216F NrfA	84
3.5 Discussion	89
Chapter 4 – The interaction of Nitrite with H264N NrfA.....	96
4.1 Introduction.....	96
4.2 Thermodynamic description of nitrite binding to H264N NrfA	97
4.2.1 Spectroscopic characterisation of nitrite binding to the oxidised WT and H264N NrfA.....	97
4.2.2 Nitrite binding to reduced H264N NrfA.....	101
4.2.3 The nature of H264N inhibition by nitrite.....	103
4.2.4 Spectroelectrochemical characterisation of nitrite bound H264N NrfA	105
4.2.5 Summary.....	108
4.3 A kinetic description of nitrite binding to H264N NrfA	111
4.3.1 Spectroelectrochemistry of H264N NrfA at non-saturating nitrite concentrations.....	111
4.3.2 PFE of hydroxylamine reduction by H264N NrfA in the presence of nitrite. 113	
4.3.2.1 Cyclic voltammetry revealing potential dependence of nitrite inhibition of hydroxylamine reduction	113
4.3.2.2 Kinetics of nitrite association and dissociation to H264N NrfA as derived by chronoamperometry	117
4.4 Discussion	121
Chapter 5 - The importance of proximal lysine ligation to the active site heme in NrfA.....	127
5.1 Introduction.....	127
5.2 The 2.3 Å structure of K126H NrfA reveals a modified active site	128

5.3 Spectroscopy revealing the coordination environment of the active site heme of K126H NrfA	131
5.4 Potential dependence of the redox cofactors in K126H NrfA.....	134
5.5 The catalytic properties of K126H NrfA	139
5.6 Discussion	142
Chapter 6 - Summary and Future Perspectives.....	148
References	153

Abbreviations

ADP	Adenosine diphosphate
ATP	Adenosine triphosphate
Ccm	Cytochrome <i>c</i> maturation
E_M	Midpoint potential
EPR	Electron paramagnetic resonance
GPES	General purpose electrochemical system
HAO	Hydroxylamine oxidoreductase
HEPES	4-(2-hydroxyethyl)piperazine-1-ethanesulfonic acid
I_{max}	Maximum catalytic current magnitude
k_{cat}	Turnover number
K_d	Dissociation constant
K_i	Inhibition constant
K_M	Michaelis constant
LMCT	Ligand metal charge transfer
MCD	Magnetic circular dichroism
NrfA	Pentaheme cytochrome <i>c</i> nitrite reductase
OTR	Octaheme tetrathionate reductase
OTTLE	Optically transparent thin-layer (spectro) electrochemistry
PDB	Protein data bank
PEG	Polyethylene glycol
PFE	Protein film electrochemistry
PGE	Pyrolytic graphite edge
SHE	Standard hydrogen electrode
TvNir	Octaheme Cytochrome <i>c</i> nitrite reductase from <i>Thioalkalivibrio nitratireducens</i>
V_{max}	Maximum turnover rate

Chapter 1

Introduction

Chapter 1 - Introduction

1.1 The Nitrogen Cycle

Microbial respiratory chains are both diverse and variable. Many bacteria are able to draw upon numerous different electron donor and acceptor compounds to facilitate respiration. Due to this flexibility bacteria are able to colonize a vast array of different habitats, whereas higher animals and plants are limited to aerobic environments. The variation of bacterial respiration can be seen in the biogeochemical nitrogen cycle. This illustrates the ability of bacteria to interconvert nitrogen compounds via numerous redox processes. The nitrogen species are present in oxidation states ranging from +5 to -3 and include nitrate (+5), nitrite (+3), nitric oxide (+2), hydroxylamine (+1), nitrous oxide (+1) dinitrogen (0) and ammonia (-3).

The nitrogen cycle includes assimilatory and respiratory processes. The assimilatory processes form ammonia which is incorporated into biological molecules such as peptides, nucleotides and enzyme cofactors, thus allowing growth. Ammonia can be produced in two processes. Firstly, the fixation of dinitrogen by the nitrogenase enzymes, which are found in free living and symbiotic soil bacteria, and secondly by the reduction of nitrate and nitrite by reductase enzymes found within the cytoplasm of animals, plants and bacteria[1]. The respiratory processes are coupled directly or indirectly to the generation of an electrochemical proton gradient across the cellular or inner membrane. This gradient is then utilised by ATP-synthase to catalyse the phosphorylation of ADP to ATP [2].

The respiratory pathways of the nitrogen cycle, nitrification, denitrification, anammox and dissimilatory nitrite reduction to ammonia (DNRA), are depicted in Figure 1.1 with the enzymes which facilitate these processes. The structures of the enzymes found within the nitrogen cycle reveal that, although the enzymes are interacting with molecules that contain nitrogen, they also include a wide range of transition metal ions such as iron, copper and molybdenum. These metal centres allow the different nitrogen molecules to bind and undergo catalyses so are therefore fundamental in the activity of these enzymes.

As well as metal ions being present within the active site of these proteins they are also involved in electron transfer within the proteins. These ions include copper, iron containing hemes and iron sulphur clusters. The variation of metal cofactors found within the enzymes that form the nitrogen cycle suggests that the enzymes evolved at different stages in time, with the iron sulphur and heme proteins likely to have been present first in an anaerobic

environment. The copper-containing proteins, are likely to have evolved later when copper became bioavailable as the earth become increasingly oxic [3]. The metal cofactors present within the catalytic subunits of the enzymes depicted in Figure 1.1 are listed in Table 1.1

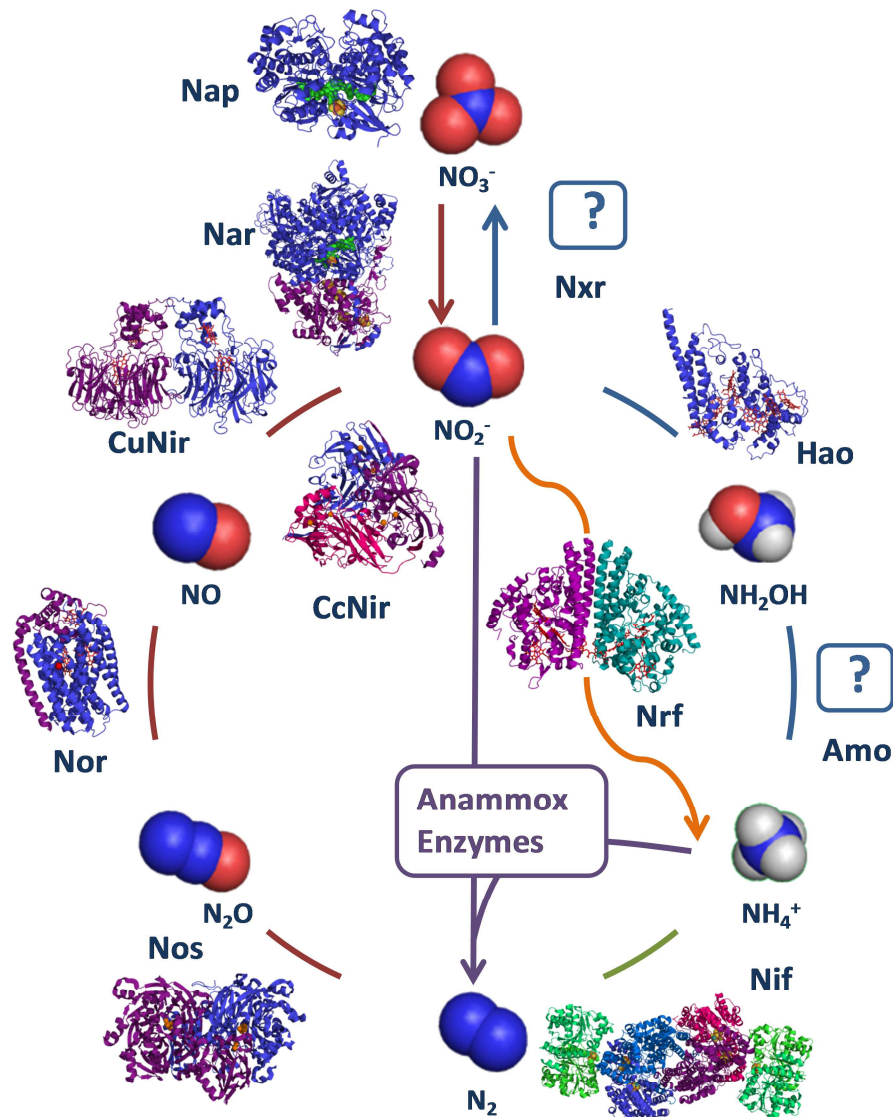


Figure 1.1 - The biogeochemical nitrogen cycle and the respiratory enzymes responsible for the interconversion of the nitrogen species. Respiration pathways: light blue represents nitrification, red denitrification, orange dissimilatory nitrite ammonification, dark blue anammox and green nitrogen fixation (a non-respiratory process). Blue spheres represent nitrogen atoms, red spheres oxygen atoms and white hydrogen atoms. The question marks represent enzymes for which a high resolution structure is not available. Anammox enzymes represents the group of enzymes that facilitate anaerobic ammonium oxidation, the structure of the enzymes are unknown.

Process	Enzyme	Active site cofactors	Electron relay cofactors	PDB and reference
Nitrification				
$\text{NH}_4^+ \rightarrow \text{H}_2\text{NOH}$	Ammonia mono-oxygenase, (Amo) (no structure)	Cu	-	-
$\text{H}_2\text{NOH} \rightarrow \text{NO}_2^-$	Hydroxylamine oxidoreductase (Hao)	c-type heme	7 x c-type heme	1FGJ [4]
$\text{NO}_2^- \rightarrow \text{NO}_3^-$	nitrite oxidase (Nxr) (No structure)	Mo-bis-MGD	-	-
Denitrification				
$\text{NO}_3^- \rightarrow \text{NO}_2^-$	Membrane-bound nitrate reductase (NarG)	Mo-bis-MGD	[4Fe-4S]	1Q16 [5]
	Periplasmic nitrate reductase (NapA)	Mo-bis-MGD	[4Fe-4S]	2JIM [6]
$\text{NO}_2^- \rightarrow \text{NO}$	Copper nitrite reductase (CuNir)	Type II copper site	Type I copper site	1SNR [7]
	Cytochrome cd_1 nitrite reductase (cd_1 Nir)	d_1 heme	c-type heme	1AOQ [8]
$\text{NO} \rightarrow \text{N}_2\text{O}$	Nitric oxide reductase (NorB)	di-nuclear site comprising <i>b</i> heme and non-heme iron	<i>b</i> heme	3O0R [9]
$\text{N}_2\text{O} \rightarrow \text{N}_2$	Nitrous oxide reductase (NosZ)	tetra-nuclear CuZ	di-nuclear CuA	1FWX [10]
Dissimilatory nitrite reduction (DNRA)				
$\text{NO}_2^- \rightarrow \text{NH}_4^+$	Cytochrome <i>c</i> nitrite reductase (NrfA)	c-type heme	4 x c-type heme	2RDZ [11]

Table 1.1- The metal centres present within the respiratory enzymes responsible for the conversion of the nitrogen species within the bacterial nitrogen cycle.

1.2 The physiological role of Cytochrome c Nitrite Reductase, (NrfA)

Cytochrome c Nitrite reductase also known as NrfA (**N**itrite **R**eduction by **F**ormate) catalyses the six electron and eight proton reduction of nitrite to ammonium. This facilitates the final step of the metabolic pathway of dissimilatory nitrite ammonification. The reduction of nitrite enables it to be used as a terminal electron acceptor, allowing respiration to continue under anaerobic conditions. NrfA is found in a wide variety of proteobacteria from the ϵ , δ , γ subclasses from which it has been characterised from species including *Desulfovibrio desulfuricans*, *Wolinella succingogenes* in addition to *E. coli* [12].

The NrfA protein itself is highly conserved across the three classes of proteobacteria which are able to perform dissimilatory nitrite ammonification. However there is variation in the electron delivery system to NrfA, Figure 1.2. There have been two forms of electron delivery system described. The first is found in the γ -proteobacteria such as *E. coli* [13, 14]. The system in γ -proteobacteria is comprised of NrfD, an integral membrane protein that functions as a quinol dehydrogenase. The NrfD protein itself is not predicted to contain any redox cofactors based upon the gene sequence. Therefore the electrons liberated from the oxidation of menaquinol are directly passed to NrfC. The NrfC protein is membrane-associated by the formation of a complex with NrfD and contains four iron-sulphur clusters (4 x [4Fe-4S]). The crystal structures of NrfCD proteins have not been solved to date. However, the structure of an homologous electron delivery system has been solved for polysulphide reductase (PsrBC) from *Thermus thermophilus* [15]. The PsrBC structure has been used to represent the NrfCD complex in Figure 1.2B. From NrfC the electrons are then passed to NrfB, a small pentaheme protein that shuttles electrons from the membrane-bound NrfCD complex to NrfA, which is free within the periplasm. The structure for *E. coli* NrfB has been solved and revealed a closely packed heme motif [16].

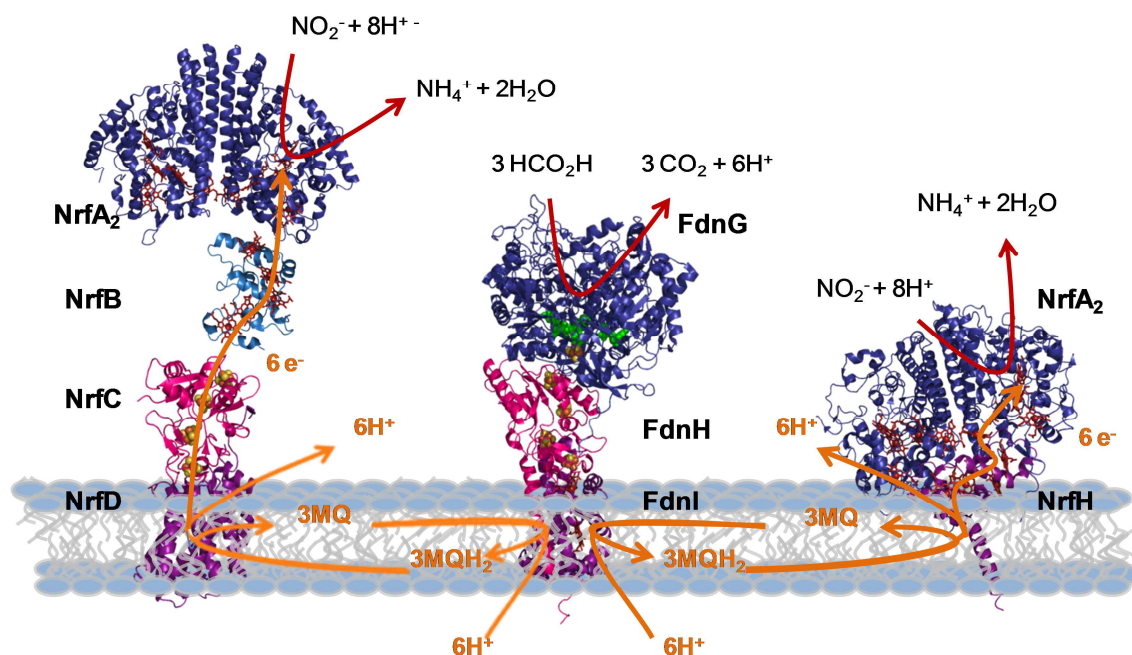


Figure 1.2- The localisation of the catalytic and electron transfer proteins of the Nrf system from different classes of proteobacteria. **(Left)** *E. coli* representing the γ-proteobacteria, NrfA (PDB:2rdz) and NrfB (PDB:2OZY) localised in the periplasm, NrfC membrane associated by the formation of a complex with NrfD, the membrane-bound quinol dehydrogenase. (The structures for NrfCD have not been solved so are modelled by the polysulphide reductase (PsrBC) from *T. thermophilus* (PDB:2VPZ)). **(Centre)** *E. coli* formate dehydrogenase (FdnGHI) (Pdb:1KQF) which couples the reduction of formate to the oxidation of menaquinone. **(Right)** *D. vulgaris* NrfHA proteins representing the ε and δ-proteobacteria, with NrfA membrane associated via interaction with NrfH (PDB), the membrane bound quinol dehydrogenase.

The second electron delivery system is found in the ε- and δ-proteobacteria such as *W. succinogenes* and *D. desulfuricans*. In contrast to the 3 protein electron transfer system in γ-proteobacteria most other proteobacteria use a single quinol dehydrogenase, NrfH, which passes electrons directly to NrfA. NrfH belongs to the NapC/NirT family of c-type cytochrome quinol dehydrogenases. It is a membrane-bound tetraheme protein which forms a stable complex with the NrfA dimer [17]. The structure of the NrfHA complex has been solved for *Desulfovibrio vulgaris* protein, Figure 1.2 [13]. The crystal structure revealed that under the crystallographic conditions NrfH formed a dimer, with each NrfH monomer interacting with a NrfA dimer, generating a complex of NrfH₂A₄ stoichiometry. It is not known if the NrfHA₂ or NrfH₂A₄ is the physiologically relevant form of the complex or an artefact of the crystallographic process.

The electrons required for the reduction of nitrite are delivered from the menaquinol pool, which is supplied by primary dehydrogenases such as formate dehydrogenase. The oxidation of formate to carbon dioxide results in the release of two protons into the

periplasm and the transfer of two electrons to a menaquinone molecule, concurrently with the uptake of two protons from the cytoplasm. This forms a fully reduced quinol molecule, which is then oxidised at a dedicated Nrf quinol dehydrogenase (NrfCD/NrfH) which translocates the two quinol protons into the periplasm and passes the two electrons on to the NrfA catalytic subunit [12, 14]. As the protons and electrons are delivered to the same side of the membrane, the reduction of the nitrite to ammonia is an electroneutral process. The charge of electrons and protons cancel each other out as the nitrite molecule is reduced. Therefore, the reduction of nitrite itself does not generate a proton motive force across the cell membrane. The generation of the proton motive force is consequently dependent on the electron input into the quinol pool from the primary dehydrogenase [2].

Apart from a role in respiration NrfA has been proposed to fulfil a secondary role as a detoxification enzyme. A number of studies have demonstrated that NrfA is able to reduce not only its proposed reaction intermediates of nitric oxide and hydroxylamine but also other cytotoxins including sulphite and hydrogen peroxide [18-20]. The ability to be able to detoxify compounds which are able to cause oxidative and nitrosative stress is believed to be an important factor in determining the pathogenicity of proteobacteria [19].

NrfA is believed to be one of the first nitrogen cycle enzymes to have evolved in an anoxic earth [21]. The original function of NrfA has been proposed to be similar to that of extant NrfA, although it has been suggested that these early enzymes may have been able to leak reaction intermediates. The generation of reactive nitrogen species such as nitric oxide and hydroxylamine by early NrfA enzymes may have been one of the driving forces in the evolution of the annamox pathway. This is able to use both nitric oxide and hydroxylamine as substrate in the generation of N_2 whilst generating a proton motive force [3]. NrfA is also proposed to be an evolutionary ancestor of many other multi-heme proteins which have links to the nitrogen cycle, including octaheme nitrite reductase (TVNir), hydroxylamine oxidoreductase (HAO) and octaheme tetrathionate reductase (OTR) [21, 22].

1.3 NrfA Structure

1.3.1 Overview of the structure of NrfA

The presence of NrfA has been confirmed in a large number of organisms, including *E. coli* [23], *D. desulfuricans* [24], *Campylobacter sputorum* subspecies *bubulus* [25], *W. succinogenes* [26], *Sulfurospirillum deleyianum* [27] and *Desulfovibrio vulgaris* [28]. When NrfA was discovered it was identified as a *c*-type cytochrome. However it was unknown exactly how many heme groups it contained. Originally it was proposed that NrfA was a hexaheme protein, based upon spectroscopic studies [26]. This model was later challenged when the gene sequence of NrfA was determined, which identified the presence of four conventional heme binding motifs. The motif consists of two cysteine residues separated by two variable residues and followed by a histidine residue (CxxCH). The two cysteine residues form covalent attachments to the heme while the histidine residue forms the proximal ligand to the heme iron. The observation of only four heme binding motifs suggested that NrfA was in fact a tetraheme protein [29]. The sequence also contained a CxxCK motif that was not believed to be a site of heme attachment as the conventional histidine residue was not present. It was first proposed this motif was a site of heme attachment by Berks *et al* [1] and later experiments confirmed this [30]. Further to the identification of a novel heme binding site, mutational studies in which the lysine residue was replaced by histidine, leucine or isoleucine resulted in an almost complete loss in nitrite reductase activity. This supported the idea that the lysine ligated heme forms the active site of NrfA [30].

The first crystal structure of NrfA was solved in 1999 for *S. deleyianum* NrfA. Subsequent structures have also been obtained for *E. coli*, *W. succinogenes* and others [31-35]. These enzymes are homologous and share a highly conserved three-dimensional structure. The structures of all NrfA proteins solved to date reveal NrfA to be a decaheme homodimer with each monomer ~45 Å x 55 Å x 30 Å in size and a mainly alpha helical secondary structure (Figure 1.3). The NrfA dimer is formed by the interaction of a three helix bundle of one monomer and the corresponding three helix bundle of the other monomer. The interaction is predominantly hydrophobic with a contact area which corresponds to ~9 % of the surface area of a single monomer.

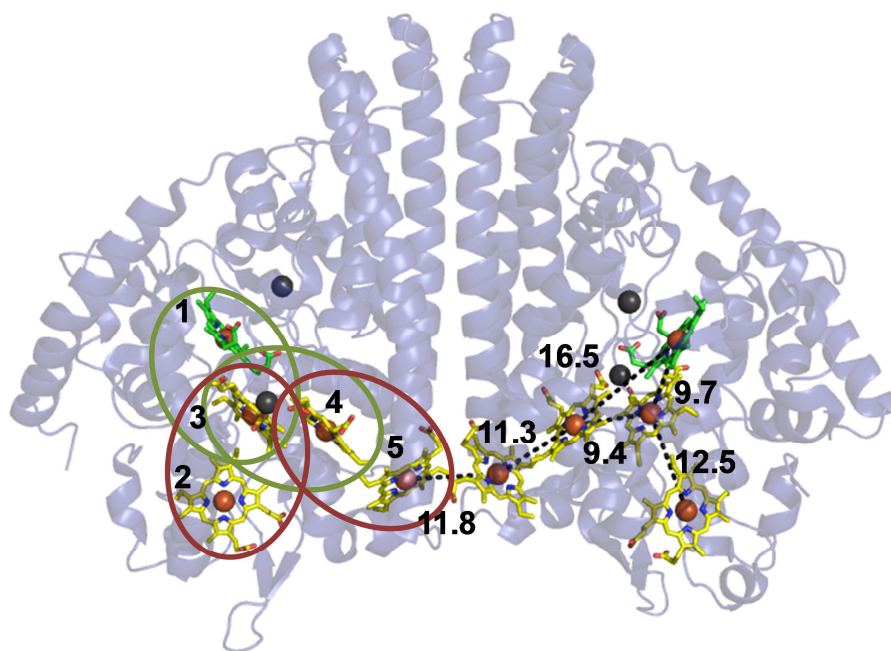


Figure 1.3 - The crystal structure of *E. coli* NrfA. Illustration of the predominantly alpha helical secondary structure of NrfA, the electron transfer hemes are shown in yellow, while the active site heme is highlighted in green. The hemes of NrfA monomer of the left have been numbered according to their order in the *nrfA* gene sequence. The green ellipses highlight the heme pairs that form parallel stacking motifs and the red ellipses highlight the heme pairs that form heme elbow motifs. The NrfA monomer on the right depicts the iron to iron distances (Å) between neighbouring hemes. The calcium ions are shown as grey spheres. Figures were prepared from PDB 2RDZ using Pymol.

The interaction between NrfA monomers has been characterised using purified NrfA from *E. coli*. Within these studies it was identified that NrfA is in dynamic equilibrium between NrfA_2 and 2 NrfA species. This dynamic equilibrium can be described by a K_d of 4 μM for the dissociation of the NrfA dimer [36]. The obtained K_d value is likely to indicate the NrfA is present as a dimer within the periplasm of γ -proteobacteria. NrfA is also likely to be a dimer in the NrfH expressing proteobacteria. The NrfHA proteins co-purify, indicating a strong interaction. The structure of NrfHA₂ complex from *D. vulgaris* shows that the NrfH protein binds tightly to NrfA through interaction with both monomers [13]. This creates a contact area of $\sim 3000 \text{ \AA}^2$ between the NrfH and the NrfA dimer. The contact surface exhibits a high level of complementation and there is strong electrostatic contribution due to formation of ionic and hydrogen-bond interactions. The interaction between the NrfA dimer and NrfH is further strengthened by one of the NrfA monomers donating a lysine residue to form the proximal ligand to a heme within the NrfH protein [13].

Each NrfA monomer contains five tightly packed covalently attached hemes numbered according to the position of the CxxCH/K heme binding motif in the gene sequence. Four of the hemes are bis-histidine coordinated with the proximal ligand provided by the histidine originating from the conventional CxxCH motif (hemes 2-5). The remaining heme is attached via the novel CxxCK heme binding motif and has a proximal lysine ligand (heme 1). The distal position of this heme is free of endogenous ligand and is occupied by a water molecule or a hydroxide ion [32].

1.3.2 Heme arrangement within NrfA

The structure of NrfA is dominated by a core of five covalently attached hemes, which are attached after the unfolded protein has been exported into the periplasm via the Sec pathway [37, 38]. The *c* type hemes are incorporated into protein by cytochrome *c* maturation machinery, which is able to identify the CxxCH binding motif [39, 40]. However the novel CxxCK motif in NrfA is not identified by the typical cytochrome *c* maturation machinery present within the bacterium. Instead adapter proteins modify the system to allow the novel motif to be recognised and the heme inserted [30, 41]. The genes that encode the adapter proteins are present within the *nrf* operon and are located downstream of the *nrfA* gene. The Nrf heme maturation proteins vary between bacteria with three different Nrf operons known to date. These are depicted in Figure 1.4. The only *nrf* operon not to contain heme maturation proteins is found in a small number of ϵ -proteobacteria including *C. jejuni* [42]. The NrfA protein from *C. jejuni* encodes five CxxCH motifs and no novel CxxCK motif. It is not known if the active site heme within this protein is ligated by the histidine residue provided by the heme binding motif, or if there is an advantageous lysine ligation during the folding of the protein. Such a ligation is seen in the crystal structure of the octaheme tetrathionate reductase from *Shewanella oneidensis*. Within this protein the active site heme is present in a CxxCH motif but a lysine residue forms the distal ligand to the active site heme [43].

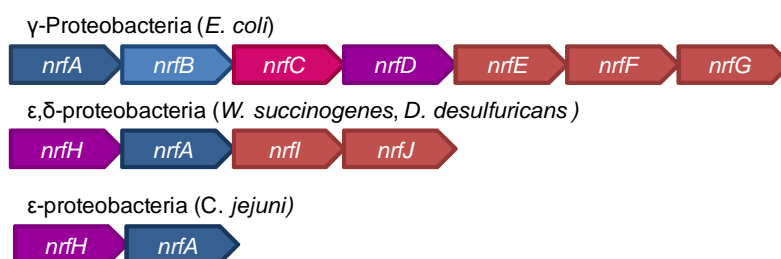


Figure 1.4 - The structure of the *nrf* operon and the coupling of formate oxidation to nitrite reduction by formate dehydrogenase and cytochrome *c* nitrite reductase. The composition and

organisation of the Nrf operon in different proteobacteria families. The γ -proteobacteria has three genes (*nrfBCD*) downstream of the *nrfA* gene that code for the quinol dehydrogenase and electron transfer proteins as well as three genes (*nrfEFG*) which code for proteins responsible for the active site heme insertion. The ϵ and δ proteobacteria have a single gene (*nrfH*) that codes for a single quinol dehydrogenase that passes electrons directly to NrfA and two genes (*nrfIJ*) which code for heme insertion proteins. A small group of ϵ -proteobacteria have a Nrf operon which only contains the *nrfHA* genes and does not contain genes that code for heme insertion proteins. This is due to the NrfA catalytic subunit not containing a CxxCK motif.

With the increase in the number of cytochrome *c* protein structures solved it has been possible to compare the heme arrangements within these proteins. This has revealed that complex heme arrangements found within many multi heme proteins can be described by two distinct diheme motifs which, when arranged together, can create an efficient electron conduit. The two diheme motifs are a parallel stacking pair motif, in which the hemes are in an offset parallel arrangement and a diheme elbow motif, in which the hemes are perpendicular to each other. The hemes pairs 1-3 and 3-4 are examples of the parallel stacking motif and hemes pairs 2-3 and 4-5 are examples of the diheme elbow motif [44] (Figure 1.3, left monomer).

The arrangement of hemes within the NrfA monomer means that the iron to iron distance are no greater than 13 Å and edge to edge distances no greater than 7 Å. This arrangement facilitates fast electron transfer between hemes (Figure 1.3, right monomer). The distance between the hemes at the dimer interface (heme 5) is also close enough to allow direct electron transfer between monomers, thus creating a ten heme complex [32]. It is however not known if electrons pass across the dimer interface under physiological conditions. The connection between the NrfA monomers will be more critical within the NrfHA system as the positioning of the NrfHA complex only allows electrons to enter via either heme 2 or 5 of a single monomer. If electrons could not pass between the hemes at the interface, the monomer not in direct electrical contact with NrfH would not be able to receive electrons from the quinol pool and therefore would be unable to carry out the reduction of nitrite. The electron transfer between the monomers becomes less important within the NrfABCD system as electrons can be delivered directly to each monomer via heme 2 [16].

1.3.3 Calcium binding sites

As well as redox active metal cofactors NrfA also contains non-redox active metals in the form of two calcium ions. The position of these ions within *E. coli* NrfA is shown in Figure

1.3 (grey spheres). In all NrfA structures to date, a conserved calcium ion (calcium I) with octahedral coordination is present near the active site, while a second calcium ion (calcium II) has been shown to be present in the majority of NrfA structures, but not all.

The conserved calcium I site is located close to the active site, at a distance of 10-11 Å from the iron atom of heme 1. The calcium ion is coordinated by the two oxygen atoms of the carboxylate group from Glu215, the oxygen of the amide group from Gln265, and the main chain carbonyls of Tyr216 and Lys261. The coordination sphere of the calcium ion is completed by two water molecules (Figure 1.5, small blue spheres). The calcium ion carries out a structural role in maintaining the architecture of the active site cavity. This interaction with Tyr216 positions the side chain of this residue towards the active site where the substrate binds. The ligation of calcium ion by Gln265 also orientates the adjoining residue His264 in the active site and prevents it from forming the distal ligand to the active site heme [11].

The calcium ion introduces a positive electrostatic charge into the vicinity of the NrfA active site and the proposed substrate ingress channel in *E. coli* NrfA. The positive electrostatic potential of the active site will be able to counteract the negative charge that will be present upon binding the nitrite oxyanion, making this interaction more favourable. The two water molecules that ligate the calcium ion form part of the hydrogen bond network that connects the conserved water molecules, found within the active site, with the bulk solution surrounding the protein. This connection is likely to be vital for the translocation of protons into the active site to enable catalysis to occur [45].

The second calcium ion is more distant from the active site and is therefore unlikely to have a direct effect on nitrite binding and reduction. The function of the second calcium ion is believed to be related to the tuning of the reduction potentials of hemes 3 and 4, as the irons of these hemes are located ~11 Å away and a single propionate from each heme also forms a ligand to the calcium ion. The coordination sphere of the second calcium varies in the known structures of NrfA. Within the γ - and ϵ -proteobacteria, as represented by the structures of NrfA from *E. coli* and *W. Succinogenes* show that the calcium ion is ligated by a propionate group from hemes 3 and 4, a carbonyl group from Pro91 and two or three conserved water molecules. A different mode ligation is seen in δ -proteobacteria. The structure of NrfA from *D. vulgaris* and *D. desulfuricans* reveals that the calcium ion is positioned in the same location and remains ligated by propionate groups of hemes 3 and 4, with the remaining ligands provided by an additional protein loop that is absent from *E. coli* and *W. succinogenes* enzymes [34].

The second calcium ion within *E. coli* and *W. succinogenes* NrfA has been shown to be labile as it can be replaced by other cations. Structures of NrfA from *E. coli* have shown an europium ion bound in the calcium (II) site while a structure of *W. succinogenes* has been solved with an yttrium ion bound [45]. Studies of *E. coli* NrfA have also revealed that NrfA is potently inhibited by Zn^{2+} . One possible cause of this inhibition could be due to the Zn^{2+} replacing the calcium in the calcium (II) site, causing a change in the midpoint potentials of heme 3 and 4 which inhibits catalysis [46]. The Zn^{2+} is unlikely to replace the calcium ion located closest to the active site, as this ion is too deeply imbedded in the protein to be easily replaced. The presence of the protein loop within the δ -proteobacteria would make the calcium ion less labile and therefore less likely to be replaced by other cations. The presence of the loop would also limit the solvent exposure of heme 3 and 4 and thus will help to mediate their midpoint potentials [34].

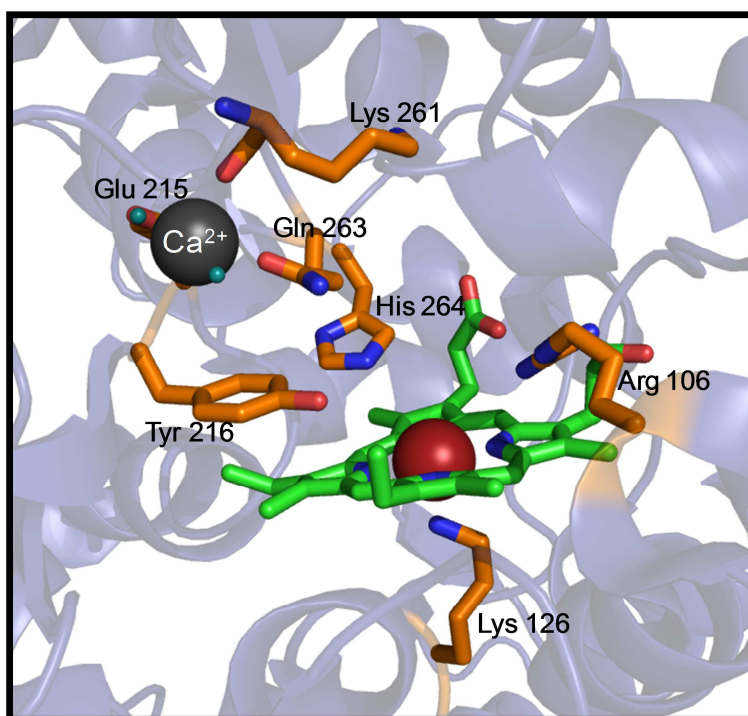


Figure 1.5-The active site cavity of NrfA, with key residues thought to be involved in substrate reduction and calcium ion ligation highlighted in orange and labelled according to *E. coli* numbering. The calcium ion is shown as a large grey sphere with two water ligands shown as small blue spheres. The active site heme is shown in green with the heme iron represented by a red sphere. Figure was prepared from PDB 2RDZ using Pymol.

1.4 Heme reduction potentials

The ability of hemes to act as centres of electron transfer is due to their ability to redox cycle between the ferric (Fe(III)) and ferrous (Fe(II)) states. Hemes and other redox cofactors are characterised by their midpoint potentials which reflects the potential where two redox states of the cofactor are present at equal concentration. The midpoint potential of the heme Fe(III)/Fe(II) couple varies depending upon a number of factors, including the axial ligands of the heme iron and their position relative to the iron and each other, the heme environment, and any ruffling of the porphyrin plane that affects the positioning of the heme iron [47].

The midpoint potentials for the hemes within a number of NrfA proteins have been determined by monitoring changes in their spectroscopic properties as individual heme groups are oxidised and reduced. The first visible absorbance study of NrfA midpoint potentials was carried out by Eaves, D. J. *et al* [30] on *E. coli* NrfA. The study used NrfA at pH 7, reduced with sodium dithionite, and plotted the height of the α -band (552nm) against potential (vs. SHE). The interpretation of the data revealed that one heme had a midpoint potential of +45 mV, two hemes had midpoint potentials of -90 mV and a further two hemes had midpoint potentials of -210 mV. The study only looked at changes in the α -peak and therefore fitted the five hemes as low spin hemes.

The most recent studies of the reduction potentials of *E. coli* NrfA have been carried out using SnO₂ electrodes. This technique uses nanocrystalline mesoporous SnO₂ electrodes. These allow protein to be absorbed on to the surface of the electrode, placing the protein under direct electrodic control. The tin oxide electrode is transparent to visible light, allowing the visible electronic absorbance spectrum of the protein to be recorded at discreet potentials. The reduction potentials of the low spin hemes within NrfA were determined by monitoring the increase in absorbance of the 552 nm band as the NrfA protein was reduced. The change in absorbance at 552 nm fit to four independent one electron reductions with midpoint potentials of +22, -117, -189 and -275 mV (vs. SHE) [48]. The midpoint potential of the active site heme was determined by monitoring the increase in absorbance at 442 nm, which relates to the appearance of a reduced high-spin heme. The change in absorbance of the 442 band fitted to a one electron process with a midpoint potential of -56 mV (vs. SHE).

Further characterisation of the reduction potentials of NrfA have been carried out using EPR spectroscopy [32, 34]. EPR spectroscopy is a valuable tool when studying transition

metal cofactors within proteins as this technique is able to characterise centres that contain an unpaired electron. The unpaired electron when placed in a magnetic field is able to adopt one of two orientations or spin directions (with or against the applied field). The transition between the two states occurs at a defined field that is dependent on the electron environment. Within NrfA the heme irons in the oxidised state contains unpaired electrons and therefore can generate an EPR signal. However reduced hemes contain no unpaired electrons and are therefore EPR silent.

The use of EPR spectro-potentiometric titrations, when coupled with structural information, allows the midpoint potentials to be assigned to individual heme centres. This is due to the ability of EPR to discriminate between different hemes based upon their environment, such as the orientation of the axial histidine ligands. The midpoint potentials of the individual hemes within *E. coli* NrfA at pH7 were assigned by Bamford *et al* [32] using electrochemical poised protein samples to avoid interference caused by the presence of dithionite. The samples were poised from 272 mV to -430 mV and EPR spectra recorded. The first signal to disappear was the rhombic trio at $g = 2.92, 2.3$ and 1.5 with an E_m of -37 mV which was assigned to heme 2. Samples poised between -88 mV and -235 mV revealed the decrease in the intensity of the EPR feature at $g = 10.8$ and 3.5 which was described by an E_m of -107 mV, this signal was attributed to the coupled hemes 1 and 3. The last signal to disappear from the NrfA EPR spectra titrated between -236 mV and -430 mV and was described by an E_m of -323 mV and was attributed to heme 4 and heme 5.

The midpoint potential of the hemes in NrfA determined by EPR and visible absorbance spectroscopy are in same potential window. EPR spectroscopy was only able to resolve three independent reduction potentials due to coupling between hemes 1 and 3 and hemes 4 and 5, whereas the midpoint potentials determined by visible absorbance spectroscopy was able to determine five independent reduction potentials. However the absorbance spectroscopy is only able to distinguish between the low- and high-spin hemes. Combining the data from both spectroscopic techniques allowed the midpoint potentials determined by absorbance spectroscopy to be assigned to the hemes with only uncertainty over the midpoint potential of the hemes 4 and 5 remaining, Figure 1.6.

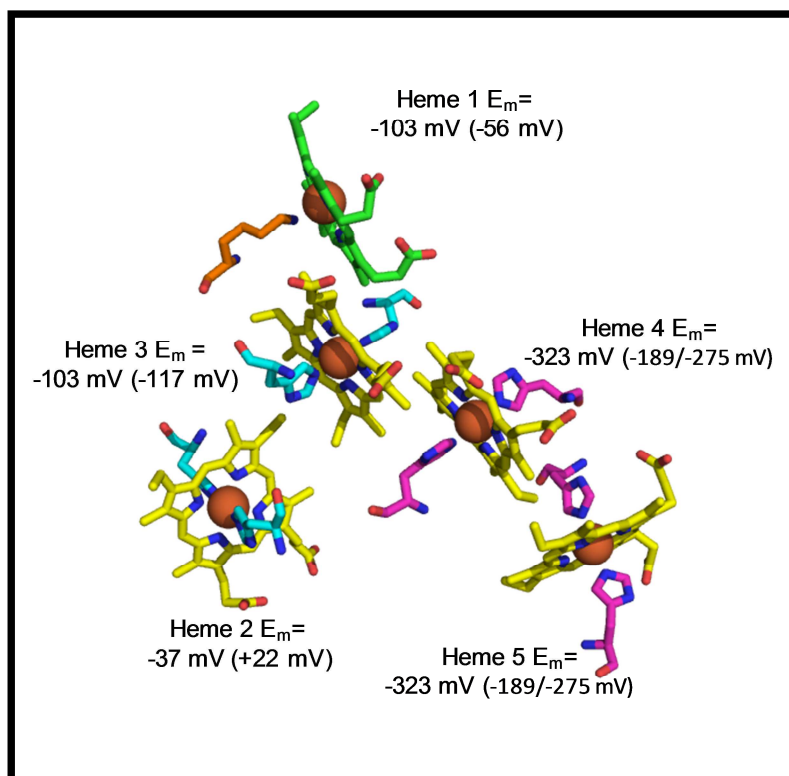


Figure 1.6 - The reduction potentials for the hemes within NrfA as determined by EPR spectroscopy which absorbance spectroscopy in brackets. Low spin bis-histidine coordinated hemes are shown in dark green with parallel axial histidine residues shown blue and perpendicular axial histidine residues shown in pink. The high spin active site heme is shown in light green with its single axial lysine ligand shown in orange.

1.5. Catalytic chemistry of NrfA

1.5.1 The active site structure of NrfA

The active site pocket of NrfA is formed on the distal face of lysine coordinated heme 1 and a catalytic triad of highly conserved residues, His264, Tyr216 and Arg106 (*E. coli* numbering) form NrfA. The catalytic triad creates a positive electrostatic environment within the active site, which will act to attract and counter the negative charge of the nitrite oxyanion. The positive electrostatic environment will also help to stabilise negatively charged reaction intermediates that might be formed during the reduction of nitrite.

The crystal structures of a number of NrfA proteins to date has revealed that the active site cavity contains a number of conserved water molecules that may act as hydrogen donors to reaction intermediates or to active site residues [45]. The conserved water molecules

within the active site of *E. coli* NrfA are connected to the bulk solution via two channels that have been proposed to be the substrate and product ingress and egress channels. The proposed ingress channel is positively charged and therefore is likely to be important in substrate recognition [49]. The egress channel has a net negative electrostatic charge and is likely to be the exit site for the positively charged ammonium product. The characteristics of the ingress and egress channels vary in the known structures of NrfA and are likely to contribute to the different characteristics observed in NrfA proteins from different organisms [49].

In the absence of nitrite it has been shown that the active site heme is bonded to either a water molecule or a hydroxide ion as identified by the crystal structure of NrfA and magnetic circular dichroism (MCD) spectroscopy performed on *E. coli* NrfA [32]. In the presence of nitrite the water/hydroxide ion is replaced, as seen in the nitrite bound *W. succinogenes* NrfA structure [50, 51]. Within the active site the nitrite molecule adopts an N-binding mode, which is stabilised by the interaction with two active site residues His264 and Arg106. These residues are each located within 2.6 Å and 2.8 Å respectively of the nitrite molecule allowing each residue to form a hydrogen bond with a different oxygen atom, thus stabilising the negative charge of the nitrite oxyanion. The crystal structure of the NrfA with nitrite bound clearly implicates the histidine and arginine residues in a stabilisation role however the tyrosine does not directly interact with the bound nitrite molecule.

1.5.2 Determination of NrfA activity

NrfA from a number of different bacteria have been characterised for their ability to reduce nitrite, nitric oxide and hydroxylamine to ammonia (Table 1.2). Despite the high sequence homology and conserved active site the rate at which they catalyse these reactions has been shown to vary. The most common method used to determine the rate of reduction is the use of redox active dyes with different optical properties in the reduced and oxidised states. This enables the dyes to act as electron donors to NrfA and for the reduction of substrate to be followed spectrophotometrically by monitoring the re-oxidation of the dye. For most assays performed on NrfA methyl viologen is used as the redox active dye, as it is colourless in the oxidised state and blue in the reduced state with an absorbance maximum at 600 nm. The rate of oxidation of methyl viologen directly represents the rate of reduction of the substrate of NrfA, by varying the concentration of substrate used within the reaction the kinetic parameters of K_M and V_{max} can be determined. The amount of enzyme added to

the assay is known which enables the V_{\max} to be converted to a k_{cat} value. The kinetics of a number of NrfA proteins are shown in Table 1.2.

NrfA	Nitrite		Nitric oxide		Hydroxylamine	
	k_{cat} (s^{-1})	K_{M} (μM)	k_{cat} (s^{-1})	K_{M} (μM)	k_{cat} (s^{-1})	K_{M} (μM)
<i>E. coli</i>	770	28	840	300	2,380	30,000
<i>W. succinogenes</i>	779	100	-	-	-	-
<i>S. deleyianum</i>	1102	-	3.6	-	514	-
<i>D. vulgaris</i>	641	-	-	-	-	-
<i>D. desulfuricans</i>	490	1140	-	-	-	1,135
<i>S. oneidensis</i>	824	23	-	-	2,380	8,300

Table 1.2 - The k_{cat} and K_{M} values for the nitrogenous substrates of NrfA from various proteobacteria. The compiled data from solution assays and PFE experiments [20, 28, 32, 35, 52-54].

The reduction of methyl viologen is often carried out using sodium dithionite which has been shown to inhibit NrfA [48]. To avoid this potential interaction with dithionite and its oxidative product sulphite, the methyl viologen can also be reduced by zinc removing the need to use sodium dithionite as the reductant [11].

An alternative technique used to study NrfA has been protein film electrochemistry (PFE). The approach has been used to investigate the activity of numerous redox enzymes, such as hydrogenase, nitrate reductase (Nap), and copper dependent nitrite reductase (CuNir) as well as NrfA [55]. In a PFE experiment the protein to be studied is immobilised on to the surface of an electrode as a sub-monolayer under which conditions each protein molecule will be in direct contact with the electrode. This ideally mimics the *in vivo* conditions with the electrode acting as the electron donor/receptor. The direct transfer of electrons to the protein negates the need for chemical reductants/oxidants and mediators which can interfere with the protein and catalytic processes.

The PFE experiment enables the rate of catalysis to be monitored by measuring the current produced at various potentials. One PFE technique, chronoamperometry, measures the current output at a constant applied potential as a function of time. The potential can also be stepped between values rapidly, and the resulting change in current monitored. In another technique, cyclic voltammetry, the potential of the electrode is swept linearly back

and forth between two extremes. The rate at which the potential is changed, the scan rate, can be controlled, while the current is recorded as a function of the applied potential.

As in the solution assay the variation of the concentration of substrate changes the rate of catalysis, which allows the enzymatic constants of K_M and i_{max} to be determined. The i_{max} parameter is the maximum catalytic current and is equivalent to V_{max} , i_{max} can be converted into k_{cat} if the amount of enzyme present within the protein film can be determined. However, this is not always possible due to the low protein coverage [56].

The characterisation of nitrite reduction by NrfA using PFE revealed that catalysis commences when the potential is swept below 0 mV (vs. SHE). This can be seen by the negative wave in Figure 1.7. The onset of catalysis below 0 mV is much lower than the reduction potential of the NO_2^-/NH_4^+ redox couple (+ 340 mV). The potential where the rate of nitrite reduction increases the most is -100 mV which corresponds to the midpoint potential of the active site heme reflecting the potential required to reduce substrate is dependent on the active site potential. At low nitrite concentrations (below K_M) when the potential is swept below -300 mV there is an attenuation in the rate of catalysis. The reason why this occurs is still not known but may be linked to the reduction of heme 4 and heme 5 which have both been proposed to have midpoint potentials of -300 mV. At nitrite concentrations at K_M or higher the attenuation feature is not present.

The technique of PFE has also been used to characterise the ability of *E. coli* NrfA to reduce nitric oxide and hydroxylamine. The study by Van Wonderen *et al* revealed that reduction of nitric oxide and hydroxylamine occurs over a similar range of potentials with the fastest increase in the rate of catalysis occurring at a potential of ca. -100 mV, which is similar to that seen for nitrite reduction [52]. The similarity in the positioning of the catalytic wave suggests the reduction of nitric oxide and hydroxylamine is likely to occur at the same location as that of nitrite reduction. The overall shape of the catalytic wave does, however, vary with substrate as do the kinetic constants.

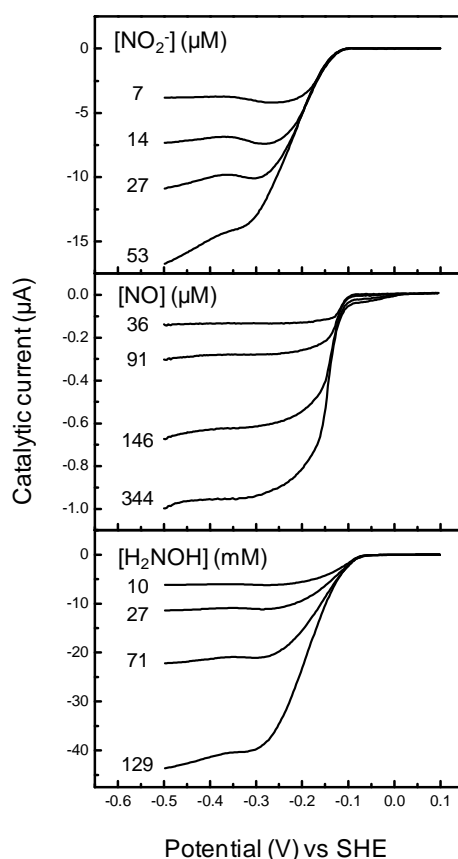


Figure 1.7- The catalytic response from PFE of native NrfA in the presence of nitric oxide, nitrite and hydroxylamine at concentrations presented in the figure. Voltammetry was conducted in buffer-electrolyte containing 2 mM CaCl_2 , 50 mM HEPES pH 7, scan rate of 0 mV s^{-1} with electrode rotation at 100 rpm for nitric oxide and 3000 rpm for nitrite and hydroxylamine and at 20°C .

1.5.3 Reaction mechanism

The characterisation of NrfA not only as a nitrite reductase but also as nitric oxide and hydroxylamine reductase implicated the later two molecules as intermediates in the reduction of nitrite to ammonia. The combination of the biochemical characterisation of NrfA and the elucidation of the structure of NrfA bound to water, nitrite and hydroxylamine allowed a mechanism for the six electron and eight proton reduction of nitrite to ammonia to be proposed by Einsle, *et al* [50].

In the oxidised resting form the active site heme of NrfA is proposed to have a distal water ligand bound. Upon reduction the $\text{Fe}^{2+}\text{-OH}_2$ bond becomes weakened. The weakening of this bond allows the water to be more easily displaced by a substrate molecule. The nitrite

adopts an N-bonding mode to the heme iron, which is calculated to be lower energy state compared to the O-bonding mode. The nitrite molecule is believed to bind tighter to the reduced active site heme than the oxidised heme, even though the oxidised has a greater positive charge and therefore is likely to form a more favourable electrostatic interaction with the negatively charged nitrite molecule. The reason why nitrite bonds tighter to the reduced heme is attributed to the back-bonding effect that allows the electron-rich iron to transfer charge onto the nitrite molecule which strengthens the Fe-NO_2^- bond, this can only occur in the reduced complex.

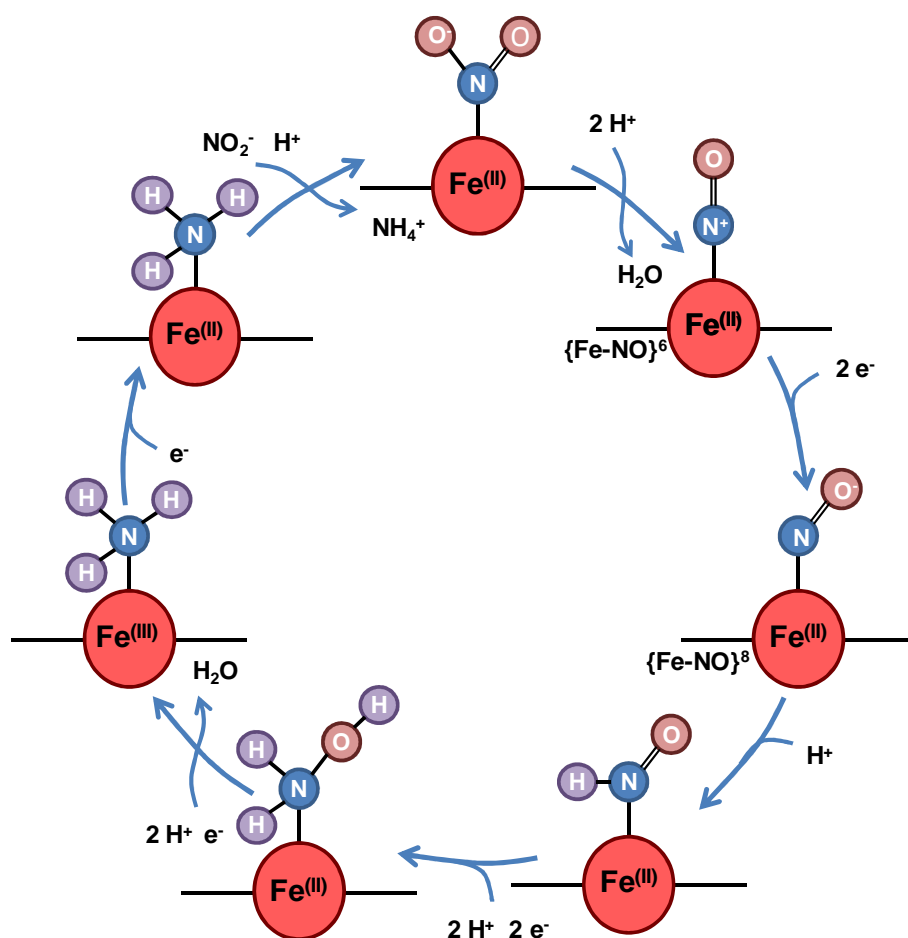


Figure 1.8- The proposed mechanism for the reduction of nitrite to ammonia by NrfA. The catalytic cycle is initiated by nitrite binding to the reduced active site heme and the heterolytic cleavage of the first N–O bond. Subsequent alternating proton and electron transfer steps lead to the enzyme-bound intermediates $\text{Fe}^{(II)}-\text{HNO}$ and $\text{Fe}^{(II)}-\text{H}_2\text{NOH}$ and eventually yield the product, ammonium, which can be released and replaced by another substrate molecule [50].

Upon the binding of nitrite to the active site heme iron, one of the N–O bonds is broken in a heterolytic cleavage. This generates a $\{\text{FeNO}\}^6$ adduct (the superscript number indicates the number of metal d-electrons plus the number of electrons in the π^* of NO, according to the Enemark and Feltham notation. This notation is necessary as it is difficult to determine the location of electrons in heme-NO complexes). The cleavage of the first N–O bond is facilitated by two electronic effects. First is the back-bonding interaction, which transfers electron density into the lowest unoccupied molecular orbital (LUMO) of the nitrite molecule which is the π^* orbital. The transfer charge into the π^* orbital of the nitrite molecule has the affect of weakening the conjugated π system that is delocalised over all three atoms, thus decreasing the soluble bond character of both of the N-O bonds within the nitrite molecule. Although weakening the intramolecular (N-O) bonds of the nitrite molecule, the intermolecular (Fe-NO₂) bond is strengthened. The second electronic effect that contributes to the heterolysis of the N–O bond is the creation of asymmetry within the nitrite molecule by the formation of hydrogen bonds between His264 and Arg106 and the two oxygen atoms of the nitrite molecule. This provides one N-O bond with greater double characteristics while the other bond adopts single bond characteristics and is therefore weakened and as a result is cleaved. The comparison of the crystal structures of the active site with nitrite and hydroxylamine bound suggests that it is the oxygen atom that is hydrogen bonded to the His264 that is cleaved. The cleavage of this bond also suggests that the His264 is likely to be present in the doubly protonated imidazolium form to enable it to donate a proton to the cleaved oxygen atom.

The linear $\{\text{FeNO}\}^6$ adduct formed from the heterolytic cleavage of the nitrite molecule is highly unstable and is quickly reduced to the more stable $\{\text{FeNO}\}^8$ adduct. This reduction is believed to occur in a rapid two electron process, as to avoid the formation of the non-linear $\{\text{FeNO}\}^7$ adduct which is highly stable and would probably form a kinetic trap in the reduction of nitrite. The injection of two electrons into active site must be rapid as the linear $\{\text{FeNO}\}^6$ adduct must be reduced to the $\{\text{FeNO}\}^8$ adduct before the $\{\text{FeNO}\}^7$ adduct can rearrange into a non-linear conformation. The positioning of hemes 3 and 4 are ideally suited for the fast and efficient transfer of two electrons into the active of NrfA that would be required to fulfil this step of the reduction process.

The reduction of the $\{\text{FeNO}\}^8$ complex creates a more nucleophilic species, which is able to undergo protonation on the nitrogen atom to form a Fe-HNO species. The HNO adduct undergoes further reduction with the alternating transfer of two electrons and two protons to form a $\text{Fe}^{2+}\text{-H}_2\text{NOH}$ species. The Hydroxylamine adduct shown in the crystal structure

confirms hydroxylamine remains bound to the iron via the nitrogen, with the oxygen atom hydrogen bonding to Arg106.

A further injection of one electron into the Fe^{2+} -hydroxylamine species causes the heterolytic cleavage of the remaining N-O bond. The subsequent re-oxidation of the heme iron coupled to a single protonation event would form an ammonium bound ferric heme species. The Fe-NH₃ bond is predicted to be weak, allowing dissociation of the product and its exit to the surface of the protein via the negatively charged egress channel.

1.6 Mutational studies of NrfA

A number of studies have characterised NrfA variants generated by site directed mutagenesis, including the role of glutamine 263 and tyrosine 216, in order to gain an insight into the roles of conserved residues within NrfA. The methods used to characterise these variants include x-ray crystallography and both solution and PFE experiments.

The role of the conserved glutamine residue 263 within *E. coli* NrfA was investigated by mutational studies conducted by Clarke *et al* [11]. Within this study the atypical monodentate glutamine ligand residue was substituted with the bidentate glutamate residue, which is a more common metal ligand. The study revealed that the coordination of the calcium ion remained unchanged with the glutamate residue adopting a monodentate ligation of the calcium ion in a similar orientation to the native residue. The characterisation of the WT and Q263E mutation using methyl viologen assays resulted in over a 10-fold increase in the K_M from $\sim 33 \pm 15 \mu\text{M}$ to $413 \pm 63 \mu\text{M}$, whilst the V_{max} remained unaltered with values of $629 \pm 25 \text{NO}_2^- \text{s}^{-1}$ and $641 \pm 41 \text{NO}_2^- \text{s}^{-1}$ for WT and Q263E, respectively.

The Q263E was further characterised by PFE which enabled the enzyme activity to be studied as a function of potential, allowing a more detailed understanding of nitrite reduction. The PFE experiments of Q263E revealed a similar catalytic profile to that of WT NrfA, although the catalytic wave had shifted to a more negative potential suggesting a higher driving force was required to reduce nitrite. When the protein films of WT and Q263E NrfA were exposed to nitrite concentrations at or below their respective K_M values, both proteins displayed a peak of activity followed by an attenuation of activity at more negative potentials, which is a well documented feature of nitrite reduction by NrfA. The results from this study indicated that the native glutamine residue is likely to be an important component in stabilising the hydrogen bond network within the active site. This which impacts on substrate binding as indicated by the increase in K_m but does not have an effect on the rate

of reduction, as the V_{\max} for nitrite reduction has not significantly altered in the Q263E NrfA compared to the native enzyme.

Another study conducted by Lukat et al characterised the active site tyrosine residue of *W. succinogenes* NrfA [45]. The tyrosine 218 residue (*W. succinogenes* numbering equivalent to Tyr216 in *E. coli* NrfA) was substituted by a phenylalanine residue, which allowed an aromatic residue to remain while removing the phenol group. The Y218F mutation resulted in significantly lower nitrite reductase activity, less than 1% of that of the native enzyme. Although the mutation had a clear impact on the rate of nitrite reduction the ability of the Y218F NrfA to reduce sulphite, a secondary substrate, remained unchanged. The decrease in nitrite reductase activity suggests that the tyrosine residue must play a direct role in nitrite reduction at some point in the catalytic cycle. The comparison of the crystal structure of the native and Y218F variant revealed that nitrite was bound in a similar conformation in both proteins. The study, however, only looked at the rate of reduction of a fixed concentration of substrate and measured the reduction of nitrite by the production of ammonia. This could potentially mean that nitrite is still able to be reduced but ammonia may not be the product. Instead, nitric oxide or hydroxylamine could be formed.

Mutational studies to identify the importance of the lysine ligation of the active site heme of NrfA have been carried out using site directed mutants of the *W. succinogenes* NrfA [41]. Two mutants were studied in which the active site lysine was substituted for either a histidine (K134H) or a leucine (K134L) residue. The K134L strain was unable to grow with nitrite as a terminal electron acceptor and had no detectable nitrite reductase activity, as assayed using reduced benzyl viologen. Western blot analysis revealed that there was no NrfA protein present suggesting that the K134L mutation resulted in an unstable protein that is degraded within the cell. The K126H strain was also unable to use nitrite as a terminal electron acceptor. However benzyl viologen assays revealed that it was still able to reduce nitrite to ammonium although at a slower rate than the WT enzyme. The presence of the active site heme was confirmed by delayed extraction matrix-assisted laser-desorption/ionization time-of-flight (DE-MALDI-TOF) mass spectrometry as the K134H protein had a similar mass to that of the WT NrfA protein. The substitution of the proximal ligand to the active site heme of NrfA revealed that the CxxCK heme binding motif could be altered to the more conventional CxxCH motif and the heme still be inserted. However the resulting protein was a less proficient nitrite reductase compared to the WT protein.

The mutational studies of both *E. coli* and *W. succinogenes* identified that the substitution of conserved active site residues within NrfA can result in observable and, more

importantly, measurable changes in the activity of the NrfA enzyme. The combination of a number of techniques enabled conclusions to be drawn on the possible role of the K126, Y216 and Q263 residues within the native NrfA enzyme.

1.7 Aim of thesis

The aims of this thesis were to investigate the mechanism by which NrfA is able to catalyse the reduction of nitrite to ammonia. The reduction of nitrite is facilitated by the active site of NrfA which is highly conserved in all known NrfA proteins. To gain a better understanding of the role the key active site residues play in the reduction of nitrite in *E. coli* NrfA, these residues were mutated and the protein expressed, purified and characterised. The variant NrfA proteins were compared to the WT enzyme in the expectation that any change in activity will help to elucidate the role of the residue within the active site of the native enzyme.

An array of techniques were deployed to characterise the native and variant NrfA proteins. The techniques included structural determination by X-ray crystallography to confirm the mutation and to determine the structural affect of the mutation allowing the enzyme kinetics to be placed in a structural context. The enzyme kinetics of the native and variant NrfA proteins were characterised for their ability to reduce the enzymes native substrate of nitrite and the proposed reaction intermediates of nitric oxide and hydroxylamine, which have been previously reported to be reduced directly to ammonia by NrfA. The reduction of nitrogenous substrates were monitored by PFE to allow catalysis to be measured as a function of potentials, which revealed novel features of substrate reduction. The mutation of individual residues indicated that each active site residue serves a discrete purpose during the NrfA catalytic cycle.

Chapter 2

Materials and Methods

Chapter 2 – Materials and Methods

2.1 Expression of recombinant WT and NrfA variants

2.1.1 Bacterial strains and plasmids

The WT and variant NrfA proteins were produced and purified using *E. coli* strain JCB4083a ($\Delta narZ::\omega \Delta narL::Tn10 \Delta napGH \Delta nrfAB \Delta nirBDC::Kan^R$) which is unable to produce the NrfAB proteins and is kanamycin (kan) resistant. The *E. coli* JCB4083a strain was freshly transformed with two plasmids. The first is the pEC86 plasmid that expresses the cytochrome *c* maturation system (*ccmABCDEFGH*) and is chloramphenicol (chl) resistant [11, 46]. The role of the pEC86 plasmid is to maximise heme insertion into the NrfA apo-protein, which should result in the production of high levels of fully functional NrfA. The second plasmid (pJG1.9) contains the *nrfB* gene and either the WT or a mutated *nrfA* gene and is ampicillin (amp) resistant. The mutant *NrfA* genes were prepared by site directed mutagenesis of the WT pJG1.9 plasmid and resulted in the substitution of active site residues within the of NrfA protein Table 2.1. The plasmid and strains were provided by Jeff Cole at the University of Birmingham. The mutations were confirmed previously by sequencing and within this work by the elucidation of the crystal structures of the recombinant WT (rWT) and the variant NrfA proteins. These structures will be discussed in more detail in subsequent chapters.

NrfA Variant	Genes encoded	Mutations	Antibiotic resistance
pJG1.9 (WT)	<i>nrfAB</i>	-	Ampicillin
pJG1.9H264N	<i>nrfAB</i>	His-264-Asn	Ampicillin
pJG1.9Y216F	<i>nrfAB</i>	Tyr-216-Phe	Ampicillin
pJG1.9K126H	<i>nrfAB</i>	Lys-126-His	Ampicillin
pJG1.9R106K	<i>nrfAB</i>	Arg-106-Lys	Ampicillin
pEC86	<i>ccmABCDEFGH</i>	-	Chloramphenicol

Table 2.1 - Plasmids used within this study.

2.1.2 Growth of the recombinant WT and variant NrfA strains

Cultures for purification were grown by picking a single colony from an LB media chl (30 µg/mL) and amp (100n µg/mL)) agar plate. The transformed *E. coli* strains were grown on

minimal salts (MS) media with glycerol (0.4% v/v) as the sole carbon source and fumarate (40 mM) as the sole terminal electron acceptor (table 2.2) [57]. Trace metal stock solution and antibiotics were added to the media at the time of inoculation. Liquid cultures of the strains were grown anaerobically at 37°C by filling the growth vessel to the brim and incubating without aeration.

To produce the cell mass required for purification typically 40 – 50 L of cells were grown for each NrfA variant. A single bacterial colony was picked and used to inoculate a 20 mL MS media overnight culture, the 20 mL overnight was then used to inoculate a 1 L overnight of MS media, 300 mL of this overnight was then used to inoculate a final 5.5 L vessel which was left to grow for 20- 24 h. Cells were then harvested by centrifugation and stored as cell pellets at -80°C until purification.

Media		
Compound	Concentration (g L ⁻¹)	
KH ₂ PO ₄	2.25	
K ₂ HPO ₄	5.5	
(NH ₄) ₂ SO ₄	1.0	
Na ₃ citrate	0.5	
MgSO ₄	0.05	
Na ₂ fumarate	3.2	
NaNO ₃	1.9	
NaCl	0.5	
Yeast extract	0.5	
Tryptone	1.0	
Glycerol	4 ml	
Media Additions		
Antibiotics	Concentration (µg ml ⁻¹)	
Ampicillin	100	
Chloramphenicol	30	
Trace metals	Volume (ml in 1 L)	Metal stock solutions (g L ⁻¹)
(NH ₄) ₆ Mo ₇ O ₂₄	1.0	1.23
Na ₂ SeO ₄	0.152	1.23
MgCl ₂ .6H ₂ O	0.25	300.0
MnCl ₂ .4H ₂ O	0.25	40.0
FeCl ₃ .6H ₂ O	0.25	50.1
CaCl ₂ .2H ₂ O	0.25	18.5

Table 2.2 – Recombinant NrfA expression media.

2.1.3 NrfA purification

The NrfA purification was carried out following the protocol outlined by Bamford et al [32]. In brief, the cell pellet was re-suspended in spheroplastic buffer containing 0.5 M sucrose, 100 mM Tris-HCl, pH8, 1 mM Ethylenediaminetetraacetic acid (EDTA), 100 mg L⁻¹ DNase 1 and 1 g L⁻¹ lysozyme. The cell buffer solution was stirred continually for 30 - 45 minutes at 30°C. Then the solution was centrifuged at 9,000 g at 4°C for one hour. The centrifugation separated the spheroplasts from the periplasmic contents, which remained in the supernatant. The pellet was discarded and the supernatant containing the NrfA protein was retained. A 65% (w/v) ammonium sulphate cut was carried out on the supernatant to precipitate the NrfA protein. Ammonium sulphate was slowly added and the solution stirred for 3 h at 4°C. The ammonium sulphate containing supernatant was then centrifuged at 30,000 g at 4°C for 1 h to pellet the precipitated protein. The pellet was retained and re-suspended in a small volume (150 mL) of 50 mM Tris-HCl, pH 8. The re-suspended protein was then extensively dialysed against 4 x 5 L 50 mM Tris-HCl over 36 - 48 h. The dialysed protein was centrifuged again at 30,000 g at 4°C for 1 h to remove any material that precipitated during dialysis.

The dialysed material was loaded onto an anion exchange Q-Sepharose column (Amersham) equilibrated with 50 mM Tris-HCl, pH 8.0. Any unbound protein was removed by washing the loaded column with one to two column volumes of 50 mM Tris-HCl, pH 8.0 buffer until the baseline absorbance had stabilized. The bound proteins were then eluted from the column using a gradient of 0–150 mM NaCl over 200 ml, followed by 150–1000 mM NaCl over 150 mL, at a flow rate of 2 ml min⁻¹. The fractions containing the NrfA protein typically eluted between 75-100 mM NaCl. The fractions containing NrfA were identified by the presence of a 53 kDa band on a sodium dodecyl sulphate polyacrylamide gel electrophoresis (SDS-PAGE) gel stained for covalently attached cytochrome c proteins. The fractions containing NrfA were pooled and concentrated using a 30-kDa Amicon filter. The concentrated NrfA sample was then passed through a Superdex 200 26/60 column (Amersham) equilibrated with 50 mM Tris-HCl, pH 7.0, and 50 mM NaCl buffer. Fractions containing NrfA were identified by Coomassie-stained SDS-PAGE gel. The NrfA containing samples were pooled and dialysed into 50 mM Tris-HCl, pH 7.0 buffer and the sample was loaded on to an anion-exchange column equilibrated with 50 mM Tris-HCl, pH 7.0 and washed with two to three column volumes of the same buffer. The NrfA protein was eluted using a gradient of 0-200 mM NaCl, 50 mM Tris-HCl pH 7.0. Typically NrfA eluted around 75 mM NaCl. Purified NrfA was identified by a single band on Coomassie-stained SDS-PAGE gel and by the A_{280}/A_{410} absorbance ratio which is 3.5 for purified NrfA [46].

Once purified samples of NrfA were stored in 50 mM HEPES and 2 mM CaCl₂ pH 7.0 at -80°C.

2.2 Protein visualisation

SDS-PAGE was used to identify the chromatography fractions that contained NrfA protein and confirm the purity of the final samples. SDS page gels were cast and run in a Hoefer vertical gel system. The gels consisted of a resolving layer of 12% (v/v) bis-acrylamide, Tris-HCl pH 8.8 and a stacking layer of 6.5% bis-acrylamide, Tris-HCl pH 6.8. Protein samples were mixed with 2 times loading buffer which contained 6 M urea, 5% SDS (w/v), 0.1% glycerol (v/v) and 0.05% bromophenol blue (v/v) and was incubated at 100°C for 15 minutes. Into each well was loaded 10-15 µL of sample. The running buffer used contained 25 mM Tris-HCl, 200 mM glycine, 3.5 mM SDS at pH8.8. The gel was run at 30 mA until the loading dye front had reached the bottom of the gel, approximately 1 h. The gels were stained for all protein using InstantBlue coomassie stain. They were covered with the stain and left shaking for 20-30 minutes to allow the blue bands to develop.

SDS page gels were run as described above and stained specifically for proteins containing c-type cytochromes [46]. The gel was first placed into 45 mL of 50 mM sodium acetate pH 5 for 15 minutes in the dark. In a light impervious container, 20 mL methanol containing 1 mg mL⁻¹ 5-tetramethylbenzidine dihydrochloride hydrate was then prepared. This was added to the gel in the sodium acetate solution and it was then incubated for a further 15 minutes. After this time 200 µL of 30% (v/v) hydrogen peroxide solution was added and the gel was left to develop in the dark until dark blue bands appeared, this was typically within three hours.

2.3 Solution spectroscopy

Ultraviolet and visible (UV-Vis) electronic absorbance spectra were recorded on a JASCO V-550 spectrophotometer. Concentrations of air-equilibrated NrfA monomer were calculated using an extinction coefficient of 497,650 M⁻¹ cm⁻¹ [46]. Reduced NrfA electronic absorbance spectra were obtained by preparing an anaerobic sample of NrfA in a sealed cuvette and adding small aliquots of sodium dithionite until the spectra no longer altered.

2.4 Protein structure determination

2.4.1 Crystallisation

The conditions needed to crystallise *E. coli* NrfA have been previously described [11, 46]. These conditions were used as a guide to set up the crystal screens for all the NrfA proteins within this study. The conditions used were 12 – 22% (v/v) polyethylene glycol 10k in 100 mM HEPES at pH 7, 7.5 and 8. Both vapour diffusion hanging drop and sitting drop methods were used in a 24 well format, with each well containing 1 ml mother liquor solution. The protein sample was concentrated to 5 mg mL⁻¹ and was centrifuged for 15 minutes at 13,000 rpm at 4°C prior to use. Drops were set up containing 1 µL mother liquor and 1 µL protein sample. The screens were incubated aerobically at 4°C.

Crystals formed over the range of conditions within one to two weeks of setup. Crystals were harvested using a loop or a mesh loop and placed into cryoprotectant for 2 -3 minutes prior to flash freezing and insertion into a crystallography puck submerged in liquid nitrogen. The cryoprotectant was 20% (v/v) ethylene glycol, 20% (v/v) PEG 10K, 100 mM HEPES pH 7.5. For substrate soaks the cryoprotectant contained 10 - 50 mM NaNO₂ and the crystal was exposed to the cryoprotectant for a longer time period of 10 – 30 minutes. Sample filled crystallography pucks were stored in a liquid nitrogen storage dewar prior to being transported in dry dewars.

2.4.2 Data collection

All diffraction data was collected at the Diamond Light Source synchrotron radiation facility (DLS, Oxford) on various beam lines. Data was collected both at the facility and also remotely from UEA. Samples were stored in liquid nitrogen, robotically loaded on to the goniostat, and cooled to 100 K by a cryojet of gaseous nitrogen. Initially three test images of each single protein crystal were taken at 0°, 45° and 90° to determine diffraction and potential resolution. The integration of the three images using MOSFLM allowed the cell parameters and space group to be determined. The STRATEGY tool in MOSFLM was used to identify the best approach to record a complete data set including start angle, degree oscillation and total number of degrees needed, Table 2.4.

Data collection	rWT	H264N	R106K	Y216F	K126H
Wavelength (Å)	0.9700	0.9778	0.9795	0.9760	0.9700
Resolution (Å)	82.45 - 2.10 (2.15 - 2.10)	45.79 - 2.15 (2.21 - 2.15)	53.86 - 2.20 (2.26 - 2.20)	57.74 - 2.11 (2.17 - 2.11)	60.61 - 2.3 (2.36 - 2.3)
Unique reflections	119,089 (8792)	57,951 (4,153)	107,322 (7,791)	111,068 (8104)	85,041 (6,213)
Completeness (%)	99.9 (99.9)	99.7 (98.2)	99.9 (98.6)	97.6 (96.9)	97.4 (96.9)
R merge	0.118 (0.279)	0.084 (0.327)	0.102 (0.353)	0.067 (0.255)	0.059 (0.252)
I/sigma	4.6 (2.4)	7.3 (2.1)	6.7 (2.1)	10.1 (3.0)	12.6 (3.1)
Mean I/sigma	8.4 (5.0)	13.4 (6.4)	11.4 (4.4)	11.5 (3.9)	13.7 (3.7)
Multiplicity	3.4 (3.5)	4.9 (5.0)	4.4 (4.3)	2.5 (2.5)	2.4 (2.3)
Space group	P2 ₁	P2 ₁ 2 ₁ 2 ₁	P2 ₁	P2 ₁	P2 ₁
Cell dimensions length (Å)	90.42, 82.45, 141.41	42.24, 89.49, 274.72	91.18, 83.02, 144.33	89.69, 79.69, 143.19	89.65, 79.56, 142.59
Cell dimensions angles (°)	90.00, 101.03, 90.00	90.00, 90.00, 90.00	90.00, 101.24, 90.00	90.00, 100.67, 90.00	90.00, 100.76, 90.00
Monomers in asymmetric unit	4	2	4	4	4

Table 2.3 - Summary of the X-ray data for rWT and NrfA variants, collected at Diamond Light Source, Oxford. Number in brackets indicates the values for the outer shell.

2.4.3 Crystal structure determination

Reduction and analysis of collected X-ray diffraction data was carried out using Xia2 [58]. This programme utilises existing indexing, integration and scaling tools to allow faster and simplified data analysis. The Xia2 programme can function automatically in 3 modes which draw on different software suites, Figure 2.1. These include LABELIT, MOSFLM and XDS for indexing and integration and SCALA and XSCALE for scaling. Limited manual alterations can be made to these three processes by the alteration of the input file (.xinfo). A 5% subset of the data was excluded from the data processing to allow the calculation of the free R factor during model refinement.

Molecular replacement was carried out using the program PHASER with the monomer NrfA from the PDB file 2RDZ as the template [59]. The structures obtained by molecular replacement were in a space group of either $P2_1,2_1,2_1$ or $P12_11$, both of which have been previously reported for NrfA [46]. Inspection of the structure within COOT with reference to $2mF_{\text{obs}}-DF_{\text{calc}}$ and $mF_{\text{obs}}-DF_{\text{calc}}$ Fourier electron density maps revealed that the five covalently attached hemes and the two calcium ions were present and correctly positioned within the structures, Table 2.4.

The active site mutation for each NrfA variant was modelled manually in COOT and underwent restrained refinement using REFMAC5 [60, 61]. Highly ordered water molecules were initially placed automatically, using the program ARP/WARP, into unoccupied density between sigma levels of 1.2 and 2.2 sigma [62]. The model underwent a further cycle of restrained refinement and then the placement of all water molecules was checked manually with further water molecules added or deleted where appropriate. Validation of the final crystal structures with Ramachandran plots was carried out using MOLPROBITY software [63].

	rWT	H264N	R106K	Y216F	K126H
Refinement					
R_{work}	0.1863	0.1555	0.15693	0.15147	0.16512
R_{free}	0.2405	0.2109	0.21436	0.2119	0.22076
Model					
Total Atoms	15973	8159	16469	16619	16079
Protein atoms	13948	6971	13940	13951	13952
Water	1137	744	1638	1780	1238
Heme	860	430	860	860	860
Other	28	14	31	28	28
Bond length RMSD (Å)	0.0195	0.019	0.02	0.02	0.017
Bond angle RMSD	2.69	2.65	2.69	0.657	2.601

Table 2.4 - Summary of refinement and model parameters of the rWT and H264N NrfA structures. The R_{work} and R_{free} values are calculated from $R = \sum |F_{\text{obs}} - F_{\text{calc}}| / \sum F_{\text{obs}}$ where F_{obs} and F_{calc} are the observed and calculated structure amplitude factors, respectively.

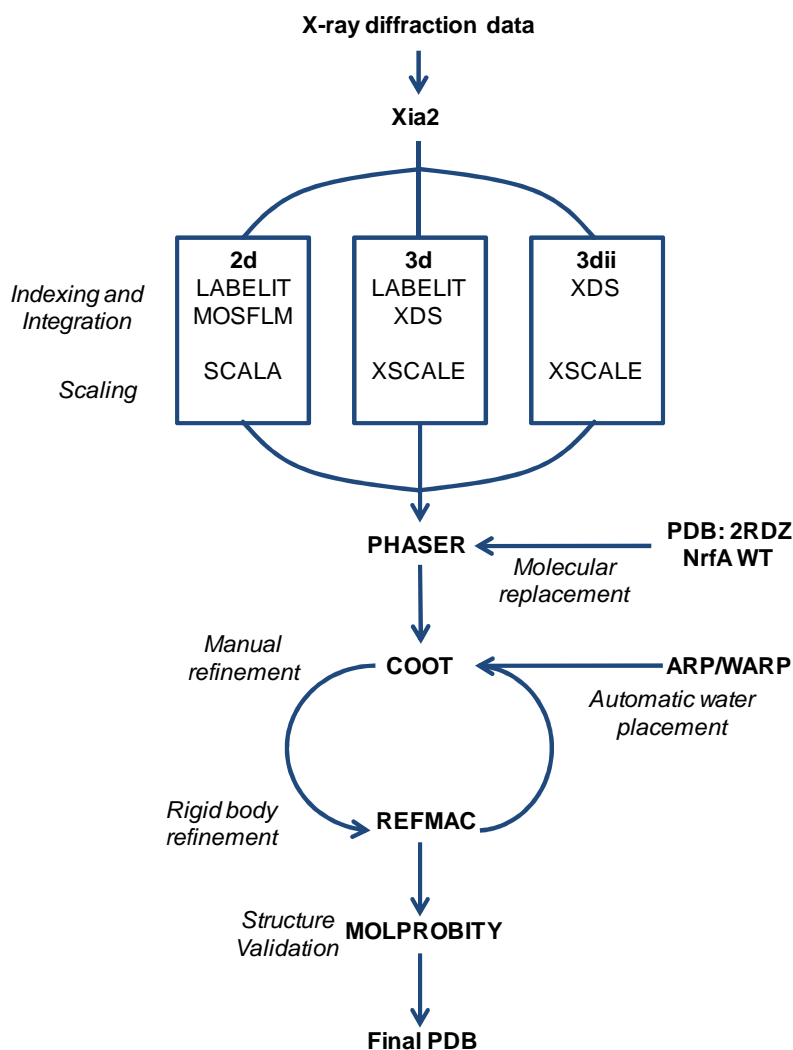


Figure 2.2- Flowchart showing the method for structure determination of NrfA WT and variants using molecular replacement. X-ray diffraction data was collected at the DLS synchrotron, Oxford. The data was processed using the Xia2 software. The molecular replacement was carried out using PHASER and a previously solved structure of *E. coli* NrfA as the template (PDB 2RDZ).

Composite simulated annealing omit maps were prepared using PHENIX AUTOBUILD software. These maps divide the asymmetric unit into overlapping omit regions. The number of regions varies depending on the size of the asymmetric unit (24 for P2₁2₁2₁ and 27 for P1 2₁ 1). The overlap between the omit regions was 2 Å. The electron density for each omit region is then calculated from atomic model excluding the atoms within that omit region. By carrying out this process for each of the omit regions, and then combining them together an electron density map ($2mF_{\text{obs}} - DF_{\text{calc}}$) is generated that is not biased by the protein model.

2.5 Characterisation of the catalytic and redox activities of NrfA

2.5.1 Reagent preparation

The sensitivity of protein film electrochemistry to trace impurities required all reagents to be prepared from Analar quality chemicals and Milli-Q water with a resistivity of $>18 \text{ M}\Omega \text{ cm}^{-1}$. The pH of all solutions were measured using a Radiometer Copenhagen PHM 82 pH meter, with a Russell pH electrode, which was calibrated prior to each use using pH standards (4.0, 7.0 and 9.2). When required, solutions were brought to the correct pH by the addition of aliquots of either 5 M NaOH or 5 M HCl.

The buffer-electrolyte used in all electrochemical experiments was 50 mM HEPES, 2 mM CaCl_2 , pH 7. The high turnover rate and low K_M for nitrite reduction by NrfA required additional care to be taken to avoid contamination of buffers with nitrite. A fresh stock of 1 M NaNO_2 was prepared each day by dissolving the appropriate mass of NaNO_2 in buffer-electrolyte. For lower nitrite concentrations a serial dilution of the original 1 mM stock was carried out with further additions of buffer-electrolyte. The hydroxylamine stock (typically 2 M) was prepared each day, as required. The appropriate mass of $\text{H}_2\text{NOH}\cdot\text{HCl}$ was dissolved in buffer-electrolyte and the pH adjusted to 7. The acidity of the hydroxylamine solution required substantial base addition. This was achieved by adding granules of NaOH and the drop wise addition of 5 M NaOH solution until a final pH of 7 was achieved. Once the neutral pH was reached, the solution was made up to the required volume by the addition of buffer-electrolyte and the pH of the solution confirmed.

A fresh nitric oxide (NO) solution (2 mM) was prepared for each day of experiments as required from a reservoir of NO gas stored in an anaerobic glove box. To prepare a gaseous reservoir of NO, a sealed conical flask filled 0.1 M NaOH solution that was purged with dinitrogen gas. The majority of the NaOH solution was displaced by NO gas from a cylinder of 98.5 % NO purchased from Sigma-Aldrich. A small volume of the NaOH solution was left in the flask to remove contaminants such as N_2O , formed from the decomposition of the NO gas. An NO stock solution was prepared each day under anaerobic conditions by removing 3 x 2 mL of NO gas from the reservoir using a gas tight Hamilton syringe and injecting it into 3 mL of anaerobic buffer-electrolyte in a sealed 5 mL universal glass bottle. After each addition the bottle was shaken and the headspace vented to maintain the NO solution at atmospheric pressure. Once all the additions were made and the headspace

vented, the solution was left to equilibrate for 30 minutes. The resulting solution had an NO concentration of $2 \text{ mM} \pm 10\%$ based upon previous work carried out by Van Wonderen et al [52]. The NO reservoir was replenished with anaerobic 0.1 M NaOH solution each time gas was removed, to prevent the build up of negative pressure in the flask. During the preparation of the NO solution all buffers were sealed to minimise contamination with gaseous NO. Unused NO Stock and reservoir solution were removed from the glove box and opened within a fume hood to limit NO release in the glove box.

2.5.2 Spectroscopic assays

The rate of substrate reduction by NrfA was monitored using a spectrophotometric method that utilised the redox active compound methyl viologen (MV). The compound methyl viologen is colourless in its oxidised (MV^{2+}) state but when reduced (MV^+) is blue in colour with an absorbance maximum at 600 nm, an extinction coefficient of $13,700 \text{ M}^{-1} \text{ cm}^{-1}$ and a midpoint potential of -446 mV vs. SHE at 25°C [64].

The enzymatic assays were carried out in 3 mL glass cuvette (1 cm light path) containing a total reaction volume of 2 mL. Stock anaerobic 100 mM sodium dithionite solution was prepared by purging 53 mg of sodium dithionite solid in a sealed universal glass bottle for 10 minutes and injecting 3 mL of anaerobic water. Anaerobic hydroxylamine (2 M) and nitrite stock solutions (1 mM - 1 M) were prepared as in the previous section. Firstly 20 μL of a 100 mM MV^{2+} solution was added to 50 mM HEPES, 2 mM CaCl_2 , pH 7 buffer in a 3 mL glass cuvette. The cuvette was then sealed with a suba-seal and purged with oxygen free nitrogen for 5 minutes. After purging the cuvette was placed into a spectrophotometer at 20°C . The anaerobic dithionite solution was then titrated into the cuvette until the A_{600} stabilised between 0.9 -1.1. The desired volume of substrate (nitrite or hydroxylamine) was added to the cuvette and mixed. The reaction was initiated with the addition of NrfA protein (final concentration of 0.5-0.1 nM). The initial velocity of nitrite reduction was calculated by determining the change in A_{600} with time, before the availability of electrons became rate limiting. Using the extinction coefficient of MV^+ and the Beer-Lambert law the change in absorbance can be converted into the change in concentration of substrate per second by dividing by six to account for the six electron reduction of nitrite. When hydroxylamine was used as substrate the change in absorbance of the MV was divided by two to account for the two electron reduction of hydroxylamine. The initial velocities of substrate reduction by NrfA were plotted as a function of substrate concentration to generate Michaelis-Menten plots and to determine the K_M , V_{max} and k_{cat} constants, using non-linear regression through the Michaelis-Menten equation (Equation 2.1) performed using Origin software.

$$\text{Rate} = \frac{V_{\max} [S]}{K_M + [S]}$$

Equation 2.1

Where [S] is the substrate concentration, K_M is the Michaelis constant and $V_{\max} = k_{\text{cat}}[E]_t$. k_{cat} is the enzyme turnover number and $[E]_t$ is total enzyme concentration.

2.5.3 Protein film electrochemistry using graphite electrodes

The technique of protein film electrochemistry allows the catalytic activity of electro-active proteins to be reported as a function of applied potential. This provides more detailed information on the potential dependence of enzyme catalysis. The direct transfer of electrons between the protein film and the electrode surface means that no reductants or mediators are required to transfer electrons to facilitate substrate reduction. The absence of reductants and mediators minimises the potential for interference from these compounds. This is especially important when using dithionite as a reductant, as it produces sulphite as an oxidation product. Previous studies have shown sulphite to bind to the active site of NrfA and act as a competitive inhibitor of nitrite reduction as well as being a poor substrate [18]. Another advantage of this technique is that the rate of reaction is measured as an electrical current due to the electron flow through the system. This is a sensitive detection method and enables only a small amount of protein to be used in a single experiment. The small amount of protein means that the decrease in substrate concentration due to enzyme turnover is negligible over the time course of a single experiment (therefore the substrate concentration effectively remains constant). The electrochemical cell is designed to ensure that the effective substrate concentration at the film surface reflects that of the bulk solution. This is achieved by a large volume of buffer-electrolyte compared to the amount of protein and the graphite electrode is continually rotated to draw fresh substrate up to the protein film and dissipate the reaction product.

The protein film voltammetry of NrfA was carried out in a three electrode chemical cell configuration, as depicted in Figure 2.3. The working electrode was a pyrolytic graphite edge (PGE) electrode with a surface area of 7 mm². The counter electrode was provided by a length of platinum wire. The reference electrode was a Ag/AgCl Russell electrode saturated with KCl solution, positioned in the reference side-arm filled with buffer-electrolyte. The potential of the reference electrode was regularly confirmed against a 2.5 mM solution of potassium ferricyanide prepared in 50 mM HEPES, pH 7.0 and 2 mM CaCl₂

buffer-electrolyte solution which has a midpoint potential of +436 mV vs. the standard hydrogen electrode (SHE). The potential recorded by the Ag/AgCl electrode was converted to the SHE by the addition of 197 mV. All potentials in this work are quoted versus SHE.

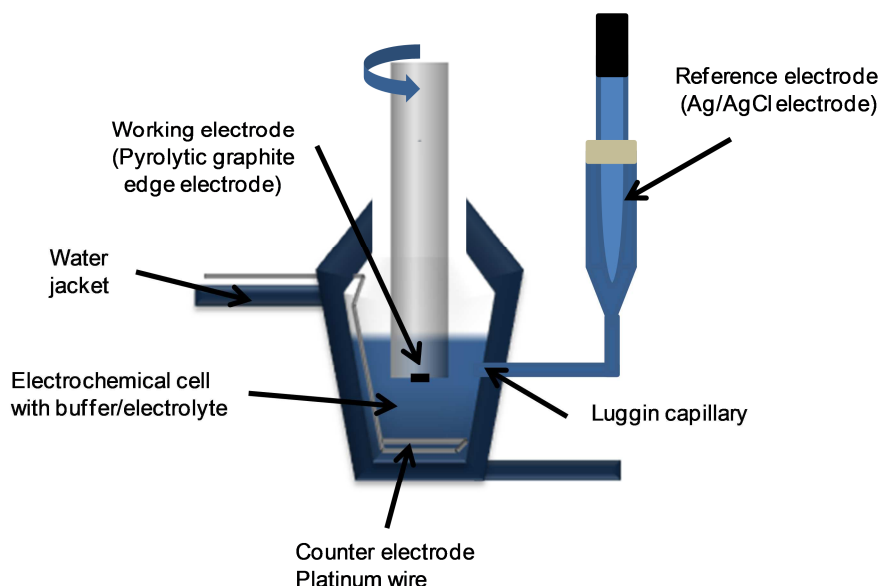


Figure 2.3 - Diagram of the three electrode electrochemical cell used for both cyclic voltammetry and chronoamperometry during protein film electrochemistry with PGE electrodes. The water jacketed electrochemical cell can accommodate 3-4 mL buffer-electrolyte.

The PGE electrode was prepared by polishing with 0.8 μm alumina slurry (to reveal a fresh graphite layer) and then sonicated to remove the alumina slurry from the surface. This process was repeated 3-5 times then the polished electrode was then taken into the glove box where 3-5 μL of an ice-cold 0.5 μM protein sample in 50 mM HEPES, 2 mM CaCl_2 , pH 7 buffer was placed onto the electrode surface and left for 30 seconds, after which time the excess protein solution was removed. The electrode was then attached to an EG&G model 636 rotator. The rotator allowed the electrode to be rotated at various speeds while maintaining an electrical connection. This enabled the mixing of the bulk solution, which continually replenished substrate and removed product from the surface of the protein film. The PGE electrode was immediately placed into the electrochemical cell so that the protein film on the electrode surface was level with the luggin capillary tip of the side arm. The cell was located inside a Faraday cage placed inside a N_2 filled glove box (Belle Technology), with the oxygen level maintained below 10 ppm. The three electrodes of the cell were linked to an Autolab PGSTAT 30 potentiostat controlled by General Purpose Electrochemical System (GPES) software and the temperature of the electrochemical cell was maintained at 20°C by the use of a thermostatically controlled water bath.

The gap between the shaft of the electrode and the wall of the cell allowed the insertion of the needle of a Hamilton syringe, enabling reagents to be added to the reaction buffer throughout the time course of an experiment. PFE experiments were carried out by using both linear cyclic voltammetry and chronoamperometry methods. To prevent the catalytic current becoming limited by the concentration of substrate at the electrode surface, the electrode rotation rate was maintained at 3,000 rpm to enable fresh substrate to be continually brought to the highly active NrfA protein film. The rate of electrode rotation was confirmed to be non-limiting by carrying out Koutecky-Levich analysis, in which the rate of electrode rotation is varied over a range of substrate concentrations. This was carried out for both nitrite and hydroxylamine. The effect of substrate depletion at the surface of the protein film was also limited by using a low concentration of NrfA (0.5 μM) to prepare the films so only a small amount of NrfA protein was present on the electrode surface [65].

During cyclic voltammetry the current was recorded as a function of potential, with the potential ramping between two set switch potentials (1st and 2nd) at a defined speed known as the scan rate, Figure 2.3. Variation of the scan rate will increase or decrease the time taken to cycle between the two switch potentials, which in turn will influence the time available for electrons to flow from the electrode to the protein or vice versa. The potential is continually cycled between the two switch potentials. This accumulates current potential data for a number of scans. Aliquots of substrate and inhibitor can be added directly into the electrochemical cell throughout the experiment and changes in the current-potential profile relate to those additions.

Chronoamperometry records current as a function of a fixed potential over time. This technique allows the protein to equilibrate fully to the applied potential, enabling steady state kinetics to be more easily observed compared to cyclic voltammetry. The chronoamperometry method also allows step changes in the potential which exposes the protein to an immediate shift in the applied potential, as shown in Figure 2.4 B. The chronoamperometry can therefore be used to resolve the effect that potential has on catalysis over time, allowing for a more in-depth kinetic analysis.

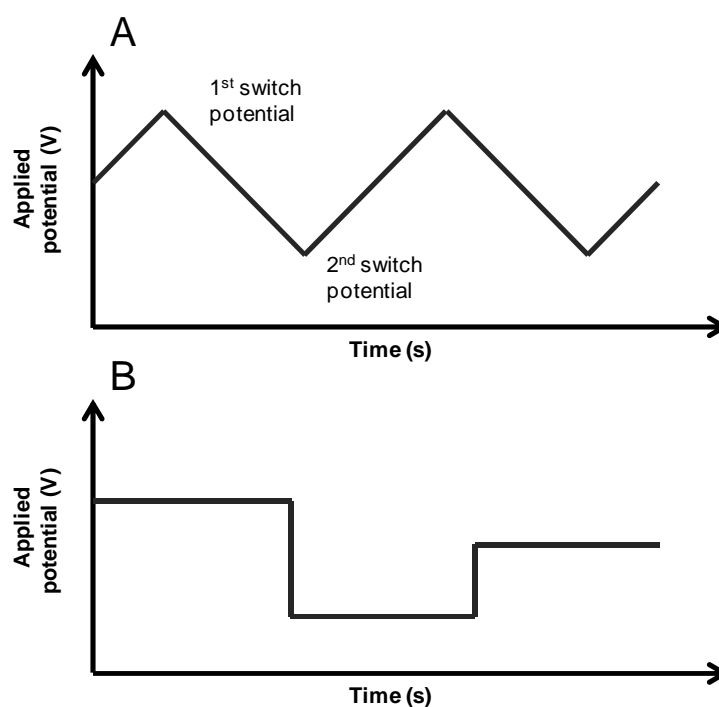


Figure 2.4- Illustration of two excitation profiles applied during protein film electrochemistry. A, cyclic voltammetry where the potential is continuously ramped between two fixed switch potentials. B, chronoamperometry where the potential is held at a single, constant value and then can be instantly switched to a new value.

At the beginning of each day cyclic voltammetry was performed scans were recorded of the bare electrode in buffer-electrolyte only to ensure a featureless charging current was observed. This confirmed that the electrode was undamaged and the electrochemical cell was correctly assembled. The scans of the bare electrode were also used as a baseline and subtracted from the scans recorded of protein coated electrode to facilitate analysis of the current generated from the protein film only.

During the time course of a PFE experiment there is a loss of signal, either due to the denaturing of the enzyme or enzyme desorption from the electrode surface. This loss in signal can be described by a first order decay. In cyclic voltammetry experiments this is accounted for by plotting the natural log of the signal magnitude at a defined potential against time for five to six scans recorded at the end of an experiment. The rate constant for the signal loss is then defined from the gradient. Data obtained in chronoamperometry experiments are analysed in the same way with the natural log of the current magnitude taken for a number of time points at a defined potential. This rate constant was then used to calculate values of i_{cat} in the absence of time decay. The corrected i_{cat} values were used to determine the K_M , V_{max} and the inhibitor constant (K_i) values.

$$i_{\text{cat}} = i_{\text{obs}} \exp^{-kt}$$

Equation 2.2

Where i_{cat} is the corrected catalytic current, i_{obs} is the observed catalytic current at a defined potential, k is the rate constant that describes the first order loss of the protein film and t is time.

The catalytic current magnitude (i_{cat}) relates to the rate of electron transfer through the protein and therefore the rate of substrate turnover. The kinetic parameters of K_M and i_{max} can be determined using the Michaelis-Menten equation (Equation 2.1) where the term i_{max} is equivalent to V_{max} . Due to the low level of NrfA protein on the electrode it is not possible to determine the exact amount of enzyme present therefore i_{max} cannot be converted into a k_{cat} constant.

2.5.4 Spectroelectrochemistry using SnO₂ electrodes

The simultaneous coupling of the techniques of visible spectroscopy and protein film electrochemistry enables the information derived from the spectroscopy to be evaluated against an applied potential. The spectroelectrochemistry of NrfA allowed the redox cycling of the hemes with the protein to be monitored. The spectropotentiometry of the NrfA proteins was carried out in a 3 electrode 'OTTLE' (Optically Transparent Thin-Layer (spectro) Electrochemical) cell, as shown in Figure 2.5. The counter electrode was a length of platinum wire. The reference electrode was a Ag/AgCl electrode prepared in the laboratory by electrolysis of a length of Ag wire in concentrated HCl. The reference electrode was calibrated against a 2.5 mM ferricyanide solution prepared in buffer-electrolyte prior to and after each experiment. Typically the addition of ~350 mV was required to give potential against the SHE. The working electrode used in OTTLE cell was a SnO₂ electrode provided by Professor James Durrant (Imperial College, London) and consist of a glass microscope slide covered with transparent conductive layer which is in turn coated with a thin layer of SnO₂ (4 μm). The three dimensional mesoporous structure the SnO₂ electrode greatly increases the surface area available for the NrfA protein to bind enabling a higher concentrations of NrfA to be reached compared to PGE electrodes.

The technique of spectroelectrochemistry offers a number of advantages over solution redox titrations. These advantages include direct electron transfer between the electrode and the protein, negating the need for mediators, and the addition of reductants and oxidants, thus removing any possible interactions between those compounds and the NrfA

protein. As mentioned previously this is especially important when using dithionite as a reductant as one of its oxidation products, sulphite, is able to bind to the active site of NrfA and inhibit nitrite reduction. If sulphite is present and interacts with the active site heme of the NrfA protein it could cause a shift in mid-point potential of that heme. A second advantage of this technique is the rate of reduction/oxidation of the protein is no longer dependent on the diffusion rate of the mediators. This enables equilibrium to be reached faster for each potential studied, allowing a quicker and more accurate titration.

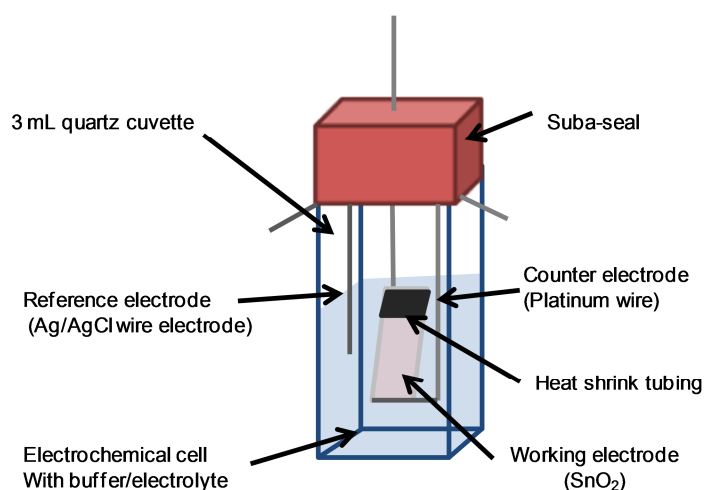


Figure 2.5 - Illustration of the configuration of the spectroelectrochemical cell used within the work of this thesis.

The SnO₂ electrode must be prepared carefully to maximise protein absorption on to the electrode and therefore maximise the spectroscopic absorbance. This was done by baking the electrode at 400°C for 30 minutes to remove any moisture, grease or dust that may have accumulated on the electrode surface. This removes any debris that could interfere with the interaction between the SnO₂ and protein. The electrode was allowed to cool to room temperature and then attached to a length of platinum wire secured using heat shrink tubing, Figure 2.4. The electrode was cooled to 4 °C and 4-8 µL of an ice cold concentrated NrfA protein solution (~80 µM) in 50 mM HEPES, 2 mM CaCl₂ buffer was placed onto the electrode surface and left for 20 minutes to soak into the porous SnO₂ but not to dry. After the 20 minutes the excess solution was removed and the electrode was rinsed in a small volume of ice cold 50 mM HEPES, 2 mM CaCl₂ buffer-electrolyte to remove any loosely bound protein.

The coated electrode was taken into an anaerobic glove box and placed in a 3 mL cuvette that contained the counter, reference and working SnO₂ electrodes, 2 mL of anaerobic 50

mM HEPES, 2 mM CaCl₂, pH 7 buffer was added and then the cuvette was sealed. Once removed from the glove box the cuvette was immediately placed into the spectrophotometer at thermostatically controlled at 4 °C. A continual argon gas flow maintained an anaerobic environment in the vicinity of the OTTLE cell. The three electrodes were attached to a potentiostat and care was taken not to disturb their orientation within the cell.

The fully oxidised (+200 mV) and fully reduced (-550 mV) absorbance spectra of the freshly prepared protein film were recorded to confirm the film is present in a redox active state. The SnO₂ electrode was poised at the desired potentials by either chronoamperometry for random potentials or by pausing cyclic voltammetry for sequential potentials. The sequential sampling was performed at a slow scan rate (5 mV s⁻¹) and pausing the scan at the desired potential before recording a spectrum. This technique ensured that the potential of the cell never jumped back to the standby potential.

The resulting spectra were analysed to enable the reduction potential of individual metal centres to be determined. The reduction potentials for the single high spin heme and the four low-spin hemes within the NrfA proteins were determined by plotting the percentage of protein reduced against the applied potential, which was calculated using Equation 2.3.

$$\frac{A_{\text{poised}} - A_{\text{ox}}}{A_{\text{red}} - A_{\text{ox}}} \times 100 = \% \text{ Reduced}$$

Equation 2.3

A_{red} is the absorbance of the fully reduced protein, A_{ox} is the absorbance of the fully oxidised and A_{poised} is the absorbance at a defined potential. All absorbance values are taken from the same wavelength.

The relationship between the concentration of an [ox] and [red] sample, the sample potential and the midpoint potential is described by the Nernst equation, Equation 2.4.

$$E = E_m + \frac{RT}{nF} \ln \frac{[\text{Ox}]}{[\text{Red}]}$$

Equation 2.4

Where E is the applied potential and E_m is the midpoint potential of the redox couple. R is the gas constant, T is the temperature in Kelvin, n is the number of electrons needed for the reduction process and F is the Faraday constant.

The Nernst equation can be rearranged to give the ratio of oxidised to reduced when the midpoint potential and the applied potential (E) is known, Equation.2.5.

$$\frac{[\text{Ox}]}{[\text{Red}]} = \exp\left(\frac{nF}{RT}(E-E_m)\right) = \theta$$

Equation 2.5

The ratio of the oxidised and reduced (θ) can then be related to the percentage of reduced protein using Equation 2.6.

$$\% \text{ Red} = \frac{100}{1+\theta}$$

Equation 2.6

Plotting the percentage of protein reduced against potential enabled the Nernst equation as presented in Equation 2.5, to be fitted to the data manually. The midpoint potential value (E_m) was manually manipulated to generate the best fit to the experimental data. The fitting was carried out using Origin software.

Chapter 3

The role of the distal pocket residues in the NrfA reaction cycle

Chapter 3 - The role of the distal pocket residues in the NrfA reaction cycle

3.1 Introduction

The reaction mechanism for the reduction of nitrite by NrfA, as proposed by Einsle and co-workers, suggests that the histidine, arginine and tyrosine residues forming the distal pocket of the active site of NrfA play a number of important roles [50]. The crystal structure of *W. succinogenes* with nitrite bound has shown that both the histidine and arginine residues form hydrogen bonds with the nitrite molecule. Another structure of *W. succinogenes* NrfA with hydroxylamine bound also revealed that arginine residue forms a hydrogen bond to the single oxygen of a hydroxylamine molecule [50]. However, the tyrosine residue does not directly interact with the bound nitrite molecule. Substituting the tyrosine residue for a phenylalanine in previous work carried out by Lukat and colleagues resulted in a decrease in activity of two orders of magnitude [45]. The loss of activity would suggest that the tyrosine residue, which does not interact with the bound nitrite, must have an important function during the reduction process.

To further experimentally assess the function of the three distal pocket residues, they have been substituted for residues that display different properties. This enables the function of the native residue to be determined by the resulting changes in catalysis. Three NrfA variants were generated in the *E. coli* enzyme by the introduction of a mutation into the recombinant plasmid containing the native *nrfA* gene. His264 was replaced by asparagine (H264N), to remove the imidazole ring of the histidine and replace it with the carboamide group of the asparagine. Arg106 was replaced with a lysine (R106K) thus replacing the guanidinium group of the arginine side chain for the amine group of the lysine residue. The Tyr216 residue was substituted for a phenylalanine (Y216F). The hydrophobic character of the residue was maintained as both contain a phenyl ring, while the phenol group of the tyrosine is lost.

Alongside the three recombinant variants of NrfA, recombinant WT NrfA (rWT) was characterised for the first time. Carrying out the structural and electrochemical characterisation of these proteins in parallel allowed for direct comparisons to be made between the variant and rWT proteins and the effects of the active site mutation to be clearly resolved.

3.2 A comparison of WT and H264N NrfA

3.2.1 Crystal Structures of rWT and H264N NrfA

3.2.1.1 The structure of rWT NrfA to a resolution of 2.10 Å

Clarke and colleagues have previously crystallised native WT NrfA purified from *E. coli* strain LCB2048, a NrfA over-expression strain [11]. The rWT purified from *E. coli* strain JCB4083a crystallised under similar conditions as those of the native NrfA. Protein crystals were harvested at 4 °C and X-ray data was collected at the Diamond Light Source synchrotron (Oxford). Analysis of the obtained data set was carried out using XIA 3dii software and identified the space group as $P2_1$ [58]. Existing structures of *E. coli* NrfA have been solved in space groups of $P2_1$ and $P2_12_12_1$ under similar conditions to those used in this work [11, 18]. The observed difference in space group is likely to reflect subtle changes in the interaction and orientation of the protein monomers within the crystal lattice that impact on the protein arrangement.

The crystal structure was solved by molecular replacement using a single monomer from an existing *E. coli* WT NrfA structure at a resolution of 1.7 Å (PDB: 2RDZ). All water molecules were removed from the search model. Molecular replacement identified two dimers within the asymmetric unit. The structure was refined to a final resolution of 2.1 Å. A summary of the data sets collected, refinement statistics for the WT NrfA, and all the NrfA variants discussed in this work can be found in Table 2.3.

The α -carbon atoms from the protein backbone of a single NrfA monomer of the native WT NrfA (2RDZ, monomer D) were structurally aligned with the four monomers present in the rWT NrfA structure. This was carried out using SUPERPOSE accessed via CCP4 [66]. The alignment generated overlaying structures with an average RMSD value of 0.30 ± 0.03 Å. The low RMSD value demonstrates that the overall 3D structure of the native WT protein and rWT protein was maintained. The five covalently attached hemes were located in the same positions with the four bis-His coordinated hemes maintaining histidine ligation. The active site heme also retained the novel lysine ligation. Comparing the electron density of the monomers present within the asymmetric unit would suggest that the heme binding sites are fully occupied. The active site calcium ion was present and maintained the same coordination sphere including two water molecules. A second calcium ion was modelled in the calcium (II) site although this atom may not be present in all protein molecules. The structural alignment of the native WT and rWT NrfA confirmed that the orientation of the

residues that form the catalytic triad, and the position of conserved water molecules within the active site cavity, were the same in both structures, as can be seen in Figure 3.1. The active site heme was modelled to be coordinated to a water molecule although this position could also be occupied by a hydroxide ion.

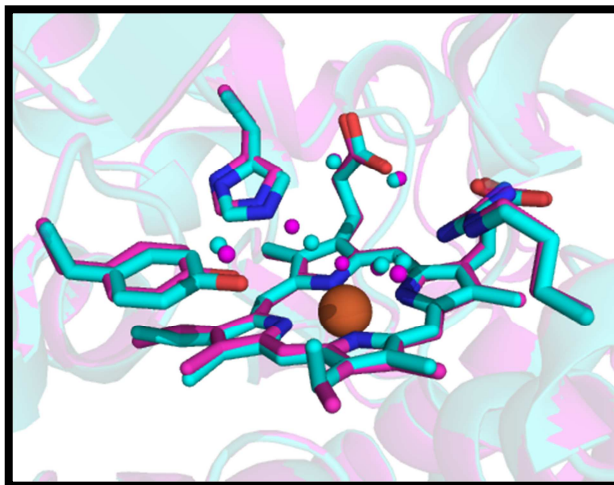


Figure 3.1 – Structural alignment of the α -carbon atoms of native WT and rWT NrfA from *E. coli*. Magenta, rWT NrfA. Cyan, the native WT NrfA (PDB: 2RDZ). Protein backbone depicted as ribbon. The residues of the catalytic triad (Histidine 264, Tyrosine 216 and Arginine 106) shown as sticks. The carbon skeleton of the active site heme depicted as sticks and with the heme iron shown as an orange sphere. Small spheres represent conserved water molecules. The structural alignment was carried out in SUPERPOSE accessed via CCP4 and the figure prepared in Pymol.

3.2.1.2 The crystal structure of H264N NrfA to a resolution of 2.15 Å

The recombinant H264N variant of *E. coli* NrfA crystallised under the same conditions as the rWT NrfA. The H264N protein crystal was in a space group of $P2_12_12_1$ [58]. Molecular replacement was carried out using the same search method as used for rWT NrfA and the structure was refined to a final resolution of 2.15 Å with the asymmetric unit containing a single H264N NrfA dimer.

A structural alignment of both monomers within the H264N dimer with a single native NrfA monomer (2RDZ, monomer D) revealed that the substitution of the active site histidine with an asparagine residue had no effect on the overall protein structure. There was an average RMSD value of $0.31 \text{ \AA} \pm (0.01)$ between the α carbon atoms of both structures. The H264N protein contained four bis-his ligated hemes, with the histidine ligands adopting the same orientation as those of the native WT protein. The active site heme was positioned as in the

native WT structure with a lysine residue as the proximal ligand to the heme iron. The sixth site was partially occupied by a water molecule. A calcium ion was also present in each of the calcium binding sites.

To confirm the substitution of the active site His264 to an asparagine composite simulated annealing omit maps were prepared using PHENIX AUTOBUILD software, methods 2.4.3. Composite simulated annealing omit maps are not biased by the protein model. The generated omit map is depicted in Figure 3.2 where it is contoured to a sigma level of 1.2 and clipped to the residues that form the NrfA catalytic triad. Comparing the omit map with the protein models in which residue 264 is either an asparagine, Figure 3.2 A or a histidine residue, Figure 3.2 B clearly shows the shape of the density closely fits that of asparagine. For the H264 model the histidine residue would require extra density to account for the entire imidazole ring. This verifies that the asparagine residue is present within the active site of the H264N NrfA.

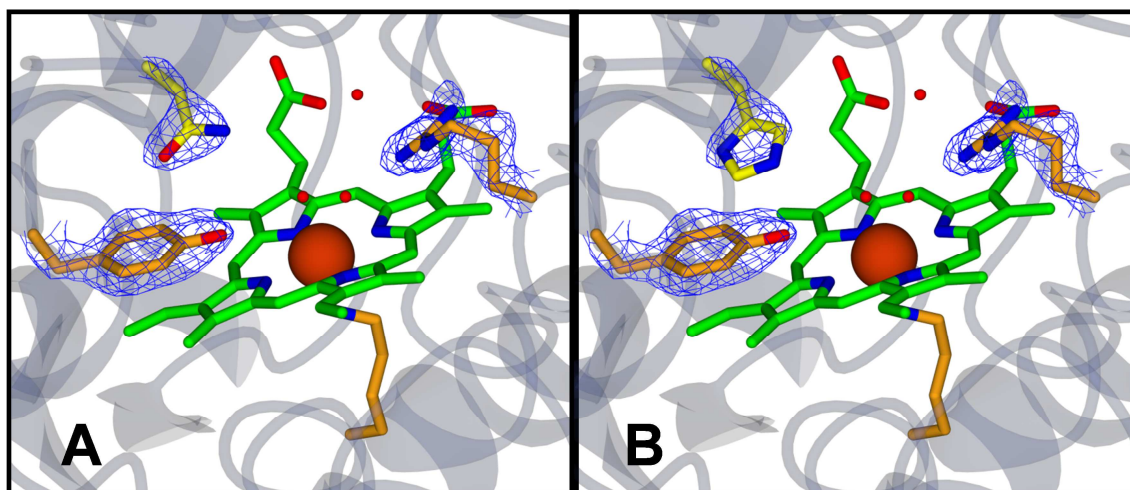


Figure 3.2 – Simulated annealing omit electron density map of H264N NrfA clipped around the residues that form the NrfA catalytic triad (blue mesh) (σ 1.2). (A) The Omit map overlaid with the protein model in which the residue in position 264 is occupied by an asparagine residue. (B) The Omit map overlaid with a protein model in which a histidine residue occupies position 264. The active site asparagine/histidine residue shown as yellow sticks, residues of R106, K126 and Y216 shown as orange sticks and active site heme shown in green sticks with the iron represented as an orange sphere. The protein is shown in blue ribbon (transparent). Figures generated using ccp4mg.

The crystal structure of H264N NrfA revealed that the asparagine residue adopts a similar position to that of the histidine residue in the native WT NrfA structure (Fig 3.3 A). It is, however, unable to resolve the precise orientation of the asparagine side chain within the

active site. This is because the electron densities of the oxygen and nitrogen atoms forming the carboamide functional group are too similar to distinguish. There are two possible orientations for this group, one with the oxygen facing the neighbouring heme propionate group and the other with the nitrogen facing the propionate group. The most favourable orientation would position the nitrogen atom nearest the heme propionate group as this avoids bringing the negative charges ($-\delta$) of the carboamide oxygen and propionate group together. In this orientation the nitrogen atom of the amide group is able to form weak hydrogen bonds with the propionate oxygen atom which are located 3.2 Å away from the upper limit of hydrogen bond formation. This conformation will further stabilise the asparagine residue, Figure 3.3 B.

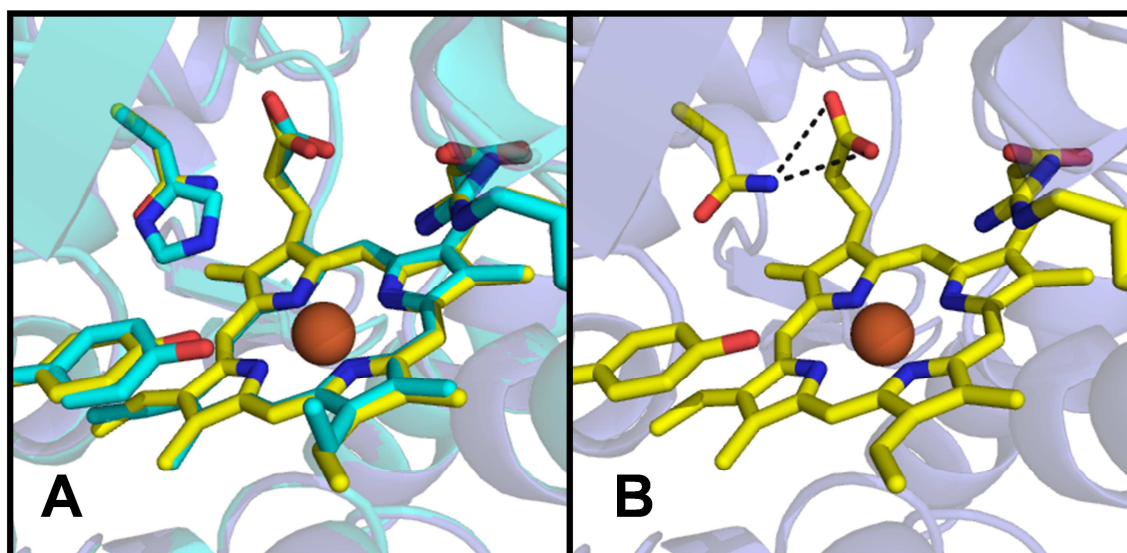


Figure 3.3 – The active site of H264N NrfA. (A) The aligned structures of H264N (yellow) and WT NrfA (PDB: 2RDZ) (cyan) showing the active site cavity. (B) The active site of H264N NrfA with dotted lines representing potential hydrogen bond interactions between the amide nitrogen of the asparagine and a propionate group of the active site heme. Both figures show His/Asn264, Tyrosine 216 and Arginine 106 residues and the active site heme in sticks whilst the iron is represented as a sphere. Figures prepared in Pymol.

The structures of rWT and H264N NrfA were further analysed using MOLPROBITY which generated a Ramachandran plot for each protein [63]. The Ramachandran plot allowed the visualisation of the dihedral angles of the amino acids within each protein, plotting them within favoured, allowed or disallowed regions. For WT NrfA the Ramachandran plot for all residues excluding proline and glycine are shown in Figure 3.4. The plot revealed that 96% of the residues fell into the favoured regions of the plot, 99.6% fell in favoured or allowed regions and 0.4% were outliers and fell into the disallowed region. The outliers were

attributable to the His264 residue, which has been reported previously to be located within the disallowed region or just within a generously allowed region [46].

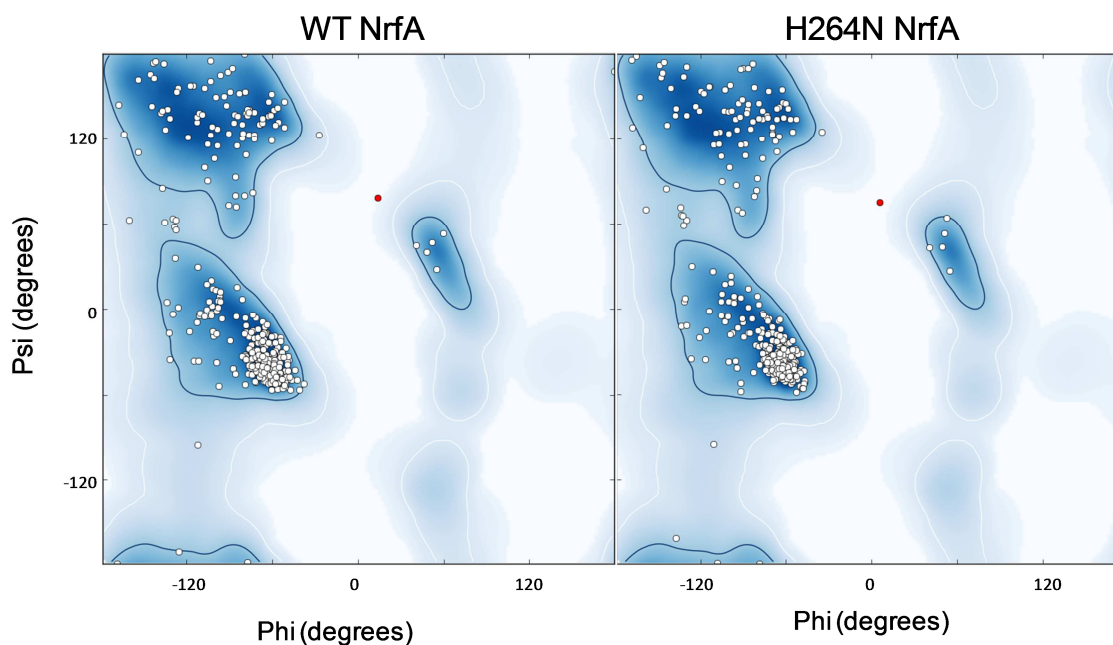


Figure 3.4 - Ramachandran plot generated from the refined structures of rWT and H264N NrfA (as labelled). The dark blue shading within the dark blue borderline represents the region that corresponds to favoured dihedral angles, the lighter blue within the white borderline denotes allowed regions and the white regions represent disallowed regions. Individual residues are represented by white circles within favoured or allowed regions or as red circles in disallowed regions. The residues within the disallowed regions are His264 within WT NrfA and Asn264 within H264N NrfA. Plot generated using MOLPROBITY [63].

The Ramachandran plot for H264N NrfA showed similar a distribution of dihedral angles as for rWT NrfA, with 97% falling within the favoured regions, 99.6% falling within favoured or allowed regions, and 0.4% outliers. The outlier was the asparagine 264 residue which appears on the plot in the same position as the native histidine residues. This shows that the backbone of the two residues share almost identical dihedral angles. This observation would suggest that the orientation of the His/Asn 264 residue is not determined by the residue itself but by the constraints placed upon it by the protein backbone. The protein backbone around residue 264 is affected by neighbouring residues most, notably glutamine 263. This residue forms a monodentate ligation to the active site calcium ion and is believed to be important in maintaining the active site architecture [11, 34].

3.2.3 Spectroscopic characterisation of rWT and H264N NrfA

UV-visible absorption spectroscopy was used to gain insight into the properties of the hemes within solutions of H264N NrfA protein. Spectra of the oxidised and dithionite reduced states of H264N NrfA are presented in Figure 3.5 together with those of rWT NrfA. The oxidised forms of both proteins display intense absorbance in the Soret region, with a maximum at 409 nm. The Soret absorbance, with the broad alpha-/beta- bands between 500 and 560 nm, is typical of low-spin ferric hemes. H264N NrfA shows a very weak absorbance maximum at 650 nm which can be seen as a shoulder on the much stronger alpha-/beta- bands. This relates to the spectral region where ligand to metal charge transfer (LMCT) bands from high-spin ferric c-type hemes are observed [67]. Studies on single heme systems including catalase-peroxidase from *Mycobacterium tuberculosis* [67] and chlorite dismutase from *Dechloromonas aromatica* [68] have been able to identify possible heme ligation based upon the 620-650 nm region of the visible absorbance spectra. If the charge transfer band that lies in this region is towards wavelengths ca 640 nm or below, it suggests that the heme is high-spin hexa-coordinated. If the band is slightly blue shifted and above 640 nm, it demonstrates a heme is predominantly penta-coordinated. The charge transfer band observed in NrfA arises from the interaction of the lysine ligand with the heme iron and is influenced by the presence and the nature of the sixth heme ligand.

There is no clear LMCT band in the 600-660 nm region for the rWT enzyme. However it has been reported previously in highly concentrated samples of *E. coli* and *D. vulgaris* NrfA to be located at 630 nm [28, 69]. Absorbance in this region would suggest a hexa-coordinated heme with either a hydroxide ion or water molecule bound [28]. The presence of a water or hydroxide ligand to WT NrfA has been confirmed by MCD spectroscopy, with the position of the LMCT band for H264N NrfA at 655 nm. This observation is supported by the crystal structure of the protein, which indicated electron density in the sixth ligand position. This is in agreement with a partially bound water molecule [32]. The change in heme ligation implicates the His264 residue in the stabilisation of the hydroxide ion or water molecule bound to the oxidised active site heme in rWT NrfA.

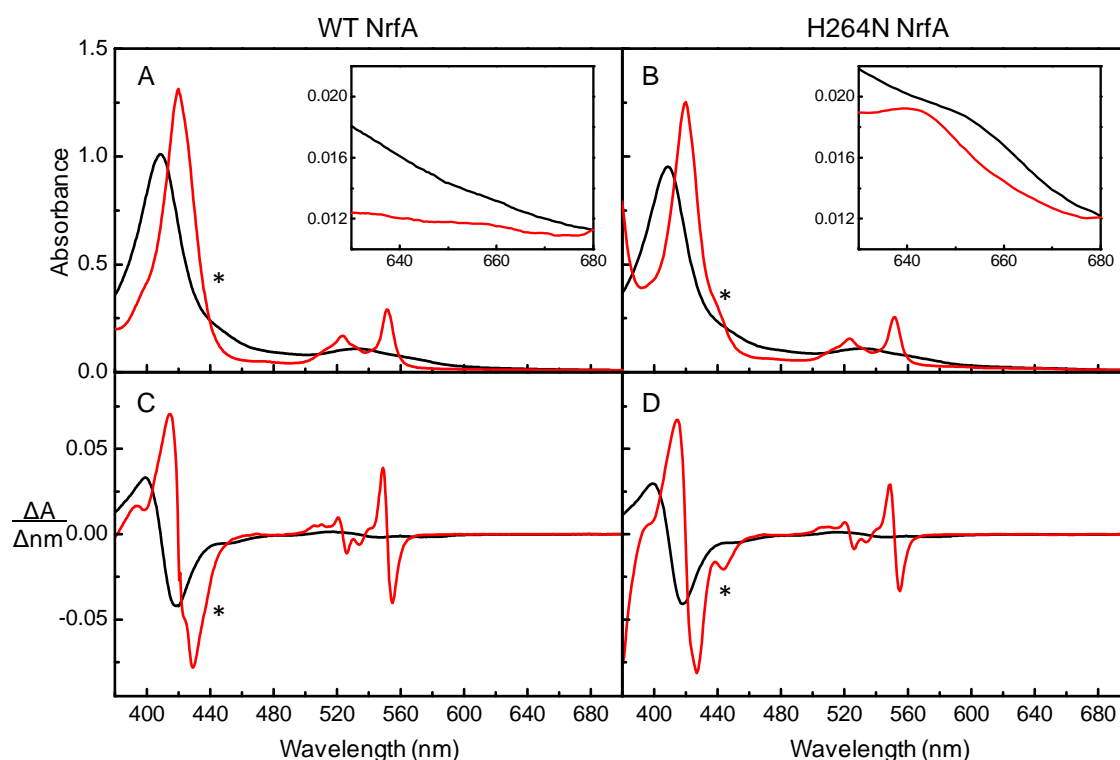


Figure 3.5 - Electronic absorbance spectra of air-oxidised and dithionite reduced rWT and H264N NrfA solutions. Panels A and B depict rWT (3.5 μM) and H264N (2.7 μM) NrfA respectively with the spectra of the oxidised (black) and reduced (red) protein shown. The spectra have been normalised to the absorbance at 409 nm for the oxidised state of both proteins. Inset depicts the 580-700 nm region in greater detail. Panels C and D show the first derivative of the data presented in panels A and B. * Denotes the features associated with high-spin ferrous heme. Buffer 2 mM CaCl_2 , 50 mM HEPES, pH 7, 4 $^\circ\text{C}$.

The dithionite reduced forms of both proteins display spectral features typical of low-spin ferrous hemes, with the Soret maximum of 420 nm and sharp features at 523 and 552 nm. A ferrous high-spin heme typically has an absorbance between 430-440 nm [70]. In NrfA this absorbance normally manifests itself as a shoulder on the side of the Soret peak at 440 nm [32]. This spectral feature is not observed for rWT, whereas the spectrum of the reduced H264N protein has a subtle shoulder on the Soret Peak. This feature becomes more apparent in the first derivative ($\Delta A/\Delta \text{nm}$) of the spectrum of the reduced protein, Figure 3.5 D. The ferrous H264N protein has an absorbance at 640 nm. This is not related to reduced high-spin heme, which should not absorb in this region. The cause of the absorbance is unknown but may be a result of dithionite breakdown, giving rise to absorption in this region.

Taken together the spectra indicate that the H264N hemes, like those of WT NrfA, are fully reduced by dithionite. In light of the structure of H264N NrfA it is most likely that the four bis-histidine coordinated hemes give rise to the spectral features from the low spin Fe^{(III)/(II)} hemes. It is also likely that the active site heme is high spin in the ferric and ferrous states. Although the spin state of the heme irons in H264N NrfA are the same as WT NrfA in both the oxidised and reduced states, there are some slight differences in the spectra of the reduced and oxidised proteins. The most notable is the appearance of a potential heme LMCT band at 650 nm in the oxidised spectra. The prominent 440 nm shoulder in the reduced protein would indicate that there has been a change in the high-spin active site heme environment introduced by the substitution of the His264, as these are not observed in the rWT protein.

3.2.4 Spectroelectrochemistry of rWT and H264N NrfA

Both rWT and H264N NrfA proteins were absorbed onto optically transparent SnO₂ electrodes in order to define the reduction potentials of these proteins by spectroelectrochemistry, as has been reported previously for WT NrfA [48]. The optically transparent electrodes enable the electronic absorbance spectra of the protein to be recorded while it is equilibrated at potentials between +240 and -600 mV. The spectra recorded at both extremes of this potential window for rWT and H264N NrfA are displayed in Figure 3.6 (panels A and B). Comparison of the spectra recorded in this manner with those attained in solution spectroscopy reveal that the Soret peak maxima for the fully oxidised and fully reduced proteins are the same across both methods. Absorbance values of 409 and 420 nm were obtained for both the WT and H264N proteins. The ferric high-spin heme signal observed at 650 nm for H264N NrfA in solution spectroscopy (Fig 3.5 inset) is not seen in the spectrum of oxidised H264N NrfA absorbed onto the SnO₂ electrode. This is due to a much lower concentration of NrfA on the electrode compared to the solution spectroscopy. Therefore, the low-intensity signal of the charge transfer band cannot be resolved over the noise that is present in experiments using SnO₂ electrodes.

Despite the inability to determine the presence of a high-spin heme in the oxidised proteins, both reduced rWT and H264N NrfA display a shoulder on the Soret band at 440 nm. This confirms the presence of a reduced high-spin heme. This can be clearly seen in the first derivative ($\Delta A/\Delta \text{nm}$) of the spectrum of the reduced protein, which displays a peak at 445 nm for both proteins, Figure 3.6 C and D. The ferrous high spin heme feature is more evident in the WT protein absorbed onto the SnO₂ electrode than in the solution spectroscopy, while the feature was clearly observed under both conditions for H264N

NrfA. The variation in the intensity for the high-spin heme feature within the reduced WT spectra would suggest that in solution the Soret band is either shifted to lower wavelengths to be masked by the Soret band of the low-spin hemes or that the high-spin ferric heme is converted to a low-spin ferrous heme. One explanation of the latter option is if the weak high-spin heme band is a result of the presence of sulphite, an oxidation product of dithionite, interacting with the active site heme [18]. Sulphite has been shown to be reduced by NrfA, although at a slower rate than nitrite. The interaction of sulphite with the active site heme has also been confirmed by a crystal structure of sulphite bound to the heme iron in NrfA from *W. succinogenes* [45]. If different affinities for sulphite explain the spectral differences between the rWT and H265N NrfA, this would indicate that the H264 residue contributes to sulphite binding to the active site heme. The interaction of sulphite with the active site of WT and variants of NrfA has not been a focus of this work but this observation suggests defining the physiological relevance of the sulphite reduction by NrfA would provide an interesting area of study.

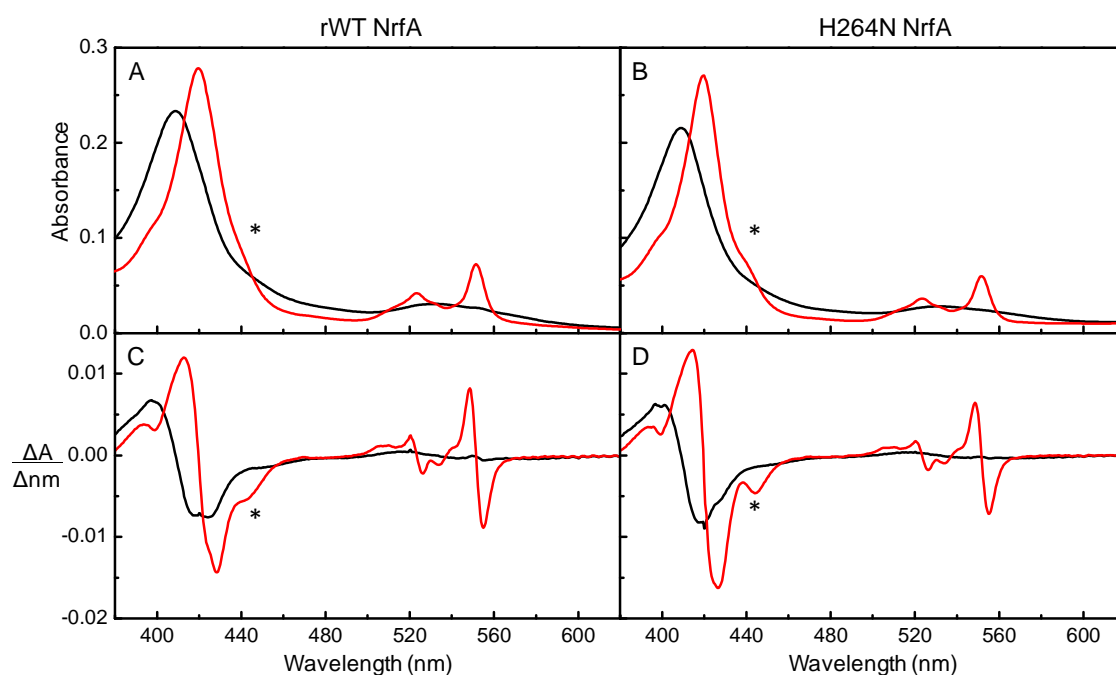


Figure 3.6 - Visible absorbance spectra of rWT and H264N NrfA absorbed onto mesoporous SnO₂ electrodes. Electronic absorbance spectra of fully oxidised poised at +240 mV (black) and fully reduced poised at -600 mV for rWT (A) and H264N (B) NrfA. First derivative of spectra presented in panels A and B, Black line fully oxidised and red line fully reduced protein for rWT (C) and H264N (D) NrfA. * Denotes the features associated with high-spin ferrous heme. Buffer-electrolyte 2 mM CaCl₂, 50 mM HEPES, pH 7, 4 °C.

Spectra recorded for adsorbed rWT and H264N NrfA that have been poised at randomly selected potentials are presented in Figure 3.7 A and B. The absorbance features in the Soret region and the alpha/beta regions for both proteins clearly display the transition from an oxidised to a reduced *c*-type heme containing protein, as the equilibration potential is varied from +90 to -390 mV. The redox transitions of the high- and low-spin hemes are more clearly resolved in the redox difference spectra (reduced – oxidised) generated for closely spaced equilibration potentials shown in Figure 3.7 panels C and D. Such spectra show positive features at 420 and 552 nm characteristic of reduction potentials for low spin hemes from +90 to -390 mV. A split Soret feature is seen at the lowest potentials. Between 430 and 460 nm a broad positive feature with a maximum at 438 nm is detected for both proteins between +90 and -150 mV. This corresponds to the redox transformation of the high-spin ferric heme, which must have a similar reduction potential in both proteins.

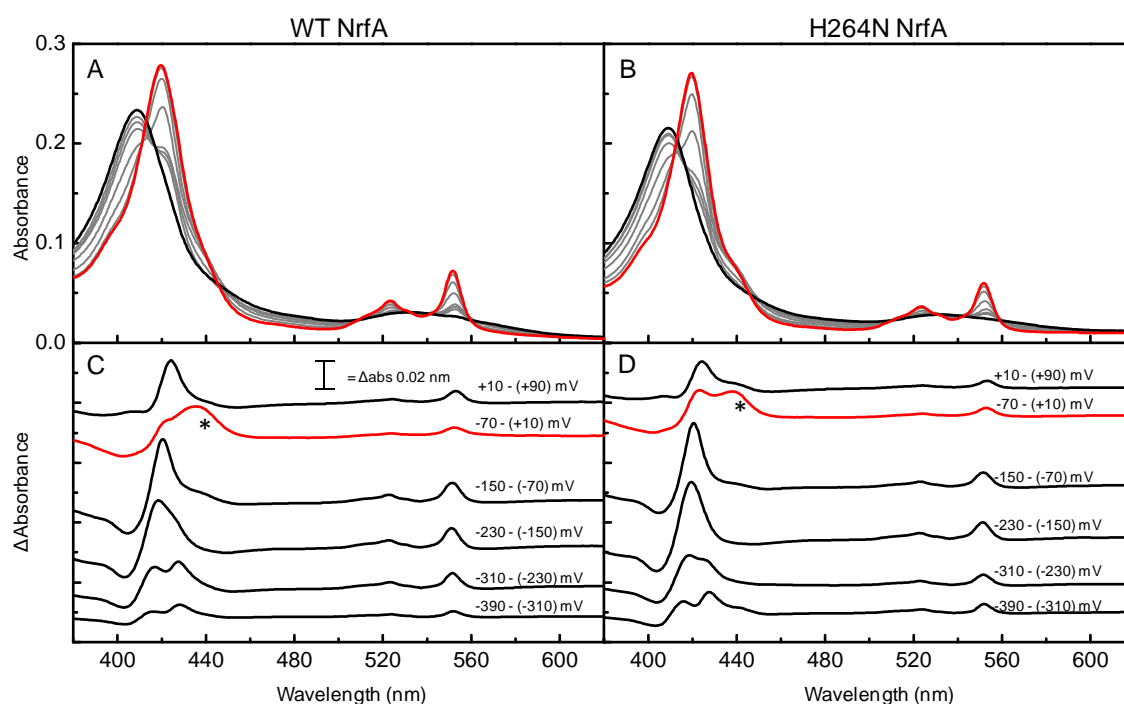


Figure 3.7 - Redox titration of rWT and H264N NrfA immobilised on optically transparent tin oxide electrodes. Electronic absorbance spectra of WT (A) and H264N (B) NrfA, fully oxidised poised at +90 mV (black), fully reduced poised at -390 mV (red) and intermediate potentials (grey). Spectra were recorded at non sequential potentials. Difference spectra (poised reduced – poised oxidised) of WT (C) and H264N (D) NrfA for the potentials stated. * Denotes the features associated with high-spin ferrous heme. Buffer-electrolyte 2 mM CaCl₂, 50 mM HEPES, pH 7, 4 °C

Mid-point potentials for the low- and high-spin hemes were resolved from the potential dependence of the absorbance intensity at selected wavelengths, Figure. 3.8. Low-spin hemes were analysed through the change in absorbance at 552 – 582 nm as high-spin hemes do not contribute to spectral features in this region. For both proteins the data was well described as the sum of four independent one-electron processes that contribute equally to the total change in absorbance (25%). This analysis yielded mid-point potentials of +15, -135, -200 and -320 mV (all ± 15 mV) for the low spin hemes in rWT NrfA at pH 7. The values determined for rWT are not significantly different to those previously reported by Marritt et al for native WT NrfA, which determined the mid-point potentials of the low spin hemes using the same spectroelectrochemical method, to be +22, -117, -189 and -275 mV (all ± 15 mV) [48]. The heme mid-point potentials are in agreement, except the lowest potential heme which appears to be shifted to more negative potentials in the rWT. The cause of this shift of ~ 40 mV is unknown as both experiments were conducted under similar conditions, with 50 mM HEPES at pH 7 used as the buffer-electrolyte. The mid-point potentials for the low-spin hemes of H264N NrfA were determined as +30, -120, -190 and -270 mV (all ± 15 mV). These values are in agreement with the published values of native NrfA.

The absorbance at 442 nm (Soret band shoulder) has contributions from both high- and low-spin hemes. To enable the absorbance resulting from the high-spin heme to be more clearly identified over the background reduction of the low-spin hemes the absorbance at 452 nm was subtracted from that of 442 nm, Figure 3.8 B. The data for both proteins fitted to a single one-electron reduction process, with a midpoint potential of -40 mV and -15 mV (± 15 mV) for rWT and H264N respectively. The value for the active site heme of rWT is in agreement with the value determined by Marritt et al of -56 mV (± 15 mV) [48]. However, the midpoint potential of the active site heme of H264N NrfA has shifted to a more positive potential by ~ 35 mV, indicating that the active site mutation has impacted on the redox properties of the nearby heme.

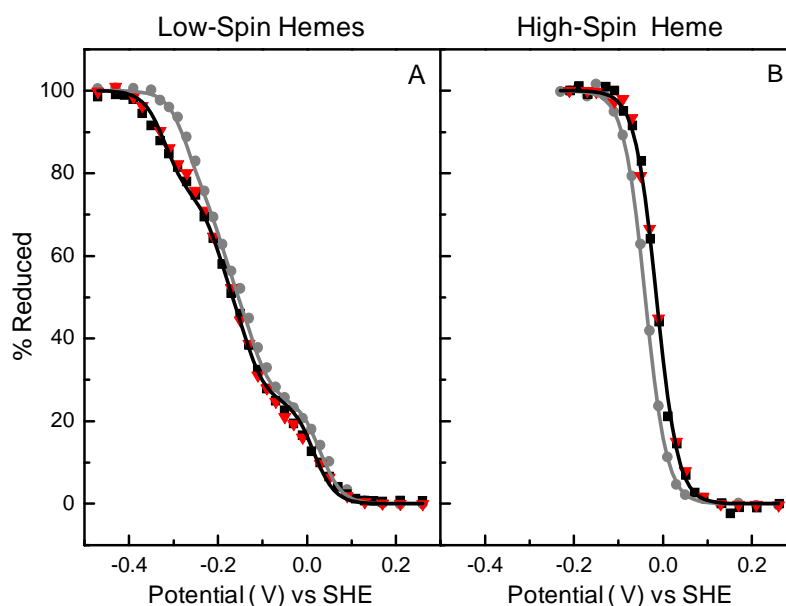


Figure 3.8 - Nernst plots for rWT (●) and of H264N NrfA (■, ▼ two independent experiments) prepared from data in Figure 3.7. (A) The extent of reduction of the low spin hemes as reported by the $A_{552} - A_{582}$, where lines show the sum of four independent one electron ($n = 1$) Nernstian responses for redox centres with midpoint potential (E_m) values of +30, -120, -190 and -270 mV (all ± 15 mV) for WT (grey) and +15, -135, -200 and -320 mV (all ± 15 mV) for H264N (black) with each redox centre contributing 25% of the total reduction. (B) Extent of reduction of high spin heme as reported by the $A_{442} - A_{452}$, where lines represent a single one electron ($n=1$) Nernstian response for centres with E_m values of -40 mV (± 15 mV) for WT (grey) and -15 mV (± 15 mV) for H264N (black). Buffer-electrolyte 2 mM CaCl_2 , 50 mM HEPES, pH 7, 4 °C

3.2.5 Spectrophotometric assays of nitrite and hydroxylamine reduction by rWT and H264N NrfA

A spectrophotometric assay was used to measure the catalytic activity of the NrfA proteins in solution. The reduction of nitrite and hydroxylamine by rWT and H264N NrfA was monitored by following the oxidation of reduced methyl viologen. Reduced methyl viologen has a blue colour and a strong absorbance at 600 nm which is described by an extinction coefficient of $13,700 \text{ M}^{-1} \text{ cm}^{-1}$, whereas oxidised methyl viologen is colourless [46]. The assay was performed at 21 °C in 2 mM CaCl_2 , 50 mM HEPES buffer at pH 7, with sodium dithionite used as the reductant. Catalytic reduction of the substrate results in the bleaching of the methyl viologen solution. The rate of bleaching, and therefore the rate of methyl viologen oxidation as measured by the decrease in absorbance at 600 nm, is directly proportional to the rate of substrate reduction.

The spectroscopic assays revealed that rWT NrfA was able to reduce both nitrite and hydroxylamine. The initial rates of substrate reduction by rWT NrfA plotted against the substrate concentration generated plots that were well described by the Michaelis-Menten equation, Figure 3.9. The kinetic parameters of K_M and k_{cat} were determined from these plots by non-linear regression using ORIGIN software. The comparison of values obtained for rWT NrfA and literature values for native WT NrfA are shown in Table 3.1. They reveal that the K_M and k_{cat} values for the reduction of nitrite are higher in the rWT protein, although not by a degree that would indicate substantial difference between the two proteins. The values determined for hydroxylamine reduction indicate that the rWT and native WT NrfA have the same K_M of 30,000 μM but the k_{cat} is higher suggesting a slightly more active protein.

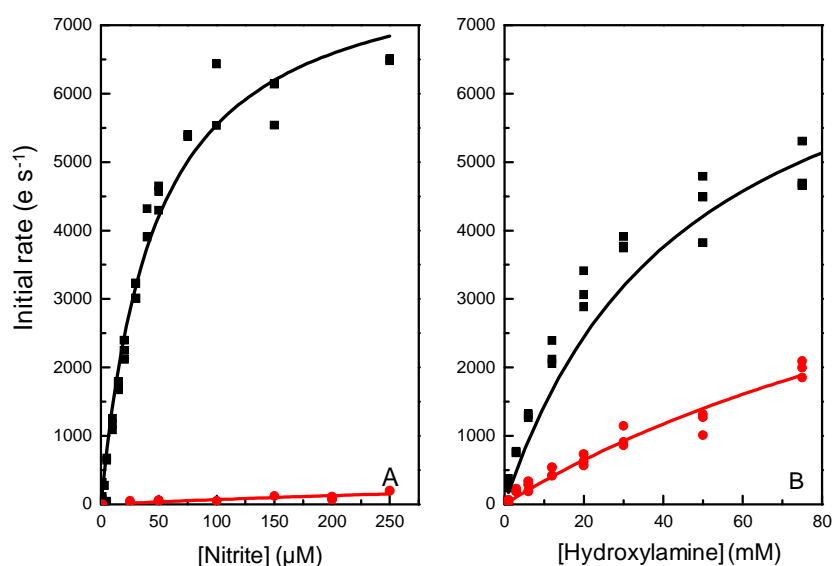


Figure 3.9 - Kinetics of nitrite and hydroxylamine reduction by WT and H264N NrfA as determined by colorimetric solution assay. (A) Initial rate of nitrite reduction plotted against nitrite concentration for WT NrfA. Line shows the fit to the Michaelis-Menten equation, fitted using non-linear regression yielding a K_M of $46 \pm 5 \mu\text{M}$ and a k_{cat} of $1352 \pm 50 \text{ e s}^{-1}$. (B) Initial rates of hydroxylamine reduction plotted against hydroxylamine concentration for WT (black) and H264N (red). Lines show the fit of the data to the Michaelis-Menten equation, giving K_M values of $30 \pm 7 \text{ mM}$ and $170 \pm 60 \text{ mM}$ and k_{cat} values of $3163 \pm 123 \text{ e s}^{-1}$ and $3089 \pm 927 \text{ e s}^{-1}$ for WT and H264N respectively. Buffer 2 mM CaCl_2 , 50 mM HEPES, pH 7, 20 °C.

The modest differences in the determined kinetics for rWT and the values for native WT NrfA are unlikely to reflect variations in the proteins. Instead they are likely to be a result of slightly different methodologies in carrying out solution assay, and varying amounts of fully functional NrfA present within the experiment. The use of dithionite reduced mediators within the assays also means that the NrfA protein is susceptible to sulphite inhibition which

will not affect the observed k_{cat} but will impact on the K_{M} value. This could be another variable that contributes the observed differences.

Solution assays of H264N NrfA conducted in the presence of nitrite up to a concentration of 1.5 mM revealed no detectable rate that would indicate enzyme-catalysed reduction of nitrite. This observation provides the first evidence that the H264N NrfA is no longer a nitrite reductase, indicating that the presence of His264 in the active site of NrfA is vital for the reduction of nitrite.

Despite not being able to reduce nitrite, H264N NrfA was able to reduce hydroxylamine. The kinetic parameters describing the reduction of hydroxylamine were determined using the same method used to calculate those values of rWT NrfA, Figure 3.9. The determined k_{cat} value was not significantly different from that obtained for the WT enzyme, indicating that both enzymes are able to reduce hydroxylamine at similar rates when substrate is non-limiting. The obtained K_{M} value was over five times that observed for rWT NrfA. This would indicate that although the substitution of the active site histidine for an asparagine does not impact on the rate of hydroxylamine reduction when substrate is unlimited, it does have an impact on the binding of hydroxylamine as a substrate. There is an increase in the error observed for values for the kinetic constants of H264N NrfA, due to the concentration of hydroxylamine used within the assay. The highest concentration of hydroxylamine assayed was 75 mM, a concentration that was less than half the predicted K_{M} value of H264N NrfA. This caused the fit to the data to be less accurate. Higher concentrations of hydroxylamine were assayed but contributed to an increase in non-enzymatic reduction of the methyl viologen. Therefore the hydroxylamine concentration was kept to 75 mM or below to minimise the impact of the non-enzymatic reduction.

NrfA variant	Nitrite			Hydroxylamine			Method	Reference
	k_{cat} (NO_2^- s^{-1})	K_M (μM)	k_{cat}/K_M (s^{-1} μM^{-1})	k_{cat} (H_2NOH s^{-1})	K_M (μM)	k_{cat}/K_M (s^{-1} μM^{-1})		
Native WT	770	25 ± 2	30.8	2,382	$30,000 \pm 4,000$	0.08	MV assay	Bamford et al
	-	28 ± 3	-	-	$127,000 \pm 25,000$	-	PFE	Angove et al
rWT	$1,352 \pm 51$	46 ± 5	29.4	$3,163 \pm 123$	$30,000 \pm 7,000$	0.105	MV assay	This work
	-	37 ± 5	-	-	$128,000 \pm 6,000$	-	PFE	
H264N	None detected			$3,089 \pm 927$	$170,000 \pm 60,000$	0.018	MV assay	This work
	None detected			-	$130,000 \pm 6,000$	-	PFE	
R106K	$1,089 \pm 70$	269 ± 33	4.1	$4,239 \pm 202$	$39,000 \pm 4,000$	0.108	MV assay	This work
	-	195 ± 8	-	Not assayed			PFE	
Y216F	457 ± 30	4.1 ± 1.1	111.5*	Not assayed			MV assay	This work
	-	4 ± 0.04	-	-	$1,500 \pm 100$	-	PFE	
K126H	75 ± 11	788 ± 221	0.095	286 ± 22	$60,000 \pm 11,000$	0.005	MV assay	This work
	-	$17,200 \pm 4,400$	-	Not assayed			PFE	

Table 3.1 - The k_{cat} and K_M values for the reduction of nitrite and hydroxylamine by native WT, rWT, and active site variants of NrfA. Values were determined by solution assays with dithionite reduced and PFE experiments. * Y216F displays substrate inhibition, which is not taken into account when calculating the enzyme specificity constant.

3.2.6 A comparison of the electrocatalytic properties of rWT and H264N NrfA adsorbed on PGE electrodes

3.2.6.1 Assessing the activity towards nitrite and hydroxylamine

A complementary perspective of the catalytic properties of the rWT and H264N NrfA was gained by PFE. In these experiments the enzyme was adsorbed onto a PGE electrode which was rapidly rotated during measurement of cyclic voltammetry and chronoamperometry. This minimised limitations to the catalytic current from substrate mass

transport to the enzyme film. As for redox titrations performed using SnO₂ electrodes, the use of graphite electrodes also avoids the need to use chemical reductants such as dithionite which produces sulphite as a breakdown product. This has been shown to be an inhibitor of nitrite reduction by NrfA [18]. However SnO₂ electrodes are less suited for catalytic studies as the mesoporous structure of the SnO₂ electrodes can cause substrate limitation. This is because the substrate has to diffuse through the structure to reach all the absorbed protein. The use of rotating graphite electrodes reduces the impact of substrate limitation, while still allowing the activity of the enzyme to be monitored across the broad potential domain. This is readily illustrated by PFE of both rWT and H264N NrfA absorbed on PGE electrodes, Figure 3.10.

The absorbed rWT enzyme in the presence of 1.1 mM NaNO₂, displays a catalytic response in contrast to the featureless voltammogram of the enzyme film in the absence of nitrite, Figure 3.10 A. The addition of 1.1 mM nitrite generates a catalytic current, with the onset of catalysis at -100 mV. The shape of the catalytic wave shows that there is a boost in catalysis observed at potentials below -300 mV. This feature has been reported previously for WT NrfA in the presence of such concentrations of nitrite [56]. Addition of 20 mM hydroxylamine to the reaction buffer results in a further increase to the catalytic current in accordance with both nitrite and hydroxylamine acting as enzyme substrates, showing that the k_{cat} of nitrite reduction is lower than that of hydroxylamine reduction at the electrode surface.

In contrast to the rWT enzyme, when the experiment is repeated with an electrode that has been exposed to a solution of H264N NrfA there is no catalysis detected after the addition of 1.1 mM nitrite, Figure. 3.10 C. The cyclic voltammetry shows a charging current, due to the migration of ions to and from the electrode as the potential shifts. Addition of hydroxylamine to the 1.1 mM nitrite containing buffer results in the production of a negative catalytic current indicative of hydroxylamine reduction. This confirms a catalytically active protein film was present and that the enzyme is able to reduce hydroxylamine, Figure. 3.10 D. These results agree with those of the solution assays. The H264N NrfA displays hydroxylamine reductase activity but does not support detectable nitrite reductase activity. It was only possible to confirm the presence of the rWT and H264N protein film by observing the reduction of a substrate, as the protein concentration was too low to detect non-turnover peaks. These could have been used to calculate the amount of protein present with the film.

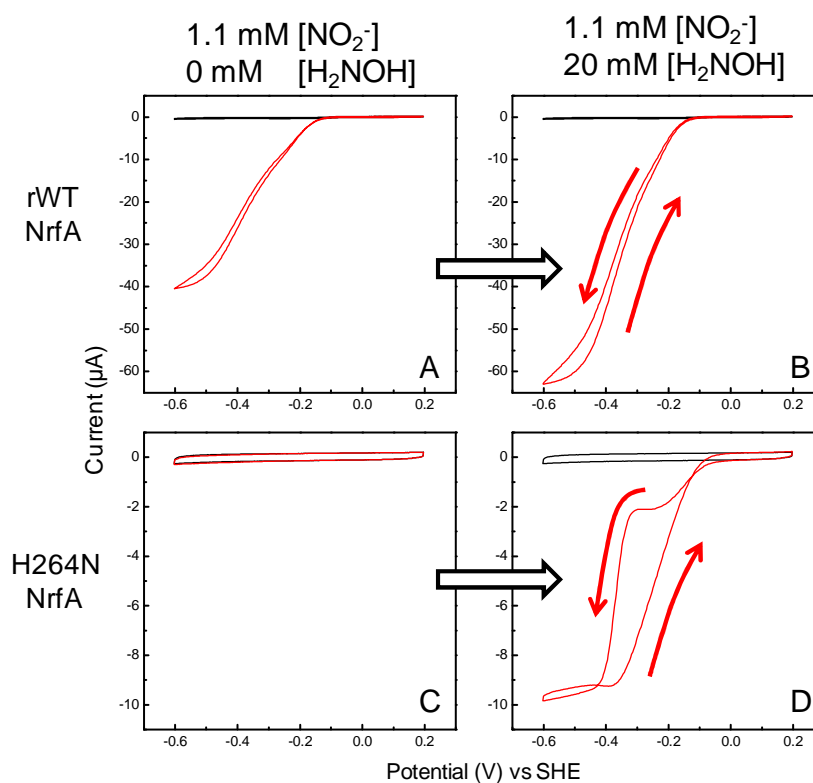


Figure 3.10 - Cyclic voltammetry of a single film of either WT or H264N NrfA, as indicated, as 1.1 mM and 20 mM hydroxylamine are introduced to the experiment. Red lines are the responses of the enzyme films for the additions indicated, and black lines are the response of the enzyme films in the presence of buffer-electrolyte alone. Buffer-electrolyte 2 mM CaCl_2 , 50 mM HEPES, pH 7, 20°C, scan rate 30 mV s^{-1} and rotation rate of 3,000 rpm.

The cyclic voltammogram displayed by the H264N NrfA film in the solution of nitrite and hydroxylamine, had a different shape to that displayed by rWT NrfA in either nitrite or hydroxylamine. For rWT NrfA in nitrite, or nitrite plus hydroxylamine, the catalytic current generated on sweeping to negative potentials almost overlays that of the positive sweep. This observation suggests the rWT catalysis was in a steady state at each potential. For H264N NrfA this is not the case. The H264N enzyme displayed a biphasic current in the negative sweep and a monophasic oxidative sweep, with both the sweeps only overlaying at potentials below -450 mV. Therefore the hydroxylamine reduction by H264N NrfA had not reached a steady state at potentials between -150 and -400 mV.

To confirm WT and H264N NrfA were behaving in a similar manner on the electrode as they were in solution, a Michaelis–Menten kinetics analysis was performed. The second scan at each hydroxylamine concentration was baseline subtracted to remove the

contribution of the charging current and corrected for the first order film loss as described in Chapter 2. The resulting titration for WT and H264N NrfA can be seen in Figure 3.11.

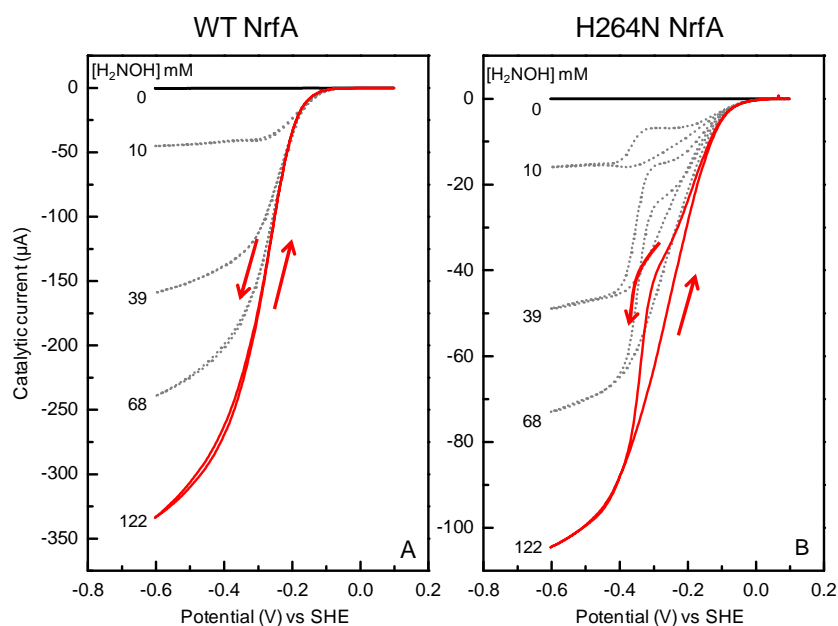


Figure 3.11 - The hydroxylamine reductase activity of WT and H264N NrfA absorbed on a PGE electrode. Voltammograms of WT (A) and H264N (B) NrfA in the presence of increasing concentrations of hydroxylamine, as indicated, have been baseline subtracted and time corrected. Arrows indicate the direction of the scan. Buffer-electrolyte 2 mM CaCl_2 , 50 mM HEPES, pH 7, 20 °C, scan rate 30 mV s^{-1} and rotation rate of 3,000 rpm.

The observed catalytic response of rWT and H264N NrfA are essentially independent of the electrode rotation rate at each hydroxylamine concentration investigated. The catalytic waves were therefore free from any significant limitations due to substrate delivery to the enzyme film, and experiments were routinely performed at a single electrode rotation rate of 3000 rpm. The observed differences in the reductive and oxidative scans in the current potential profiles of H264N were therefore not due to substrate limitation.

The catalytic waves for rWT NrfA are as previously described by Angove et al with the reductive and oxidative sweeps superimposed, with catalysis commencing ca. -100 mV [65]. The reductive and oxidative sweeps for H264N NrfA however do not overlay between -150 and -400 mV for all hydroxylamine concentrations assayed. This indicates that under the conditions of this experiment the reaction has not reached a steady state. To determine the kinetic parameters of K_M and i_{max} the catalytic current generated at -500 mV for each hydroxylamine concentration was plotted against substrate concentration and the data fitted to the Michaelis-Menten equation, Figure 3.12. The potential of -500 mV was chosen

for analysis because the reductive and oxidative scans of H264N overlay indicating that the reaction is under steady state conditions at this potential. The fit to the Michaelis-Menten equation carried out using non-linear regression. The i_{\max} values are not directly comparable as the amount of enzyme present within each experiment is unknown. Therefore the difference in observed current could be due to a higher amount of enzyme being absorbed in the WT experiment than the amount in the H264N NrfA experiment. However the K_M values can be compared. The K_M values determined for the reduction of hydroxylamine by WT NrfA when in solution and absorbed onto the electrode reveal significantly different values, Table 3.1. The variation has been noted previously by Angove et al which determined the K_M to be 127 ± 25 mM using PFV at -550 mV and pH 7, Table 3.1 [65]. The exact cause of the different K_M values for WT NrfA is uncertain but it is likely to be a result of intrinsic properties of the WT protein as the K_M values determined for H264N NrfA using solution assays and PFV techniques are in agreement.

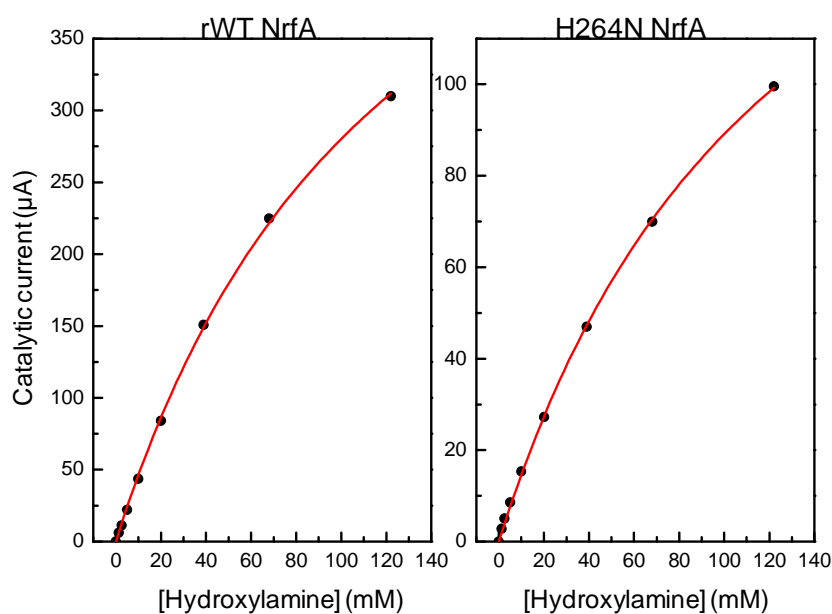


Figure 3.12 - Kinetics of hydroxylamine reduction by rWT and H264N NrfA. Catalytic current as generated at -500 mV, prepared from data presented in Figure 3.11 Red line represents the fit of the Michaelis-Menten to the data, yielding an i_{\max} of 640 ± 20 μA and K_M of 128 ± 6 mM for

3.2.6.2 Assessing the activity towards nitric oxide

Having established that H264N NrfA was unable to reduce nitrite but could still reduce hydroxylamine, a proposed reaction intermediate, left the possibility that nitric oxide, another proposed reaction intermediate, could be reduced. Nitric oxide reductase activity is difficult to determine with the solution spectrophotometric assays used to measure nitrite and hydroxylamine reduction. This is in part because nitric oxide is highly reactive with trace amounts of oxygen. Nitric oxide can also directly interact with the chemical reductants such as dithionite and reduced methyl viologen. For these reasons the nitric oxide reductase activity of rWT and H264N NrfA was characterised using PFE in a nitrogen filled glove box with an oxygen level below 10 ppm. The PFE experiments were performed as before. However the rotation rate was lowered from 3,000 rpm to 100 rpm, to limit the amount of nitric oxide gas lost from the solution while still conferring some control over the mass transport of substrate to the protein film [52].

The cyclic voltammograms presented in Figure 3.13 show rWT and H264N NrfA in 40 ± 4 μM nitric oxide. In the presence of nitric oxide, WT NrfA displays a catalytic wave which is distinct from that observed for nitrite reduction. The main difference is that there is no attenuation feature at potentials below -300 mV characteristic of nitrite reduction at low substrate concentrations. This confirms the catalytic current is due to the enzymatic reduction of nitric oxide, and not contamination caused by trace amounts of nitrite present within the nitric oxide solution.

Cyclic voltammetry of H264N NrfA under the same conditions provided no evidence of a catalytic current even up to 80 ± 8 μM nitric oxide. A small increase in current magnitude was seen below -350 mV. This current arises from the direct reduction of nitric oxide at the electrode surface and confirms the presence of nitric oxide within the buffer-electrolyte solution. Addition of 28 mM hydroxylamine to the buffer-electrolyte produced a clear sigmoidal catalytic reduction wave below -80 mV (data not shown). This confirmed the presence of an active H264N NrfA film. From these observations it was concluded that, like nitrite, nitric oxide is not a substrate for H264N NrfA.

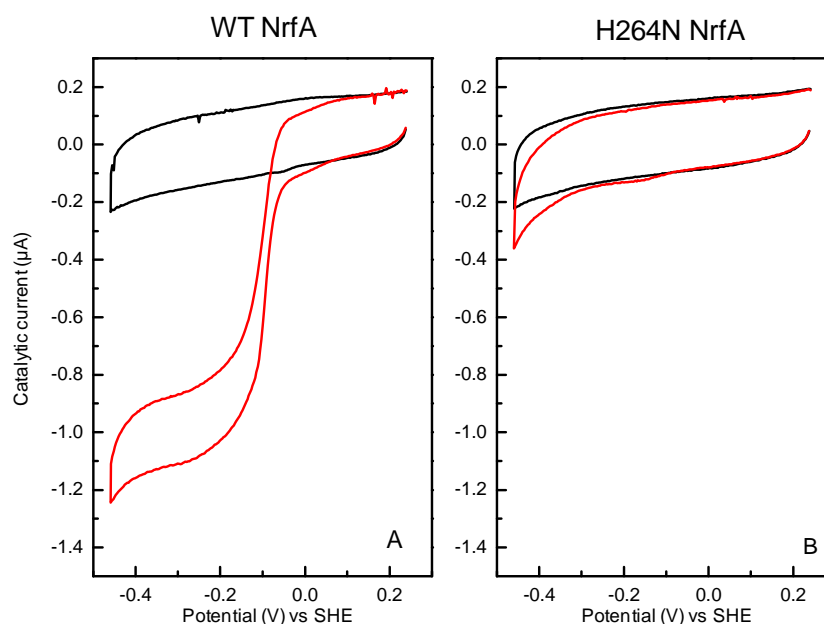


Figure 3.13 - Cyclic voltammetry of rWT (A) and H264N (B) NrfA, in the absence (black line) and presence (red line) of $40 \mu\text{M} \pm 4$ nitric oxide. Buffer-electrolyte 2 mM CaCl_2 , 50 mM HEPES, pH 7, 20°C , scan rate 30 mV s^{-1} and electrode rotation of 100 rpm.

The work presented so far in this chapter has identified that recombinant WT NrfA has the same structural, spectroscopic and catalytic characteristics as has been previously determined for native WT NrfA purified from *E. coli* strain LCB2048. Therefore in the remaining sections of this chapter and subsequent chapters rWT will be referred to as WT NrfA.

3.3 Characteristics of R106K NrfA

3.3.1 Structural aspects of the arginine to lysine substitution

The crystal of R106K NrfA used to determine the crystal structure grew under the same conditions as the other NrfA variants and crystallised in the $P2_1$ space group. The structure was solved using molecular replacement to a final resolution of 2.2 \AA . The R106K protein was essentially identical to the WT protein, with a RMSD value of $0.355 \pm 0.02 \text{ \AA}$ between the α carbons of the protein backbones of the superimposed structures. Each of the four monomers within the asymmetric unit contained two calcium and five covalently attached hemes. Four of the hemes were bis-his ligated, with the histidine ligands adopting the same

confirmation as in the WT structure. The active site heme maintained lysine ligation with the distal ligand modelled as a water molecule, although this could be a hydroxide ion.

The substitution of the active site arginine residue was confirmed by generating residue simulated annealing composite omit electron density maps. The map was clipped to the residues of the catalytic triad and overlaid with a protein model that contained either a lysine or an arginine residue in position 106, Figure 3.14 A and B. The large guanidinium group of the arginine side chain was not accounted for by the electron density, indicating it is unlikely that an arginine residue is present at that location. The lysine residue fitted completely within the observed electron density, verifying that this substitution was successful.

The presence of the lysine residue in the R106K NrfA generates a slightly larger active site cavity. This is because the lysine side chain is shorter, with only a single terminal amine group compared to the bulkier guanidinium group of the arginine side chain. In the WT NrfA structure the guanidinium group interacts with the neighbouring heme propionate group by the formation of hydrogen bonds over distances of $2.88 \pm 0.08 \text{ \AA}$ and $3.62 \pm 0.06 \text{ \AA}$ (average of the four monomers within the asymmetric unit). This interaction acts to arrange the guanidinium group so that a second nitrogen atom is positioned to face towards the active site heme. This nitrogen atom has been shown to hydrogen bond to a nitrite molecule bound in the active site of NrfA from *W. succinogenes* [45].

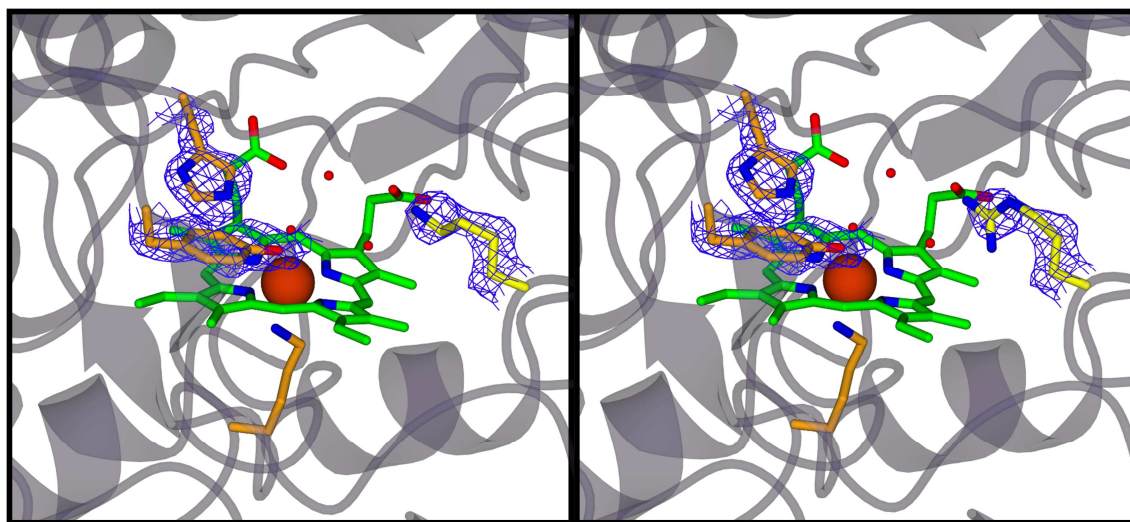


Figure 3.14 –Simulated annealing composite omit electron density map of R106K NrfA clipped around the residues that form the NrfA catalytic triad (blue mesh) (σ 1.2). (A) The Omit map overlaid with the protein model in which the residue in position 106 is occupied by a lysine residue. (B) The Omit map overlaid with a protein model with the native asparagine residue

occupying position 106. The active site lysine/asparagine residue shown as yellow sticks, residues of K126, Y216 and H264 shown as orange sticks and active site heme shown in green sticks with the iron represented as an orange sphere. Figures generated using ccp4mg.

In the R106K NrfA structure, the amine group of the lysine residue also interacts with the heme propionates group with distances of $3.09 \pm 0.22 \text{ \AA}$ and $4.02 \pm 0.33 \text{ \AA}$ from the two oxygen atoms. These form the carboxylate group of one of the active site propionates. The distance between the lysine residue and the propionates is slightly longer than those between the arginine residue and the propionates. There is also greater variance in the distance, indicating that the lysine residue may have greater flexibility within the active site. Although, in this position, the amine group is located slightly away from the active site the flexibility of the lysine residue may allow a second conformation to be adopted where the residue is able to interact with bound substrate. This shift in orientation could be brought about by the binding of the negatively charged nitrite molecule. This would attract the lysine residue which is most likely to be protonated and positively charged.

3.3.2 The nitrite and hydroxylamine reduction characteristics of R106K NrfA

To determine the nitrite and hydroxylamine reductase activity of R106K NrfA spectrophotometric assays were conducted to measure the initial rates of nitrite and hydroxylamine reduction at various substrate concentrations. The initial rates were plotted against substrate concentration and the kinetic constants were determined by fitting the Michaelis-Menten equation to the data, Figure 3.15. The R106K enzyme retained the ability to reduce nitrite at a similar turnover rate. However, the affinity of the enzyme for nitrite was negatively impacted, rendering the R106K NrfA a less efficient nitrite reductase than the WT enzyme. This can be seen by the decrease in the specificity constant ($k_{\text{cat}}/K_{\text{M}}$) from $29.4 \text{ s}^{-1}\mu\text{M}^{-1}$ in WT to $4 \text{ s}^{-1}\mu\text{M}^{-1}$ in the R106K protein. While the mutation had a clear effect on nitrite reduction, the hydroxylamine reductase activity was relatively unaffected. There was no significant change to K_{M} and only a small increase in the observed k_{cat} value, from $3,163 \pm 123 \text{ H}_2\text{NOH s}^{-1}$ in WT NrfA to $4,239 \pm 202 \text{ H}_2\text{NOH s}^{-1}$ in R106K NrfA.

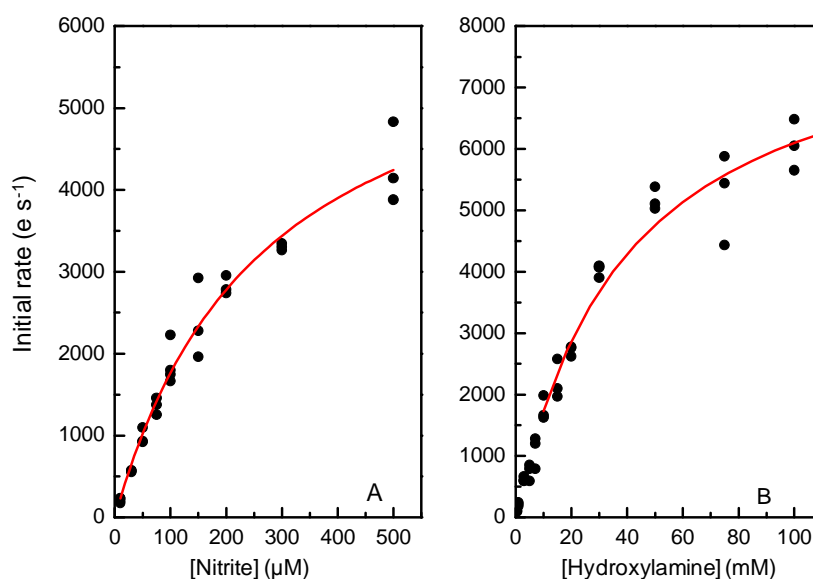


Figure 3.15 - Kinetics of nitrite and hydroxylamine reduction by R106K NrfA as determined by colorimetric solution assay. Initial rates of nitrite (A) and hydroxylamine (B) reduction plotted against substrate concentration. Line shows the fit to the Michaelis-Menten equation, fitted using non-linear regression yielding K_M of $269 \pm 33 \mu\text{M}$ and a k_{cat} of $6,534 \pm 420 \text{ e s}^{-1}$ for nitrite reduction and a K_M of $39,000 \pm 4,000 \mu\text{M}$ and a k_{cat} of $8478 \text{ e s}^{-1} \pm 404$ for hydroxylamine reduction. Buffer 2 mM CaCl_2 , 50 mM HEPES, pH 7, 20 °C.

To further explore the effect the substitution has had on nitrite reduction, PFE was carried out using graphite electrodes on which either WT or R106K NrfA protein was adsorbed. The protein film was then exposed to increasing nitrite concentrations while the potential was continually swept. The resulting voltammograms can be seen in Figure 3.16. The addition of nitrite resulted in an increase in catalytic current, in accordance with an enzyme catalysed reaction. As the amount of protein present within the WT and R106K protein films cannot be determined, it is not possible to compare the i_{max} values of the two protein films. However, the K_M values and wave shapes can be compared. The K_M value for R106K determined by PFE was slightly lower than that calculated in the solution assays, Figure 3.17. The small discrepancy in the value is due to the different method employed and not due to changes in the protein.

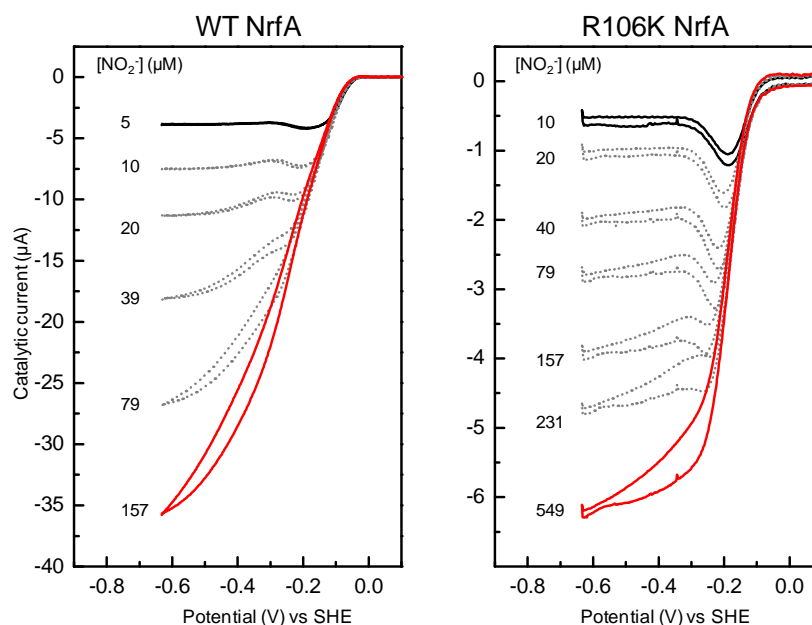


Figure 3.16 - The nitrite reductase activity of WT and R106K NrfA adsorbed on PGE electrodes. Cyclic voltammograms of WT (A) and R106K (B) NrfA in the presence of increasing concentrations of nitrite as indicated. All cyclic voltammograms baseline subtracted and time corrected. Buffer-electrolyte 2 mM CaCl_2 , 50 mM HEPES, pH 7, 20 °C, scan rate 30 mV s^{-1} and rotation rate of 3,000 rpm

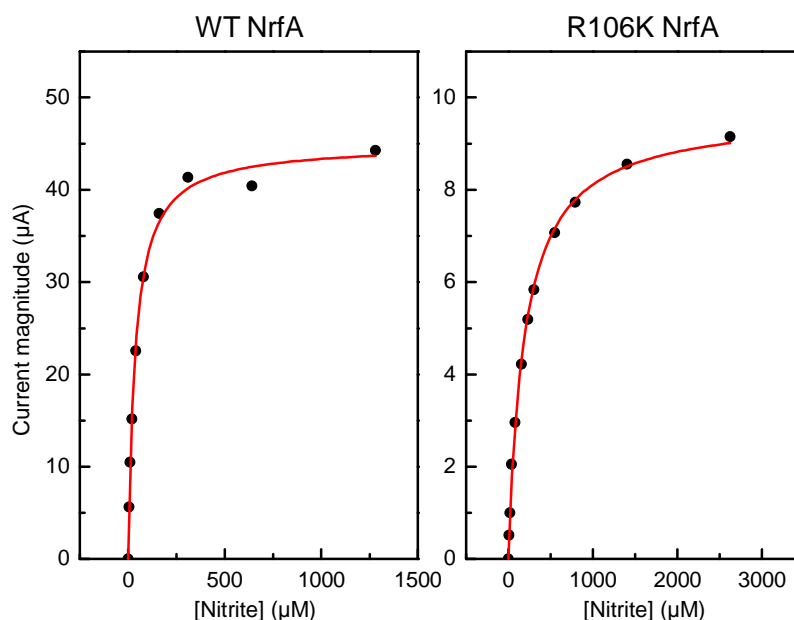


Figure 3.17 - Kinetics of nitrite reduction by WT and R106K NrfA as determined by cyclic voltammetry. Current generated at -500 mV plotted against nitrite concentration, red line shows the Michaelis-Menten equation fitted to data using non-linear regression yielding a K_M of $37 \pm 5 \mu\text{M}$ and an i_{max} of $45 \pm 1.8 \mu\text{A}$ for WT NrfA and a K_M of $195 \pm 8 \mu\text{M}$ and i_{max} of $9.5 \pm 0.4 \mu\text{A}$ for R106K NrfA.

The wave shape of nitrite reduction by WT NrfA at nitrite concentrations below 20 μM showed the catalytic current commencing at a potential around -50 mV and increasing in a sigmoidal fashion as the potential was swept more negative. Attenuation in the catalytic current is observed at -250 mV prior to a plateau in current at -400 mV. As the WT protein is exposed to increasingly higher nitrite concentrations, the attenuation feature is lost and a boost in activity is observed. This behaviour has been previously described for WT NrfA [65]. Cyclic voltammograms of R106K NrfA show the same features as the WT protein with catalysis commencing at \sim -100 mV and the attenuation of the catalytic current at -250 mV. However, the magnitude of the attenuation feature is much pronounced than that observed for WT NrfA, and it persists until higher nitrite concentrations. The cause of the more pronounced attenuation feature is likely to be linked to the lower affinity of the R106K NrfA for nitrite. The higher K_M of R106K compared to WT NrfA means at a defined nitrite concentration, there will be more WT substrate:enzyme complexes than R106K substrate:enzyme complexes. Therefore when the scans are compared of the proteins in nitrite concentrations that reflect the enzyme K_M (scan 39 μM for WT and 231 μM for R106K NrfA) the wave shapes are similar. This would indicate that the attenuation feature is linked to low nitrite conditions with the feature most pronounced when nitrite is present at concentrations below the respective K_M value for that protein.

The observation that nitrite and hydroxylamine reduction is maintained in the R106K enzyme would suggest the Arg106 although important it is not vital for nitrite reduction. The decrease in the k_{cat} value for nitrite reduction is relatively small compared to the five times increase in K_M , suggesting that the arginine residue is more important in substrate recognition and binding than reduction. However, when interpreting the data related to residue substitutions it is important to consider the role that the substituted residue is playing within the protein. The lysine could be able to partially fulfil the role of the native arginine residue, as both are positively charged and of similar length. The crystal structure of R106K revealed that in the absence of nitrite the lysine interacts with the heme propionates group. This will mean that the active site is less favourable to nitrite binding, which could account for the higher K_M . Upon nitrite binding, the introduction of the negative charge could cause the lysine residue to move into a new position in which it stabilises the nitrite molecule, allowing for its activation and reduction. This would agree with the observation that WT and R106K NrfA have the same k_{cat} , as once nitrite is bound to the heme the lysine provides the function of the native arginine residue.

3.4 Characterisation of Y216F NrfA

3.4.1 Crystal structure of Y216F to a resolution of 2.11 Å

The tyrosine to phenylalanine NrfA variant crystallised in a space group of $P12_1$. Molecular replacement generated an initial structural model containing four NrfA monomers within the asymmetric unit. The tyr216 residue present within the initial model was substituted for a phenylalanine. The substitution was confirmed by generating simulated annealing composite omit electron density maps. The omit electron density map was then overlaid with a protein model which contained either a tyrosine or a phenylalanine residue in position 216, Figure 3.18. The electron density agreed with the presence of a phenyl ring. However, it was unable to account for the phenol oxygen of the tyrosine model whereas the phenylalanine residue fitted the density well.

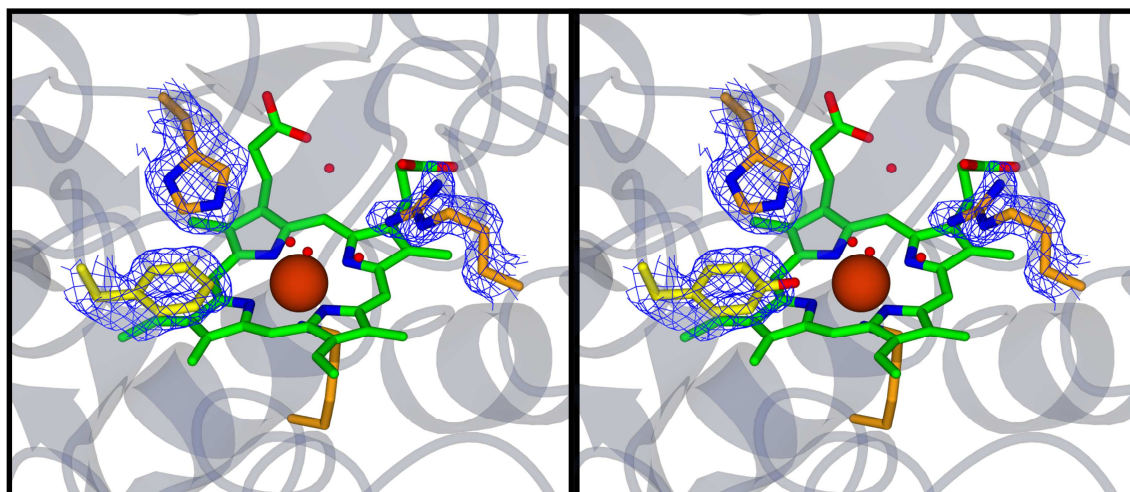


Figure 3.18 –Simulated annealing composite omit electron density map (blue mesh) of Y216F NrfA variant clipped around the residues that form the NrfA catalytic triad (σ 1.2). (A) The Omit map overlaid with the protein model in which residue in position 216 is occupied by a phenylalanine residue (as expected in the NrfA variant). (B) The Omit map overlaid with a protein model with the native tyrosine residue occupying position 216. The active site phenylalanine/tyrosine residue shown as yellow sticks, residues of R106, K126 and H264 shown as orange sticks and active site heme shown in green sticks with the iron represented as an orange sphere. Figures generated using ccp4mg.

The alignment of the α carbons of the protein back bone of each of the four monomers present within the Y216 asymmetric unit with a WT NrfA monomer (2RDZ, monomer D) generated a RMSD value of 0.36 ± 0.01 Å. This indicated that the Y216F and WT NrfA structures are essentially identical. Further inspection of the Y216F structure revealed that

all five covalently attached hemes were inserted with the correct ligands present for each heme iron. There was also electron density present within both calcium binding sites, attributed to the presence of two calcium ions. The calcium ions maintain the same ligation as in WT NrfA with both protein and water ligands forming the coordination spheres. The position of the R106, H264 active site residues were unaffected by the nearby substitution. The modelled phenylalanine residue adopted a similar position to that of the native tyrosine.

The active site heme in Y216F had a water molecule as the sixth ligand. However, this could be a hydroxide ion. There were also notable changes in the positioning of the conserved water molecules within the vicinity of the substitution. The change in position of the conserved water molecules is likely to be due to change in the hydrogen bond network caused by the loss of the tyrosine phenol group. The change in the water network could impact on proton delivery to the active site as well as substrate delivery as the mutation is located alongside the proposed substrate entry channel [49].

3.4.2 A spectroelectrochemical investigation of Y216F NrfA

The redox properties of Y216F NrfA were investigated using the OTTLE technique which has been discussed earlier in this chapter for WT and H264N NrfA. The Y216F protein was adsorbed onto a SnO₂ electrode and then poised at a range of potentials in a random order. At each potential, time was allowed for the protein to equilibrate prior to the recording of a visible absorbance spectrum. The resulting redox titration produced a range of spectra that revealed the redox properties of the hemes within the Y216F protein, Figure 3.19 A. In the fully oxidised state the protein clearly shows an intense absorption band in the Soret region (409 nm) which is contributed to by both oxidised high- and low-spin hemes. A broad absorption band with a maximum of ~530 nm is also observed that only relates to oxidised low-spin hemes. Both of these features have been described previously for WT NrfA [48]. Upon reduction the broad absorbance (~530) band becomes two distinctive peaks with maxima at 522 nm and 552 nm. The Soret band also shifts to longer wavelengths (420 nm) which relate to the reduction of the low-spin hemes. A shoulder also appears on the Soret band which indicates the presence of a reduced high-spin heme. This can be more easily resolved by comparing the first derivative of the electronic absorbance spectra for the fully oxidised and fully reduced protein, Figure 3.19 B.

To further identify the potential range at which the different heme redox transformations occur the adjacent difference spectra (reduced– oxidised) were calculated for 80 mV

windows, Figure 3.19 C. The adjacent difference spectra show that the reduction of the low-spin hemes, which is indicated by peaks at 420 and 552 nm, occurs over a wide reduction window from +90 to -390 mV. At lower wavelengths, the increase in absorbance at 420 nm becomes split with maxima at 416 and 430 nm. This has been documented previously for NrfA. The reduction of the single high-spin heme can be seen over the background reduction of the four low-spin hemes by a positive absorption peak at 442 nm.

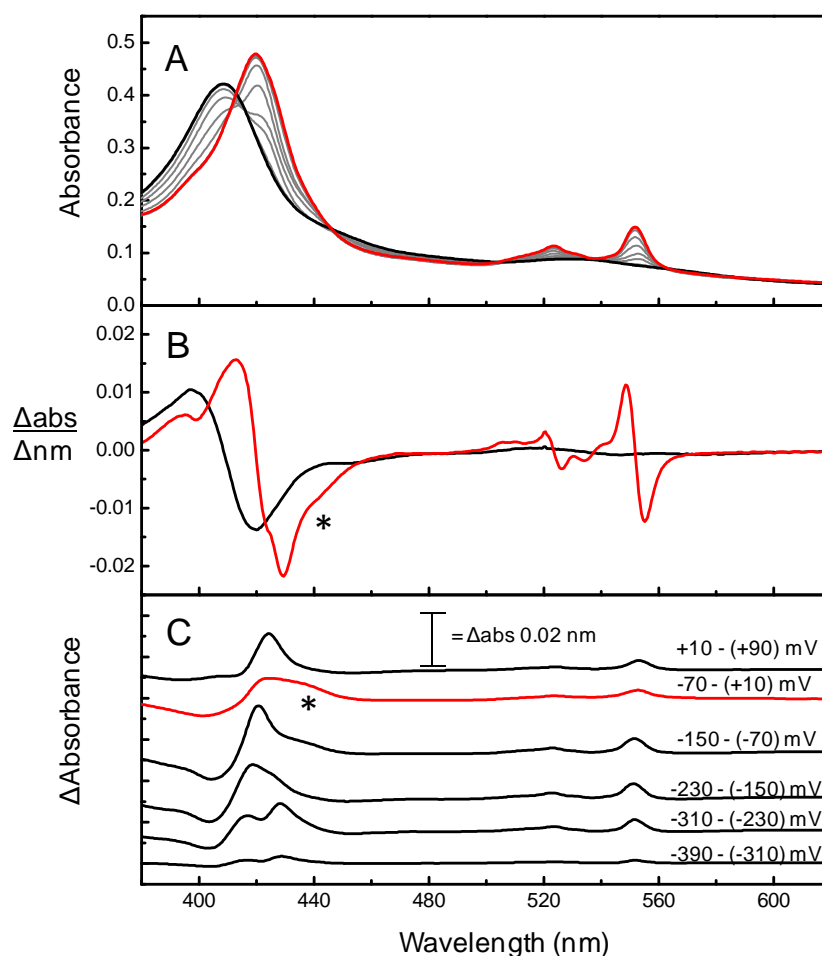


Figure 3.19 - Redox titration of Y216F NrfA adsorbed onto optically transparent SnO_2 electrode. (A) Electronic absorbance spectra of Y216F NrfA, fully oxidised poised at +90 mV (black), fully reduced poised at -390 mV (red) and intermediate potentials (grey). Spectra were recorded at non-sequential potentials. (B) First derivative of Y216F NrfA, fully oxidised (+90 mV) black line and fully reduced (-390 mV) red line. (C) Difference spectra (poised reduced – poised oxidised) NrfA for the potentials stated.* Denotes the features associated with high-spin ferrous heme. Buffer-electrolyte 2 mM CaCl_2 , 50 mM HEPES, pH 7, 4 °C.

The information gained from the redox titration of Y216F NrfA adsorbed onto SnO_2 was used to determine the reduction potentials of the hemes within the protein. The reduction

potentials of the low-spin hemes were calculated by monitoring the absorbance change at 552 nm – 582 nm as a function of applied potential. The resulting data as seen in Figure 3.20 was described by the Nernst equation in which four independent one electron processes contribute equally to the total absorbance change. The values of reduction potentials were manually adjusted to give the best fit to the data and yielded values of +15, -135, -200 and -320 mV (all ± 15 mV). The reduction potentials are in agreement within those obtained for the WT protein, indicating that the substitution in the active site has not impacted on the redox properties of the bis-his coordinated hemes.

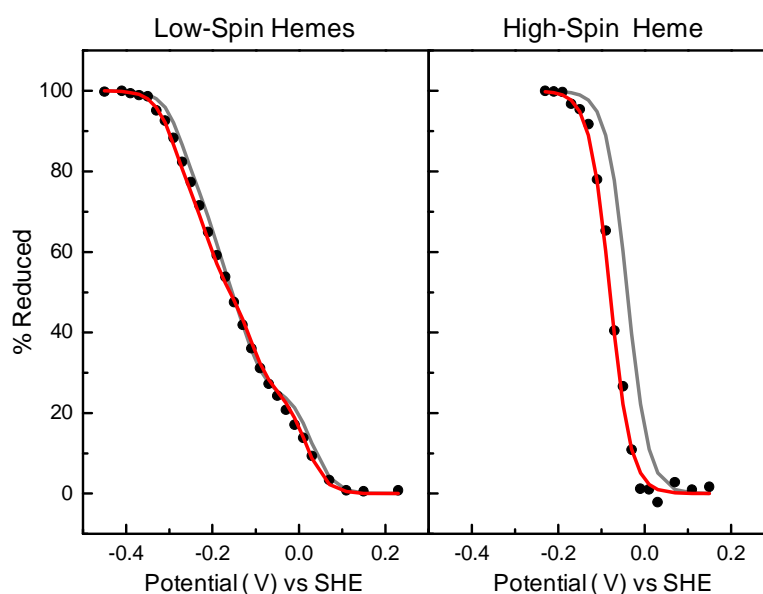


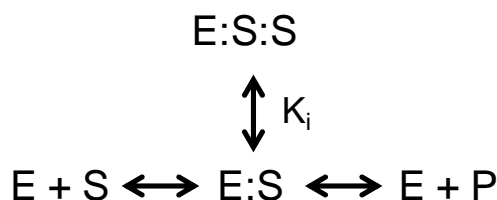
Figure 3.20 - Nernst plots for the heme centres in Y216F NrfA (●). (A) The percentage of reduction of the low spin hemes as reported by the $A_{552} - A_{582}$, where lines show the sum of four independent one electron ($n = 1$) Nernstian responses for redox centres with midpoint potential (E_m) values of +15, -135, -200 and -320 mV (all ± 15 mV) for Y216F NrfA with each redox centre contributing equally to the total reduction. (B) Extent of reduction of high spin heme as reported by the $A_{442} - A_{452}$, where lines represent a single one electron ($n=1$) Nernstian response for centres with E_m values of -80 mV (± 15 mV) for Y216F (red line). Grey line represents the reduction potentials of the high- and low-spin hemes of WT NrfA, as presented in Figure 3.8. Buffer-electrolyte 2 mM CaCl_2 , 50 mM HEPES, pH 7, and 4 °C.

The reduction potential of the single high-spin heme was determined by monitoring the absorbance change at 442 nm, with the absorbance at 452 nm subtracted to account for the low-spin heme background. The change in absorbance 442 - 452 nm as a function of applied potential could be described by the Nernst equation, with a single electron process with a reduction potential of -80 ± 15 mV. The high-spin heme reduction potential of Y216F displays a shift compared to the high-spin heme of the WT protein (-40 mV). The shift of 40

mV is small but does indicate the active site substitution has had an impact on the active site heme, especially as the reduction potential of the bis-his hemes are unchanged. The exact method by which the absence of the phenol group impacts on the heme redox properties is not known. It may be linked to a change in the conserved water arrangement.

3.4.3 Catalytic properties Y216F NrfA

Spectroscopically monitored solution assays of Y216F NrfA identified that the protein had maintained nitrite reductase activity despite the substitution of the active site tyrosine residue for phenylalanine. The plot of initial rate against nitrite concentration varied from those previously observed for WT NrfA, Figure.3.21. Initially the rate of reduction increased as the substrate concentration increased. However, above 500 μM nitrite, further additions resulted in a decrease in catalytic activity. The observed decrease in catalyses reveals that at high concentrations nitrite was inhibiting the reduction process. The classical interpretation of this would indicate that nitrite reduction by Y216F is susceptible to substrate inhibition, which can be described by the reaction Scheme 3.1 where the formation of a binary substrate complex results in an inhibited enzyme.



Scheme 3.1

Here, E represents the free enzyme and S substrate, E:S the substrate:complex, E:S:S the binary substrate complex, P the reaction product and K_i is the equilibrium constant that describes the second substrate binding the E:S complex.

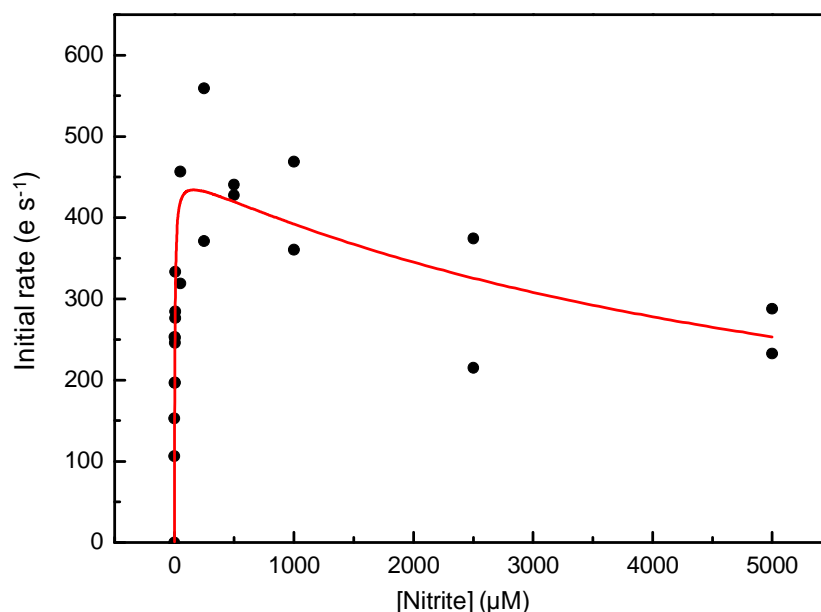


Figure 3.21 - Initial rates of nitrite reduction by Y216F NrfA as determined by colorimetric solution assay. Initial rates are plotted against nitrite concentration; line shows the fit to equation 3.1 which describes substrate inhibition and yielded kinetic constants of $k_{\text{cat}} = 457 \pm 30 \text{ e}^- \text{ s}^{-1}$, $K_M = 4.1 \pm 1.1 \text{ } \mu\text{M}$, $K_i = 6237 \pm 2360 \text{ } \mu\text{M}$. Buffer 2 mM CaCl_2 , 50 mM HEPES, pH 7, 20 °C.

$$\text{Rate} = \frac{V_{\text{max}}}{\left(1 + \left(\frac{K_M}{[S]}\right) + \left(\frac{[S]}{K_i}\right)\right)}$$

Equation 3.1

The kinetic constants of V_{max} , K_M and K_i were determined by fitting the substrate inhibition equation (equation 3.1) to the initial rates obtained for the nitrite reduction. The fit was performed with Origin software and generated values for k_{cat} of $457 \pm 30 \text{ e}^- \text{ s}^{-1}$, K_M of $4.1 \pm 1.1 \text{ } \mu\text{M}$ and a K_i of $6237 \pm 2360 \text{ } \mu\text{M}$, Figure 3.21. The results reveal that the k_{cat} of the Y216F enzyme is significantly reduced compared to the WT value indicating a slower rate of nitrite turnover. However, a 10-fold decrease in the K_M means that the Y216F has a higher affinity for nitrite. When both the K_M and k_{cat} are used to calculate the specificity constant the value is over three times higher than that of WT, suggesting a more efficient enzyme even though the maximal rate of reduction is lower. However the specificity constant does not take into account the observed substrate inhibition. This reveals that at higher concentrations nitrite is inhibiting.

To further explore the impact of substrate inhibition on the Y216F NrfA, PFE was carried out using graphite electrodes. Cyclic voltammograms measured with a protein film of Y216F NrfA, exposed to increasing concentrations of nitrite are displayed in Figure 3.22. The voltammograms have been baseline subtracted and time corrected for film loss. There is a clear increase observed in catalysis as more substrate is added (grey lines) to the chemical cell until a concentration of 160 μM nitrite is reached (red line) At this point further additions result in a decrease in reduction (blue lines), mirroring the observation made in the solution assays.

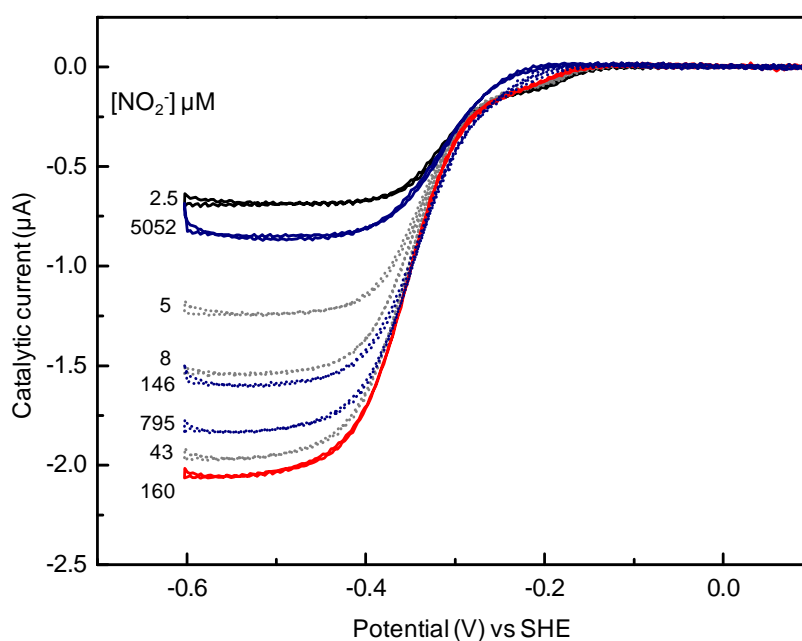


Figure 3.22– Cyclic voltammetry of Y216F adsorbed onto PGE electrodes in the presence of nitrite at 2.5, 5, 8, 43, 795, 1460, 5052 μM . Y216F NrfA nitrite titration of voltammograms show nitrite additions which result in an increase in catalytic current (black and grey) the voltammograms which displays the last increase in catalysis (red) before nitrite becomes inhibiting and voltammograms show a decrease in current upon further nitrite additions (blue). Baseline subtracted and time corrected. Buffer-electrolyte 2 mM CaCl_2 , 50 mM HEPES, pH 7, 3,000 rpm, 20 $^\circ\text{C}$, scan rate 30 mV s^{-1} and rotation rate of 3,000 rpm.

Plotting the catalytic current magnitude at -500 mV for data presented in Figure 3.22 against concentration and fitting equation 3.1 to the data allowed the i_{max} , K_{M} and K_{i} values to be determined. The fit to the data yielded an i_{max} value of $2.2 \pm 0.2 \mu\text{A}$. This cannot be compared to other i_{max} values or converted to a k_{cat} value as the amount of protein present in the film is unknown. The fit produced a K_{M} value that is in agreement with the solution assays and a K_{i} value of $3384 \pm 294 \mu\text{M}$, which is lower than the value previously obtained in the solution assays. The lower K_{i} value could reflect that the sulphite present within the

solution assay has an effect on the degree of inhibition observed. However, both methods agree the K_i value that describing nitrite binding to the enzyme substrate complex is orders of magnitude higher than the K_M value that describes nitrite binding to the free enzyme.

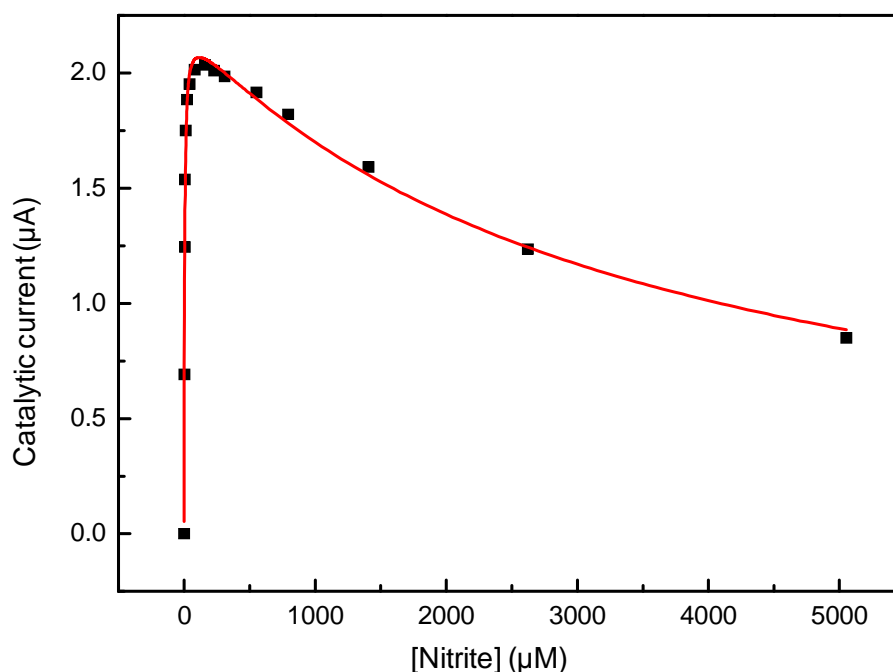


Figure 3.23- Substrate inhibition of nitrite reduction by Y216F NrfA as determined by PFE. The observed catalytic current as a function of substrate concentrated from the CV data presented in Figure 3.22. The line is the fit of equation 3.1 to the data, indicating substrate inhibition with kinetic constants of i_{\max} $2.2 \pm 0.2 \mu\text{A}$, K_M of $4 \pm 0.4 \mu\text{M}$ and K_i of $3384 \pm 294 \mu\text{M}$. Experimental conditions as stated in Figure 3.22.

The cyclic voltammograms of Y216F not only agree with the substrate inhibition observed in the solution assays, they also provided information on the potential dependence of nitrite reduction with increasing nitrite concentrations. The onset of catalysis in Y216F NrfA is at -130 mV which is 50 mV more negative than the WT protein. The onset of catalysis in WT NrfA is the start of a sigmoidal wave that describes the main catalytic wave resulting from the reduction of nitrite, Figure 3.16. In the Y216F protein the onset of catalysis results in a small catalytic wave with a second much larger sigmoidal wave commencing at a potential of -230 mV. With increasing nitrite concentrations up to 160 μM , the initial small catalytic wave shows a decrease in catalytic current generated and shifts to more negative potentials. The second wave also shifts to more negative potentials but displays an increased current generated, in agreement with nitrite acting as a substrate. As nitrite is added to concentrations above 160 μM the initial wave continues to decrease in size until only the single wave is observable at 5052 μM nitrite. At the higher nitrite concentrations

the second wave generates a decreased catalytic current, reflecting a decrease in the rate of nitrite reduction. The catalytic wave also shifts to more negative potentials. The observation that with a higher substrate concentration the catalytic wave shifts to lower potentials has been documented for WT NrfA in which it is thought to reflect a need for an increased driving force to bring about substrate reduction [65].

The main catalytic wave that describes the nitrite reduction is ~175 mV lower in the Y216F NrfA than that of WT NrfA. The position of the catalytic wave of WT NrfA is thought to be linked to the reduction potential of the active site heme (-40 mV) as once the active site heme is reduced, catalysis of the substrate can occur. However, the reduction potential of the active site heme of Y216F has been measured to be -80 mV. Although this is a 40 mV negative shift in the reduction potential it does not correspond to the 175 mV shift that is observed in the catalytic wave. The reduction potentials of the low-spin hemes have not changed so it is unlikely that the position of catalytic wave is a consequence of the electron transfer through the NrfA protein. Therefore another factor must be influencing the potential dependence of nitrite reduction in the active site of Y216F.

The hydroxylamine reductase activity Y216F NrfA was characterised using PFE. It revealed that hydroxylamine reduction proceeded via normal Michaelis-Menten kinetics, as increasing the substrate concentration resulted in an increase in catalysis until the rate of catalysis was independent of further substrate addition. Therefore, there was no indication of substrate inhibition occurring, with hydroxylamine as the substrate, as was observed for nitrite reduction. The position of the wave also altered as catalysis began at more positive potentials (-90 mV) compared to nitrite reduction (-130 mV). The wave still had a biphasic character with a boost in catalysis observed at potentials below -250 mV. The boost for hydroxylamine reduction occurs over a similar potential range to the second wave of nitrite reduction. This boost is not observed in hydroxylamine reduction catalysed by WT NrfA, which is shown in Figure 3.11. This suggests that even though there is no evidence for substrate inhibition the substitution has still resulted in a modification of the potential dependence of hydroxylamine reductase activity.

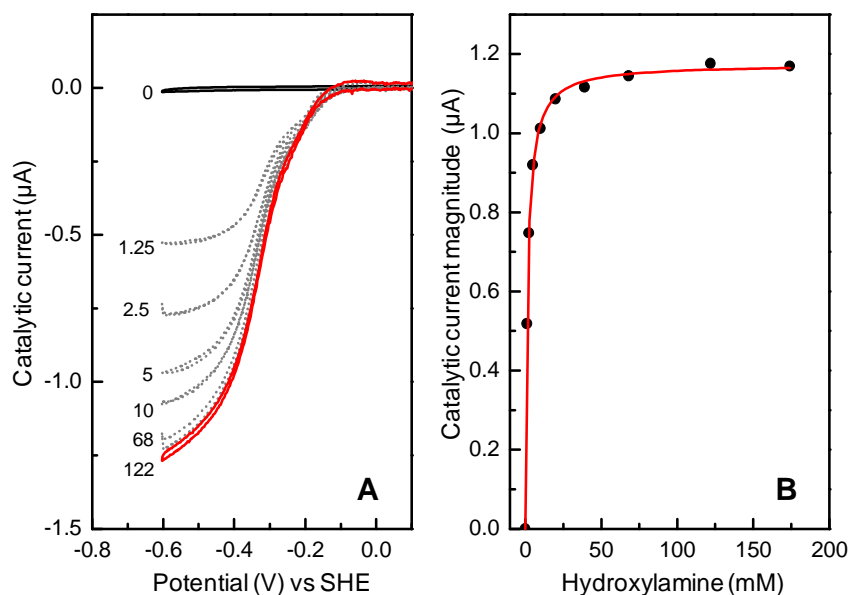


Figure 3.24 – Hydroxylamine reduction by Y2164 NrfA. (A) CVs of hydroxylamine reduction at concentrations stated. (B) Michaelis-Menten fit to the catalytic current generated at -500 mV in panel A, producing a K_M of 1.5 ± 0.1 mM and an i_{max} of 1.75 ± 0.03 μ A. Buffer-electrolyte 2 mM $CaCl_2$, 50 mM HEPES, pH 7, 20 °C.

The difference between hydroxylamine reduction by WT and Y216F NrfA is also reflected in the K_M value determined by fitting the Michaelis Menten equation to the data presented in Figure 3.24 A and B. The fit generated an i_{max} and a 1.75 ± 0.03 μ A and K_M 1.5 ± 0.1 mM at an applied potential of -500 mV. The K_M value for the phenylalanine for tyrosine substitution is much lower than that of WT enzyme (30 mM), indicating a high affinity for hydroxylamine. Y216F NrfA also displayed a higher affinity for nitrite indicating that the mutation must allow for more favourable nitrite binding. The exact reason for this is unclear, but could be as a result of the changes in the position of the conserved water molecules near the substituted residue. These could allow for easier diffusion of substrate into the active site cavity.

3.5 Discussion

The work within this chapter has illustrated the importance of the three conserved residues that form the distal pocket NrfA. Comparison of the crystal structures of the three variants with that of the rWT protein indicated that the substitute residues adopted conformations similar to those of the native residues. This resulted in no overall change to the other residues within the active site or the NrfA structure as a whole. This enabled the NrfA

variants to report characteristics arising from the substituted residue alone. The structures of all the NrfA variants maintained either a water molecule or an hydroxide ion as the sixth ligand to the active site heme, as has been documented in the native *E. coli* NrfA structures previously characterised [32, 48, 65].

The use of spectroelectrochemistry in which the protein were absorbed on to SnO₂ electrodes allowed the redox properties of the low- and high-spin hemes within rWT, Y216F and H264N NrfA to be characterised without the introduction of chemical reductants. The use of chemical reductants such as dithionite to reduce the NrfA proteins in solution was shown to interfere with the properties of the high-spin heme of the NrfA protein, partially masking the absorbance in the 440 nm region. This indicated that the sulphite, a breakdown product of NrfA was able to bind to the active site. The effect on the H264N protein was less than the rWT and Y216F proteins suggesting the H264N NrfA has lower affinity for sulphite.

The spectroelectrochemistry allowed redox titrations to be carried out under the control of a potentiostat. This enabled the midpoint potentials of the high-spin active site heme and low-spin electron transfer hemes to be determined for rWT, H264N and Y216F NrfA. The potentials of the hemes within rWT were in line with those previously reported. The substitutions of each of the three active site residues had no impact on the reduction potentials of the low-spin hemes. They did, however, affect the reduction potential of the active site heme of both proteins. The H264N mutation resulted in the reduction potential increasing while in the Y216F NrfA it decreased. Even though the residues do not directly interact with the active site, they are still able to influence the redox properties of the heme. The influence is likely to be through changes in the nature of the charge active site, either in the change in the water network or in altering the charge of the active site pocket.

In contrast to the subtle changes in the structure of the active site, the kinetic properties of NrfA were dramatically altered in the all three NrfA variants. The changes in activity provide an insight into the role that native residues play in the reduction of nitrite and other substrates of NrfA as summarised Figure 3.25.

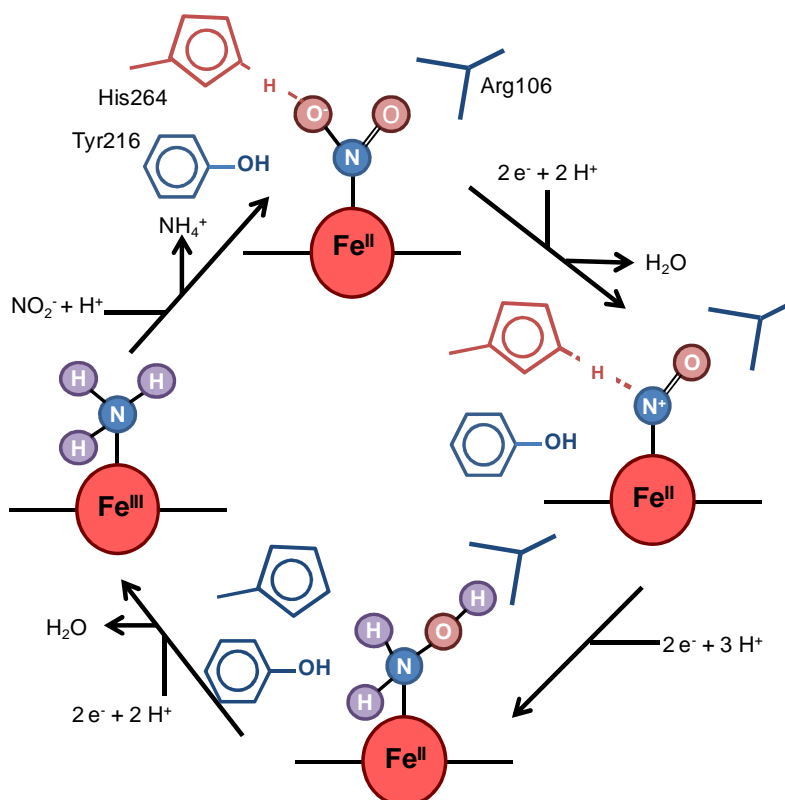


Figure 3.25 – Role of NrfA active site distal residues. Histidine residue is vital for nitrite and nitric oxide reduction (red) but is not vital for hydroxylamine reduction (blue). Arginine and tyrosine residues (blue) are not vital for nitrite and hydroxylamine reduction but negatively impact on enzyme activity when substituted. For more detail see Table 3.1.

The substitution of the active site histidine for an asparagine residue had the clearest change in activity, compared to the WT enzyme. The substitution resulted in the complete loss of nitrite and nitric oxide reductase activity. However, H264N NrfA maintained the ability to reduce hydroxylamine at the same rate as WT NrfA as both proteins displayed similar k_{cat} values. The K_M values determined by solution assays were significantly different for the WT and H264N proteins. However, these assays are susceptible to interference from sulphite binding, present due to the oxidation of dithionite. The similar K_M values of 128 mM and 130 mM for WT and H264N NrfA reveal that the reduction of hydroxylamine is likely to proceed in the same manner in the H264N NrfA variant as it does in WT NrfA. The observed activities would indicate that the His264 residue has a vital role in the reduction of nitrite and the nitric oxide intermediate, but is not vital for the reduction for the of the hydroxylamine bound intermediate.

An indication of further differences between H264N and WT NrfA is the hysteresis that was observed in the CV recorded of hydroxylamine reduction. The hysteresis was observed

only in the H264N NrfA and was reproducible over multiple cycles. It was most pronounced in the first scan but was still present in subsequent scans, recorded at a scan rate of 30 mVs⁻¹.

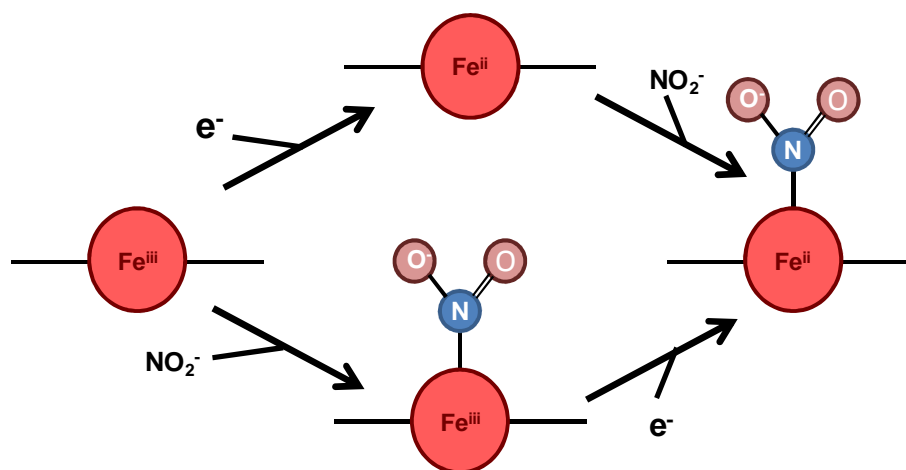
In contrast to the H264N NrfA variant, the R106K substitution had the most subtle changes in activity compared to the WT protein. Both nitrite and hydroxylamine reductase activities were maintained. The reduction of nitrite by R106K was less efficient than the WT enzyme, and this was reflected by the smaller specificity constant. The cause of this difference was that the R106K enzyme had a fivefold increase in the K_M value. The higher K_M value indicates that the enzyme has a lower affinity for nitrite. The cause of this increase is likely to be due to the loss of the guanidinium group of the arginine side chain. Positioned within the active site of NrfA to form a hydrogen bond to the bound nitrite molecule as revealed by the nitrite bound WT NrfA crystal structure [45]. In the R106K NrfA variant the structure revealed that the amine group of the lysine residue was facing away from the active site and interacting with a heme propionate group. Without the presence of a hydrogen bond to interact with the bound nitrite molecule, the active site of the R106K NrfA adapted to bind and stabilise a nitrite molecule. Even though the active site of R106K has a lower affinity for nitrite the reduction occurs at similar rates. This could indicate that the arginine residue is only involved in substrate recognition and binding and does not affect substrate reduction. It is also possible that the lysine residue is able to compensate the role that the arginine residue performs in substrate reduction. The formation of a hydrogen bond to the bound nitrite molecule is thought to be vital for the activation and reduction of the nitrite molecule [50]. Therefore it is likely that the lysine residue can fulfil the role of the native arginine residue. To do this, the lysine residue would have to change orientation upon nitrite binding and form a hydrogen bond with an oxygen atom of the bound nitrite. The flexibility of the lysine side chain and the positive charge on the amine group would allow this to occur. The reduction of hydroxylamine progressed at a slightly faster rate in the R106K variant with no significant change observed in the K_M value. This would indicate that the arginine residue plays no role in the reduction of hydroxylamine or the lysine is able to compensate.

The characterisation of the H264N and R106K NrfA clearly shows that out of the residues that have been shown to interact with the bound nitrite molecule it is the interaction of His264 that is most important to the activity of NrfA. While the Arg106 residue can be replaced with a lysine residue with minimal impact on enzyme activity. The remaining residue of catalytic triad Tyr216 is not thought to be in direct contact with bound substrate or reaction intermediates, but is still thought to be important in facilitating substrate reduction.

The nitrite reductase activity of Y216F NrfA, as characterised by both solution assays and PFE experiments, revealed an initial increase in catalysis with increasing substrate concentration until the further addition of nitrite resulted in a decrease in activity. This observation was characterised as substrate inhibition in which a binary substrate enzyme complex is formed following Scheme 3.1. The enzyme with two substrate molecules bound is inhibited and causes the observed decrease in activity. The kinetic constants determined by fitting equation 3.1 to data generated from solution assays yielded a k_{cat} half of that of the WT enzyme and a K_M of $4.1 \pm 1.1 \mu\text{M}$ indicating a tighter binding of nitrite to Y216F despite a lower rate of reduction. The K_i value which describes the binding of the second nitrite molecule was $6237 \pm 2360 \mu\text{M}$ showing the inhibition site has a much lower affinity for nitrite compared to the active site. There has been evidence for substrate inhibition of WT NrfA at much higher nitrite concentrations (>5 mM). However, the cause of the inhibition has not been resolved (Thomas Lowe, unpublished). The crystal structure of Y216F NrfA identified that there were changes in the position of active site water molecules that distorted the hydrogen bond network within the region of the mutation that forms part of the substrate entry channel. The disruption caused by the loss of the phenol group of the Tyr216 residue may have generated a low affinity nitrite binding site that could disrupt the substrate entry channel and therefore reduce the catalysis at higher nitrite concentrations. There was however no indication of this form of binding occurring in the nitrite bound structure of Y218F (Y216F equivalent) NrfA from *W. succinogenes*. The crystal of Y218F NrfA was exposed to 10 mM nitrite and only a single nitrite molecule, bound at the active site heme, was resolved in the final structure. This could indicate that a more complex process is giving rise to the observed inhibition, at higher nitrite concentrations than a second nitrite molecule binding.

Substrate inhibition has been characterised in copper dependent nitrite reductase (CuNir) from *Alcaligenes faecalis* by Wijma and colleagues and provides a second explanation of the characteristics of nitrite reduction displayed Y216F NrfA [55]. The CuNir enzyme is able to bind nitrite and reduce it to nitric oxide, carrying out an important step in the denitrification pathway [71]. It contains two copper centres, a copper 2 site binds nitrite molecule and copper 1 site that acts as an electron relay transferring electrons to the active site. The substrate inhibition of CuNir is described by a random-sequential that is comprised of two competing pathways. In the first pathway the substrate binds to the active site first, followed by the reduction of the active site and in the second pathway the active site is reduced prior to substrate binding.

At lower nitrite concentrations the pathway in which the copper site is reduced prior to substrate binding will be the predominant route. However, as the nitrite concentration is increased, the second pathway will become more dominant as the nitrite will bind prior to the active site reduction. The two pathways are described by different rates. Therefore, which pathway is followed will change the overall rate of catalysis. The rate is also dependent on pH, as at low pH a water molecule is present at the active site and at high pH it is a hydroxide ion, therefore changing the molecule that nitrite must displace to bind to the copper. At low pH the reduction of the active site with a water molecule bound is faster than with nitrite bound, therefore as the nitrite concentration is increased nitrite is able to bind prior to the reduction which results in an overall slower rate. At high pH the rate of reduction of the active site with nitrite bound is faster than with the hydroxide ion bound active site. As a result as the nitrite concentration is increased, there is no substrate inhibition observed. The random-sequential mechanism when applied to Y216F NrfA would generate Scheme 3.2.



Scheme 3.2

Substrate inhibition for Y216F according to Scheme 3.2 would suggest that nitrite binding to the active site heme results in a slower rate of reduction than if the heme was reduced before nitrite binding. The slower rate of reduction could be caused by the active site heme becoming more difficult to reduce when nitrite is bound. This would slow electron transfer to heme as well as reducing the reduction potential of the active site heme. Cyclic voltammetry of nitrite reduction by Y216F revealed that the main catalytic wave had shifted to more negative potentials by 175 mV. The shift in catalysis was not in agreement with the shift in midpoint potential of the active site heme and could reflect a reduction potential of the heme with nitrite bound. This supports a random sequential method for Y216F substrate inhibition.

Chapter 4

Nitrite interaction with H264N

NrfA

Chapter 4 – The interaction of Nitrite with H264N NrfA

4.1 Introduction

The structure of nitrite bound to the active site of NrfA from *W. succinogenes* revealed the nitrite molecule binds to the active heme iron via the lone pair of electrons on the nitrogen atom [50]. This orientation allows each of the oxygen atoms to form a hydrogen bond with both the active site histidine and arginine residues. The hydrogen bonding is thought to be critical in polarising the nitrite molecule and allowing the cleavage of first N-O bond. Work presented in Chapter 3 revealed the substitution of the active site Arg106 for a lysine residue within *E. coli* NrfA generated an enzyme that maintained its ability to reduce nitrite and hydroxylamine. By contrast, the substitution of the His264 for an asparagine residue resulted in a loss of detectable nitrite and nitric oxide reductase activity, while the ability to reduce hydroxylamine was essentially unaffected. The comparison of both substitutions reveals that out of the two residues that form hydrogen bonds to the nitrite molecule, it is the His264 residue that is vital for nitrite and nitric oxide reduction.

Examination of the structure of H264N NrfA in conjunction with the nitrite bound WT NrfA structure suggests possible reasons why the nitrite and nitric oxide reductase activities have been lost, Figure 4.1. The substitution of the His264 residue for an asparagine residue increases the distance between the hydrogen bonding groups available to interact with the bound nitrite molecule from 2.6 Å to 3.8 Å. The loss of this stabilising interaction could impede nitrite binding as well as preventing important stages of the nitrite reduction. Experiments providing direct insight into the role of His264 in nitrite binding and reduction are presented in this chapter.

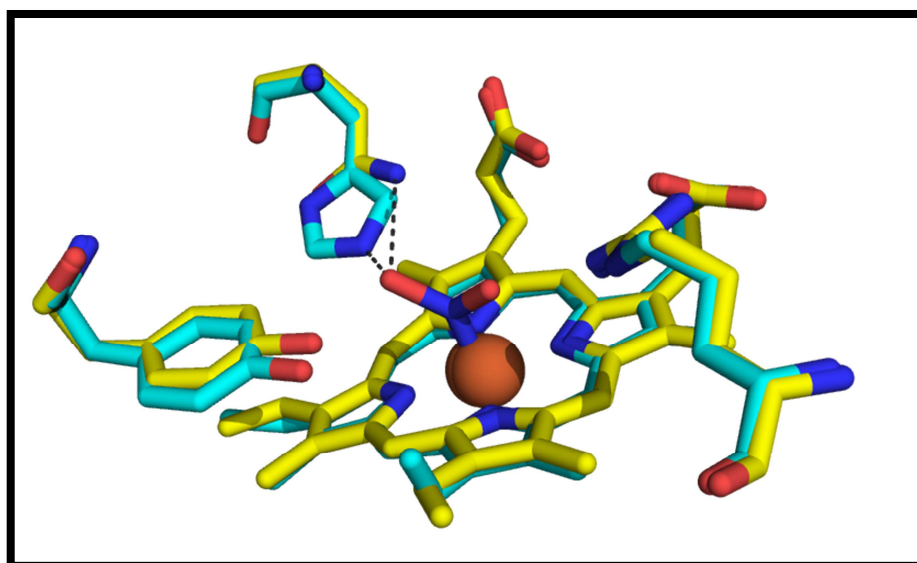


Figure 4.1– Overlaid structures of the active site of *E. coli* H264N NrfA and *W. succinogenes* WT NrfA. H264N active site structure with water bound (water not shown) overlaid with the WT NrfA structure from *W. succinogenes* (PDB: 2E80) with nitrite bound. Dashed lines represents the possible interaction between the histidine of the (*W. succinogenes*) WT NrfA, the bound nitrite molecule at a distance of 2.6 Å, and the possible interaction between the asparagine of the (*E. coli*) H264N NrfA and the bound nitrite molecule at a distance of 3.8 Å. Structures aligned based all atoms in the model using Superpose in CCP4.

4.2 Thermodynamic description of nitrite binding to H264N NrfA

4.2.1 Spectroscopic characterisation of nitrite binding to the oxidised WT and H264N NrfA

Optically monitored titrations were performed to identify if nitrite was able to bind with the same affinity to oxidised WT and H264N NrfA. Aliquots of nitrite were added to solutions of air-oxidised WT or H264N NrfA in 50 mM HEPES, 2 mM CaCl₂, pH 7 buffer. Electronic absorbance spectra were recorded after each nitrite addition. The resulting spectra were corrected by the appropriate dilution factor to account for each nitrite addition and can be seen in Figures 4.2 and 4.3 for WT and H264N NrfA respectively.

The addition of up to 3500 µM nitrite to a 3.3 µM WT NrfA solution produced no significant changes to the low-spin heme contribution in the broad alpha/beta region (490 to 600 nm) of the electron absorbance spectra, Figure 4.2. The high-spin metal ligand charge transfer

band (LMCT), observed at wavelengths around 640 nm, could not be monitored as the concentration of protein was too low to allow this low intensity feature to be observed. However a decrease in the intensity of the Soret region (409 nm), and a slight shift in intensity between 425 - 440 nm was observed with increasing nitrite concentrations. The change in absorbance at 425 nm became independent of nitrite addition after 2000 μM . It is difficult to assign the changes in the spectra at 425 nm to high- or low-spin hemes as both these features give rise to absorbance at this wavelength. Furthermore a level of error is introduced when correcting for protein dilution, which may impact on the magnitude of the observed changes.

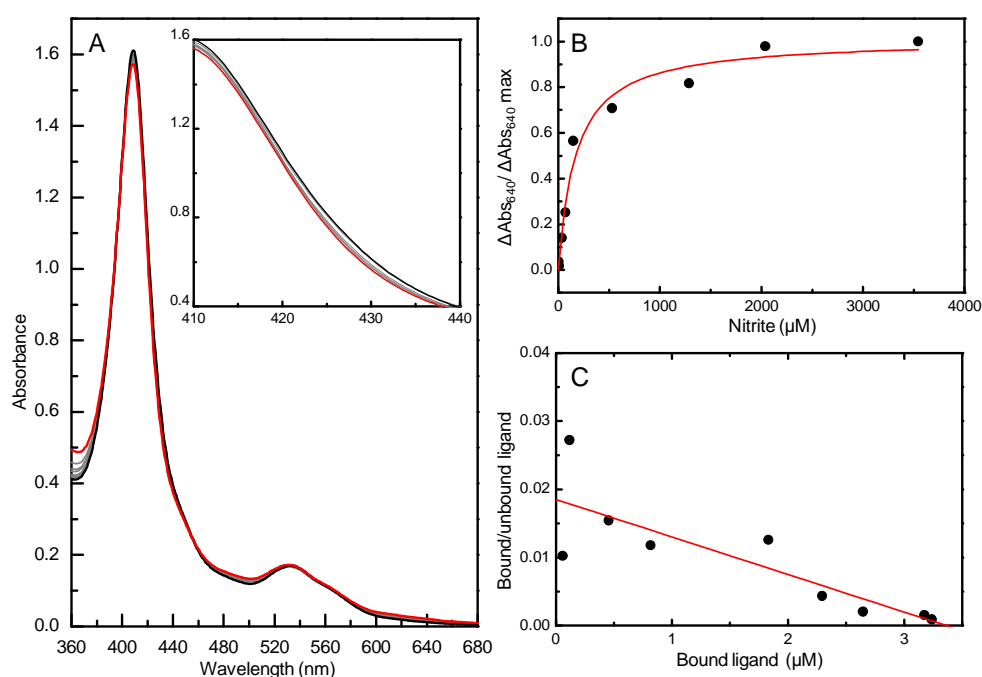


Figure 4.2- Nitrite binding to air-equilibrated WT NrfA. (A) Electronic absorbance spectra of a 3.3 μM WT NrfA solution with 0 (black line), 8, 32, 147, 529, 1287, 2039 (grey lines) and 3543 μM nitrite (red line) (inset showing magnified 425 nm region). (B) Nitrite binding curve based on the change in absorbance at 425 nm with increasing nitrite concentration fitted to equation 4.2 describing a K_d^{ox} of $172 \pm 34 \mu\text{M}$. (C) Scatchard plot of nitrite binding to WT NrfA with a K_d^{ox} of $181 \pm 56 \mu\text{M}$. Buffer 2 mM CaCl_2 , 50 mM HEPES, pH 7, 20°C.

The addition of nitrite to a 3 μM solution of H264N NrfA produced no observable changes in the broad alpha/beta region of the spectra, while the Soret band showed a small decrease in intensity with nitrite addition. The H264N protein displays a weak absorbance at 650 nm attributable to the LMCT band of oxidised high-spin heme. This results from the interaction of the heme iron with its ligand. Upon the addition of nitrite, the intensity of this weak signal

decreases at the same time as the absorbance at 640 nm increases, Figure 4.3 A inset. The shift of the 650 nm band then becomes independent of nitrite concentration above 500 μM as no further changes in the spectra are observed. The wavelength of the charge transfer band can be related to the coordination sphere of the heme. When the band is located at wavelengths greater than 640 nm, the heme iron is thought to be penta-coordinated. At wavelengths at or below 640 nm it is more likely to be hexa-coordinated. In the absence of nitrite the band in H264N is observed at 650 nm suggesting there is a significant population of the penta-coordinated high-spin heme. As nitrite is titrated into the protein solution the absorbance at 650 nm decreases while a corresponding increase is observed at 640 nm. This observation indicates an increasing population of the hexa-coordinated high-spin heme as the nitrite concentration is increased, most likely caused by nitrite forming the sixth ligand to the heme iron.

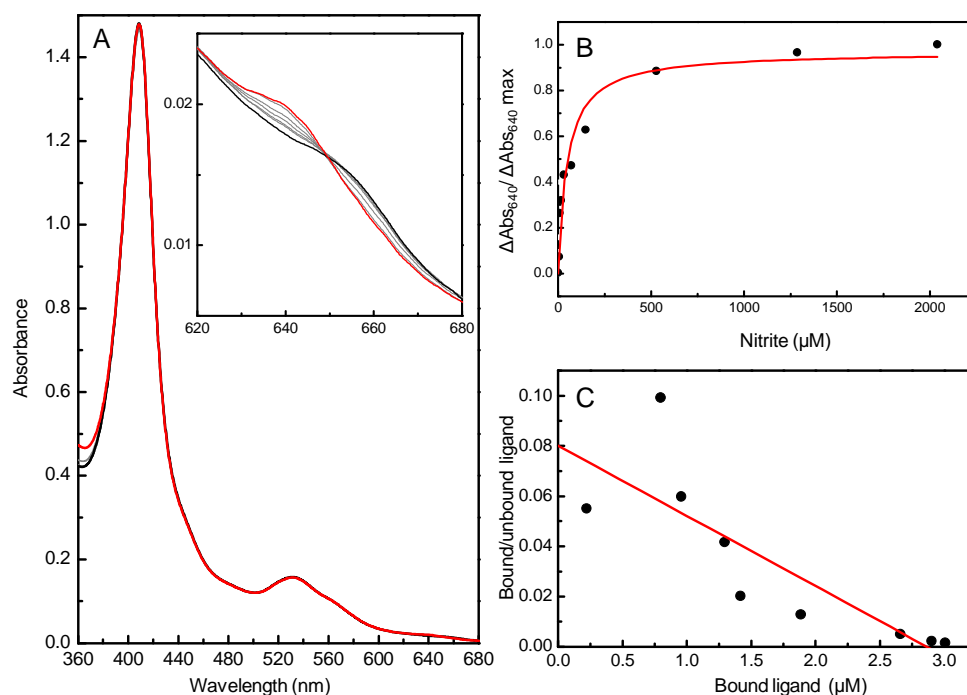
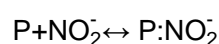


Figure 4.3- Nitrite binding to air-equilibrated H264N NrfA. (A) Electronic absorbance spectra of a 3 μM H264N solution with 0 (black line), 8, 16, 70, 147, 529 (grey lines) and 2039 μM nitrite (red line) (inset showing magnified 640 nm region). (B) Nitrite binding curve based on the change in absorbance at 640 nm with increasing nitrite concentration fitted to equation 4.2 describing a K_d of 48 ± 11 μM . (C) Scatchard plot of nitrite binding to H264N with a K_d of 36 ± 18 μM . Buffer 2 mM CaCl_2 , 50 mM HEPES, pH 7, 20°C.

The changes observed in the Soret region of electronic absorbance spectra upon the addition of nitrite would suggest that nitrite is able to interact with both the WT and H264N

proteins. The interaction is likely to occur at the active site heme, as it is features that relate to the oxidised high-spin heme that have altered. Those that arise solely from low-spin heme contributions have remained constant. This would indicate that nitrite is able to at least enter the active site cavity of both proteins.

To quantify nitrite binding to the two oxidised enzymes a reversible 1:1 binding was assumed:



Where P is the NrfA protein, NO_2^- nitrite ligand, and $P:\text{NO}_2^-$ is the protein nitrite complex.

The fractional saturation, Y, is defined as the fraction of binding sites with ligand bound and therefore Y can vary from 0 to 1. If the protein only binds one ligand the concentration of binding sites and protein are the same and the fractional saturation is determined from equation 4.1.

$$Y = \frac{[P:\text{NO}_2^-]}{[P] + [P:\text{NO}_2^-]}$$

Equation 4.1

Where [P], $[P:\text{NO}_2^-]$ and $[\text{NO}_2^-]$ are the equilibrium concentrations for the free enzyme, protein nitrite complex and free nitrite, respectively.

The dissociation constant K_d^{ox} is equal to $[P][\text{NO}_2^-] / [P:\text{NO}_2^-]$. Therefore substituting $[P:\text{NO}_2^-] = [P][\text{NO}_2^-] / K_d^{\text{ox}}$ into equation 4.1 gives equation 4.2

$$Y = \frac{[\text{NO}_2^-]}{K_d^{\text{ox}} + [\text{NO}_2^-]}$$

Equation 4.2

From electronic absorbance spectra of WT NrfA presented in Figure 4.2, the fractional saturation was obtained by monitoring the absorbance change at the wavelength most representative of the high-spin heme, this was 425 nm. The plot of Y against $[\text{NO}_2^-]$ was well described by equation 4.2 with a K_d^{ox} value of $172 \pm 34 \mu\text{M}$ determined by non-linear regression, Figure 4.2 B. While the change in the absorbance at 425 nm was small, they

yielded a K_d value that is comparable to $\sim 100 \mu\text{M}$ that was determined by EPR monitored nitrite titration of *E. coli* NrfA (B. Burlat unpublished work). The Y for H264N NrfA was calculated using the increase in absorbance at 640 nm, as this region is only contributed to by oxidised high-spin heme. The plot of the fractional saturation against nitrite concentration was described by equation 4.2 with a K_d^{ox} value of $48 \pm 11 \mu\text{M}$, Figure 4.3 B.

The spectroscopically defined K_d^{ox} values determined for WT and H264N NrfA show that not only does nitrite bind to the oxidised active site heme but it binds with similar affinities to both proteins. This would indicate the hydrogen bond that was shown to be present in the structure of *W. succinogenes* NrfA, between the His264 and the nitrite molecule, is not essential for nitrite binding to the oxidised protein. Therefore the lack of nitrite reduction activity does not arise from the inability of nitrite to bind to the H264N enzyme, but must be caused from some other aspect of the behaviour of the enzyme containing an asparagine at position 264.

4.2.2 Nitrite binding to reduced H264N NrfA

To investigate the interaction of nitrite to the fully reduced H264N NrfA, chronoamperometry experiments were performed that enabled the impact of nitrite on the hydroxylamine reductase activity to be monitored under steady-state conditions. A H264N NrfA film was immersed in buffer-electrolyte containing 28 mM hydroxylamine and poised at -500 mV. Additions of nitrite were made to the cell to a final concentration of 9.1 mM. Each nitrite addition resulted in a decrease in the observed catalytic current in line with nitrite acting as an inhibitor of hydroxylamine reduction, and so binding to the reduced enzyme, Figure 4.4 A. The catalytic current after each addition of nitrite was recorded and corrected for film loss. The catalytic current was converted into fraction of catalytic current remaining and plotted against nitrite concentration, Figure 4.4 B.

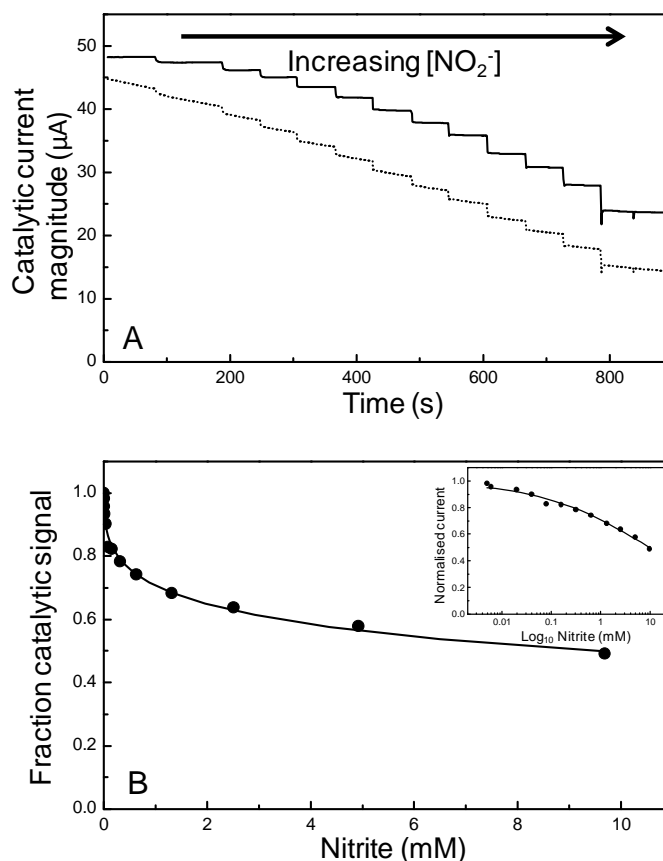


Fig 4.4- Nitrite inhibition of hydroxylamine reduction by H264N NrfA. (A) Chronoamperometry at -500 mV of H264N NrfA in the presence of 28 mM hydroxylamine and increasing concentrations of nitrite (0, 5, 10, 20, 39, 78, 155, 312, 626, 1316, 2512, 4919, 9683 µM), raw data (dotted line) and time corrected data (solid line) shown. (B) Plot of fraction of catalytic current remaining as nitrite concentration is increased, data from (A). Inset, sigmoidal fit to the data presented in (B) producing an IC₅₀ value of 9.6 ± 1.1 mM. Buffer-electrolyte 2 mM CaCl₂, 50 mM HEPES, pH 7, 20°C, electrode rotation at 3,000 rpm.

The IC₅₀ value, which represents the concentration of an inhibitor required to reduce the activity of an enzyme by half under a defined set of conditions, was determined by plotting the fraction of catalytic current remaining against the log₁₀ of the nitrite concentration. A sigmoidal fitting to the data was performed. The fit to the data determined an IC₅₀ value of 9.6 ± 1.1 mM, Figure 4.4 B. The IC₅₀ value reflects the affinity of the enzymes under the conditions of the experiment and therefore is dependent upon the substrate concentration used. The IC₅₀ value was converted to a K_i , which is equivalent to the K_d^{red} that reflects the affinity of substrate for the reduced NrfA protein, using equation 4.3. The K_M for hydroxylamine reduction was 130 mM in the absence of nitrite and the substrate concentration [S] was 28 mM. This yielded a K_d^{red} value of 7.9 ± 0.9 mM. The observed inhibition confirmed that nitrite is able to interact with the reduced active site of H264N

NrfA, although it appears to be with a much lower affinity compared to the oxidised active site.

$$K_d^{\text{red}} = \frac{IC_{50}}{1 + \frac{[S]}{K_M}}$$

Equation 4.3

4.2.3 The nature of H264N inhibition by nitrite

To determine the type of inhibition that is experienced by H264N NrfA in the presence of nitrite, further chronoamperometry experiments were performed. The catalytic current was monitored as hydroxylamine was titrated into a fixed concentration of nitrite e.g. Figure 4.5. The experiment was repeated with fresh films in solution of different nitrite concentrations. After the completion of each titration, the protein film was transferred into a buffer-electrolyte solution containing 28 mM hydroxylamine. By measuring the catalytic current in the standard solution of 28 mM hydroxylamine, the response of the films could be normalised. This allowed comparison of the i_{max} values generated in solutions of different nitrite concentrations, as it removed the dependency of the current on the concentration of protein present within the film.

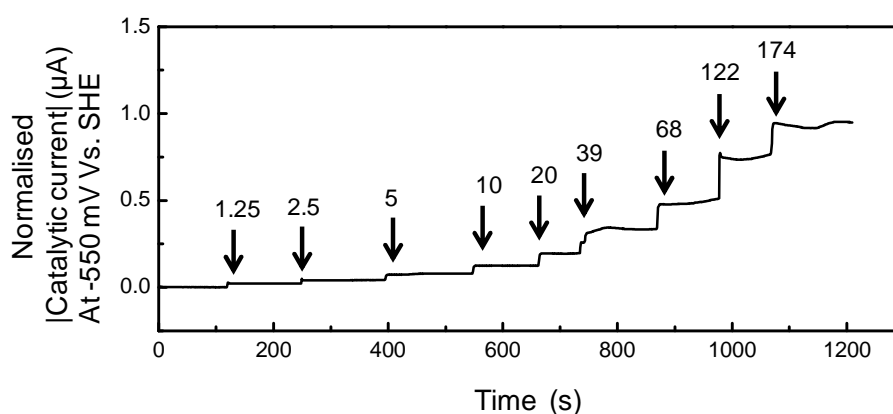


Figure 4.5—Chronoamperometry monitoring the catalytic current of a H264N NrfA protein film poised at -500 mV, in the presence of a fixed concentration of nitrite (15 mM) with increasing hydroxylamine concentrations as indicated (mM). Catalytic currents normalised to the current produced when the film was exposed to 28 mM hydroxylamine in the absence of nitrite. Buffer-electrolyte 2 mM CaCl₂, 50 mM HEPES, pH 7, 20°C, electrode rotation at 3,000 rpm.

The data was plotted as $1/[\text{Hydroxylamine}]$ vs. $1/\text{catalytic current magnitude}$ and fitted to equation 4.4, to determine K_M^{obs} and $i_{\text{max}}^{\text{obs}}$ by linear regression.

$$\frac{1}{i} = \left(\frac{K_M^{\text{obs}}}{i_{\text{max}}^{\text{obs}}} \frac{1}{[S]} + \frac{K_M^{\text{obs}}}{i_{\text{max}}^{\text{obs}}} \right)$$

Equation 4.4

The Lineweaver Burk plots constructed using linear regression enabled the K_M^{obs} and $i_{\text{max}}^{\text{obs}}$ values to be calculated as well as allowing the type of inhibition to be determined. The Lineweaver Burk plot showed that the Y intercept remained essentially constant with increasing nitrite concentration whereas the intercept of the X axis varied with increasing inhibitor concentration, this is indicative of competitive inhibition, Figure 4.6. This was supported by the K_M^{obs} and $i_{\text{max}}^{\text{obs}}$ values, determined by non-linear regression of rate vs. $[S]$. By plotting the K_M^{obs} values against nitrite concentration it is possible to determine the inhibitor dissociation constant (K_i) equivalent to a K_d^{red} value. The K_d^{red} value was determined to be 15.7 ± 1.2 mM, a value that is more than 300 times higher than the K_d^{ox} observed for nitrite binding to the air-oxidised enzyme. It is not possible to perform the same analysis on the WT NrfA, as exposure of the reduced enzyme to nitrite results in the nitrite being turned over. However, the K_M value for nitrite reduction by WT NrfA can be taken as an approximation of the K_d^{red} which gives a value of 37 ± 5 μM .

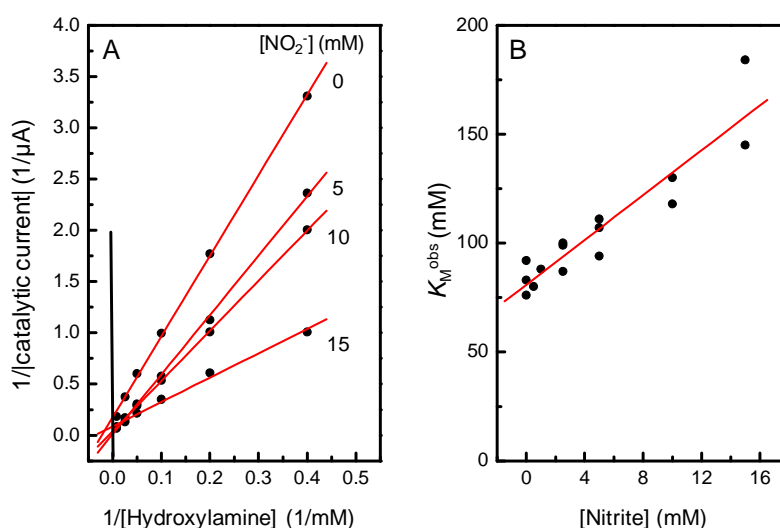


Figure 4.6- Nitrite inhibition of hydroxylamine reduction by H264N NrfA at -500 mV. (A) Lineweaver Burk plots for hydroxylamine reduction in solutions of 0, 5, 10 and 15 mM nitrite. Lines are the linear fit of the data points used to calculate K_M and i_{max} values from equation 4.4. The data was obtained from chronoamperometry of H264N NrfA films poised at -500 mV and

normalised to the current produced when the film was exposed to a solution of 28 mM hydroxylamine and films corrected for film loss. (B) K_M^{obs} values obtained from Lineweaver Burk plots of H264N NrfA films in different nitrite concentration plotted against nitrite concentration. Experimental conditions as in Figure 4.5.

4.2.4 Spectroelectrochemical characterisation of nitrite bound H264N NrfA

To determine the heme reduction potentials of nitrite bound to H264N NrfA, a SnO_2 electrode with an absorbed layer of H264N NrfA was placed in to an OTTLE cell containing anaerobic; 1 mM nitrite, 50 mM HEPES, 2 mM CaCl_2 buffer-electrolyte at pH 7. Electronic absorbance spectra were recorded with the film poised at increasingly negative potentials to generate the fully reduced protein. The film was then poised at increasingly positive potentials and spectra recorded as the protein returned to a fully oxidised state. The film was poised at each potential for 3 minutes prior to measuring a spectrum, Figure 4.7 A and B. Inspection of the absorbance spectra collected during the titration, alongside the redox difference spectra for the reductive and oxidative poisoning of the sample, showed that the enzyme behaved identically under both reductive and oxidative titrations, Figure 4.7.

The absorbance spectra of the fully oxidised and fully reduced H264N NrfA in the presence of 1 mM nitrite displayed the same spectral features attributed to low- and high-spin hemes as those observed in the absence of nitrite, Figure 3.7. The adjacent difference spectra showed the increase at 552 nm was observed over the potential range of +10 to -390 mV. The variation in the absorbance at 552 nm with potential was well described by four independent electron processes ($n=1$) with mid-point potentials of +15, -120, -190, -320 mV (all ± 15 mV). Each redox centre contributed equally to total reduction (25%). The midpoint potentials obtained for the low-spin hemes in the presence of nitrite are in agreement with those determined in its absence. The similar reduction potentials for the low-spin hemes in the absence and presence of 1mM nitrite indicates that these hemes are not susceptible to nitrite binding. Such an interaction would be unlikely, as the hemes are bis-His coordinated and buried within the protein.

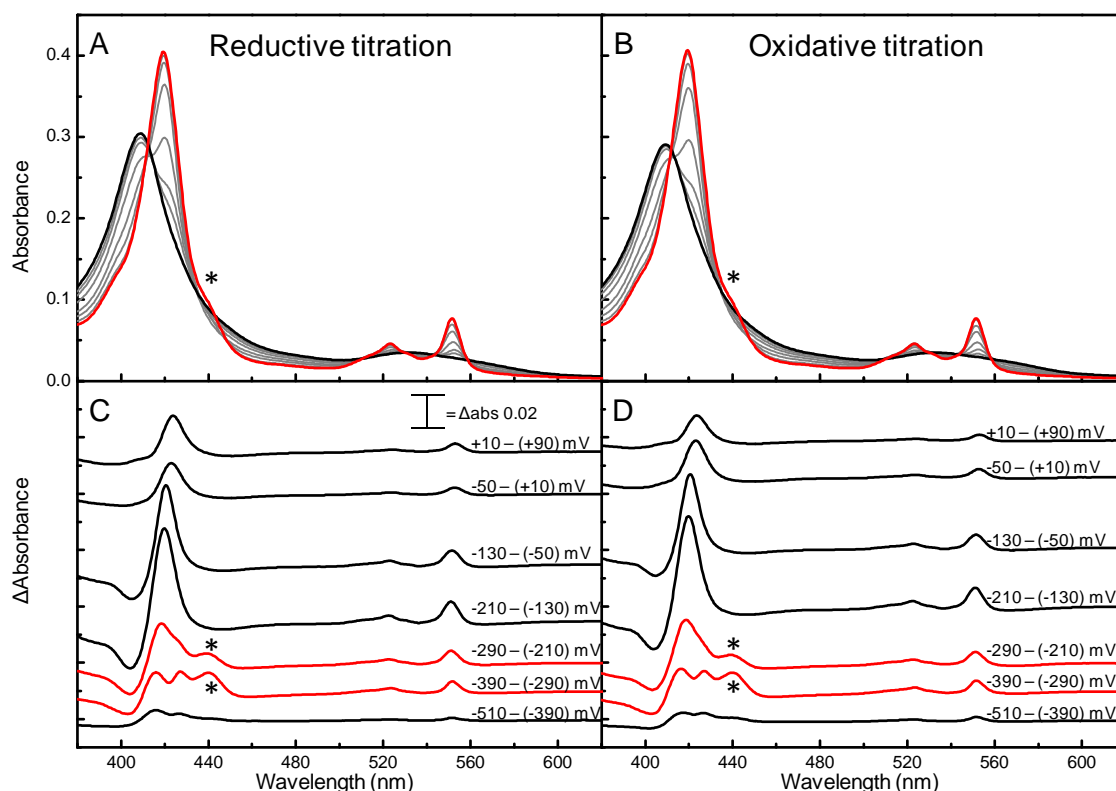


Figure 4.7- Spectropotentiometry of H264N NrfA immobilised on mesoporous tin oxide in the presence of 1 mM nitrite. Electronic absorbance spectra of the reductive (A) and oxidative (B) titration. Fully oxidised H264N poised at +90 mV (black), fully reduced poised at -510 mV (red) and intermediate potentials (grey). Spectra were recorded at sequential potentials. Difference spectra (reduced poised – oxidised poised at potentials indicated) of H264N reductive (C) and oxidative titration (D). * Denotes the features associated with high-spin ferrous heme. Buffer-electrolyte 1 mM NO_2^- , 2 mM CaCl_2 , 50 mM HEPES, pH 7, 4°C

Reduction of the active site high-spin heme increases the absorbance at 442 nm. This occurs at potentials between -210 and -390 mV for nitrite bound H264N NrfA, Figure 4.7 D. The change in absorbance at 442 nm with potential was well described by a single ($n=1$) electron reduction with a midpoint potential of -300 ± 15 mV. This is a potential range significantly below that of the high-spin heme redox potential in the absence of nitrite (-15 ± 15 mV). The significant negative shift of 285 mV in the reduction potential of the active site heme reveals that more energy is required to reduce the active site heme in the presence of nitrite. The observation that only the spectral features related to the high-spin heme are changed upon the addition of nitrite supports the hypothesis that nitrite inhibition is caused by the direct interaction of nitrite with the active site heme.

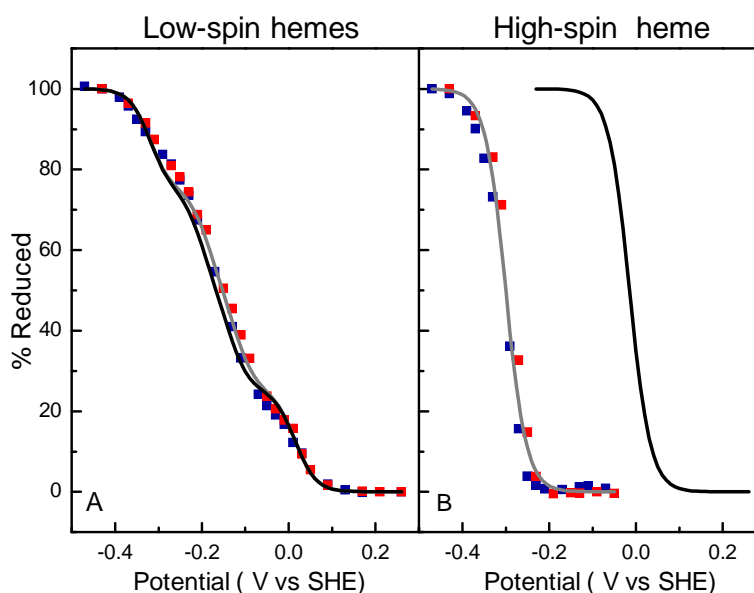
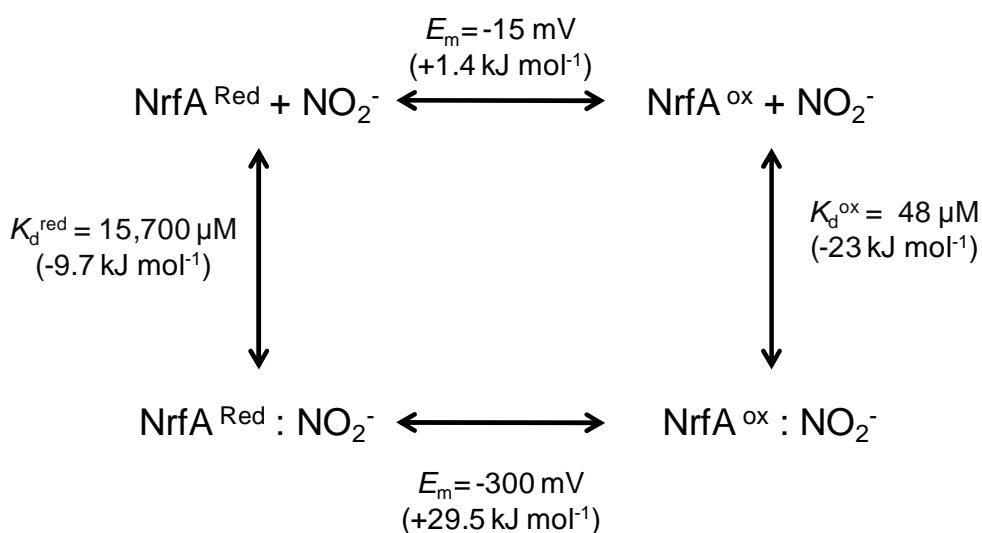


Figure 4.8- Nernst plots showing redox cycling of H264N NrfA in the presence of 1 mM nitrite. The redox profiles of the four low-spin hemes (A₅₅₂ - A₅₈₂) are shown in panel A. The reductive (■) and oxidative (■) data fits the behaviour of a four independent single electron ($n=1$) processes described by the Nernst equation with each redox centre contributing 25% of the total reduction and with E_m values of +15, -120, -190, -320 mV (grey line). Nernstian fit for the low spin hemes of H264N NrfA in the absence of nitrite, black line low-spin heme potentials from Figure 3.8. The redox profile of the high-spin heme (A₄₄₂ - A₄₅₂) is shown in panel B. The reductive (■) and oxidative (■) data fits a single electron ($n=1$) process described by the Nernst equation with an E_m value of -300 mV, grey line. The high-spin heme potentials of H264N NrfA in the absence of nitrite from Figure 3.8, black line. Experimental conditions as Figure 4.7.

Experiments presented later in this chapter indicate that H264N NrfA immobilised SnO₂ electrode becomes fully saturated, at all oxidation states of the protein, when exposed to 1 mM nitrite. This was unexpected given a K_d^{red} of 15.7 ± 1.2 mM was determined from nitrite inhibition of hydroxylamine reduction by H264N NrfA absorbed onto graphite electrodes. With this K_d^{red} value and 1 mM nitrite, only 6% of the reduced enzyme would be predicted to have nitrite bound. The most likely explanation of this is that the concentration of nitrite within the SnO₂ electrode is greater than the bulk solution. Similar effect has been reported for O₂ [72]. For nitrite, an explanation could be that the effective concentration of nitrite at the surface and within the pores of the SnO₂ electrode could be increased if the nitrite molecules are electrostatically attracted to SnO₂ electrode. The surface of the electrode is likely to experience alterations in charge as various potentials are sampled. This could also mean that the effective nitrite concentration within the SnO₂ electrode is potential dependent and not reflected by the concentration of the bulk solution. The exact implication of change in the concentration ions at the surface of the SnO₂ electrode has yet to be resolved in this work and has also not been fully acknowledged in the literature.

4.2.5 Summary of the thermodynamics of nitrite binding to H264N NrfA

In the simplest case, the binding of nitrite to oxidized and reduced H264N NrfA can be approximated by a square scheme where only the oxidation state of the active site heme is considered, Scheme 4.1. This scheme can be described with the quantitative parameters describing the reduction potential of the active site heme in the absence of nitrite, determined in the previous chapter to be -15 mV (± 15). The dissociation constants for nitrite from both the oxidized and the reduced active site were found to be 48 μM and 15,700 μM respectively, and the midpoint potential of the active site heme when bound to nitrite was found to be -300 mV (± 15). By converting these values into Gibbs free energy, any three values should allow the 4th to be accurately calculated.



Scheme 4.1- Square scheme describing nitrite dissociation from reduced and oxidized H264N NrfA. ΔG values (kJ mol^{-1}) calculated from the measured K_d values for reduced (poised at -500 mV) and air oxidized H264N NrfA, Equation 4.5. The ΔG values shown in brackets (kJ mol^{-1}) for the reduction of the active site heme were calculated from the measured E_m values, equation 4.7.

The K_d values can be converted into change in Gibbs free energy (ΔG) using Equation 4.5, where R is the gas constant, T is the temperature and K_{eq} is the equilibrium constant of nitrite association can be calculated from the K_d values using equation 4.6.

$$\Delta G = -RT \ln K_{\text{eq}}$$

Equation 4.5

$$K_{\text{eq}} = \frac{1}{K_{\text{d}}}$$

Equation 4.6

The E_m values for can also be converted into ΔG by using equation 4.7, where n equals the number of electrons ($n = 1$), F is the Faraday constant and E_m is the midpoint potential of the active site heme either in the absence of nitrite (- 15 mV) or with nitrite bound (-300 mV).

$$\Delta G = -nFE_m$$

Equation 4.7

However, taking any three measured values does not predict the fourth accurately. In fact the values predicted in this way lie well outside the uncertainty of the experimentally defined values, Table 4.1. The apparent contradiction of the values describing the simple square scheme presented above is likely to be a consequence of additional parameters that impact on the behavior of the active site heme.

Process	Measured value	Predicted value
Ox \rightarrow Red	E_m -15 mV	-160 mV
Ox:NO ₂ \rightarrow Red:NO ₂	E_m -300 mV	-150 mV
Red \rightarrow Red:NO ₂ ⁻	$K_{\text{d}}^{\text{red}}$ 0.015 M	7.05 M
Ox \rightarrow Ox:NO ₂ ⁻	K_{d}^{ox} 48 ⁻⁶ M	0.1 ⁻⁶ M

Table 4.1- Measured values for the reduction potentials of the active site heme of H264N NrfA in the presence and absence of nitrite and the affinity of the reduced and oxidised active site for nitrite. Converting the measured values into Gibbs free energy allowed any three values to be used to calculate the predicted 4th value. The measured and predicted values are not consistent.

The most likely variable impacting the parameters is the redox state of the four low-spin hemes within the H264N protein. Each of the four parameters within the square scheme were determined whilst the protein was present in different redox states, Figure 4.9. The reduction of the low-spin hemes will coincide with an increase in the negative charge of the

protein if this is not compensated by proton binding. The reduction of the active site heme in the absence of nitrite occurs in a protein which has only one other heme centre reduced. In contrast the reduction of the active site heme with nitrite bound occurs when three other heme centres are reduced.

As well as the possibility that a protein that is reduced will have an increased electrostatic repulsion for nitrite, there is also the possibility that the reduction of the heme causes change in the protein conformation. This could impact on the active site architecture, therefore affecting the affinity of the enzyme for its substrate. It is important to note that although the observed parameters do not completely fit into the square scheme the qualitative observation that nitrite has a higher affinity for the H264N enzyme in the oxidised than the reduced state fits with the data. This results in a decrease in reduction potential of the active site heme when nitrite is bound is consistent with thermodynamic predictions.

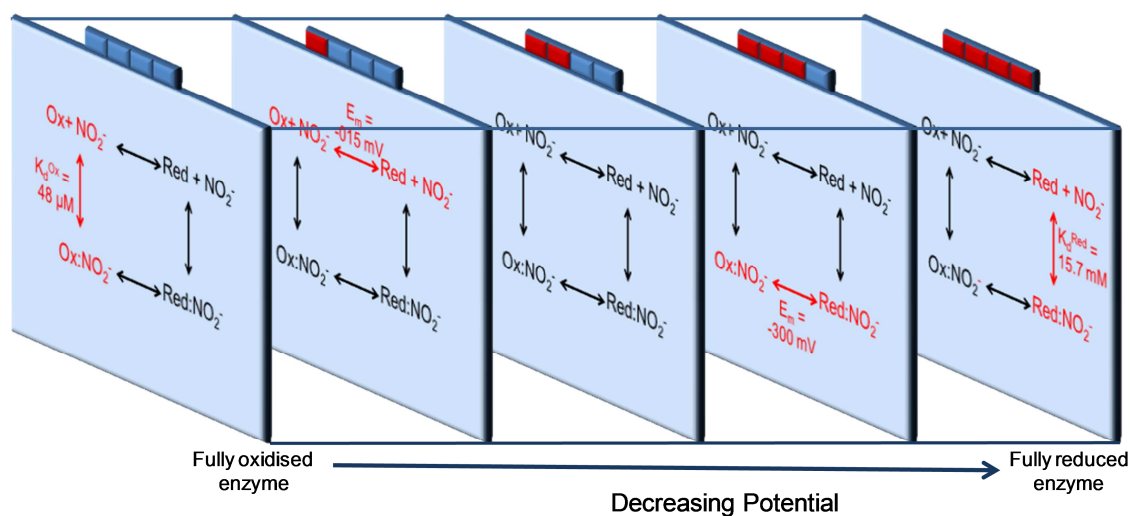


Figure 4.9– Extension of the square scheme presented in Scheme 4.1 for the high-spin active site heme to include the oxidation states of the low-spin hemes indicated at the top of the figure. The majority oxidation states of the low-spin hemes are determined from the E_m values defined in this work red font indicates the process detected for the square scheme relating the majority oxidation state.

4.3 A kinetic description of nitrite binding to H264N NrfA

4.3.1 Spectroelectrochemistry of H264N NrfA at non-saturating nitrite concentrations

To gain further insight into nitrite binding to H264N NrfA, spectroelectrochemical titrations were performed on the protein absorbed onto a SnO₂ electrode using intermediate nitrite concentrations of 5 and 50 μM. The electronic absorbance spectra obtained while poisoning the protein at potentials producing the fully reduced and oxidised protein contained the same high- and low-spin features as reported previously for H264N NrfA, in the absence and presence of 1 mM nitrite. However, monitoring the intensity of the feature at 442 nm arising from redox transformation of the high-spin heme revealed clear hysteresis in the reductive and oxidative titration, Figure 4.10 and 4.11. Importantly no hysteresis was observed in the titration of the low-spin hemes that were monitored by the $\Delta A_{552-582}$. As a consequence, the hysteresis in the $\Delta A_{442-452}$ plots reflects the kinetics of oxidation state dependent nitrite binding and release from H264N NrfA. The complete saturation of the high-spin heme of H264N NrfA with 5 μM and 50 μM nitrite is contrary to the K_d^{ox} value $48 \mu\text{M} \pm 1$, which was determined by titration of an air-oxidised solution H264N NrfA with nitrite. With this K_d^{ox} only ~50% of the high-spin should be associated with nitrite when exposed to 50 μM and even less when exposed to 5 μM. This would suggest that within the SnO₂ electrode the protein is experiencing much higher nitrite concentrations.

Rapid equilibration of nitrite with H264N NrfA would cause the midpoint potential of the high-spin heme to shift from -15 to -300 mV as the nitrite concentration is increased from 0 to 1 mM, but would not introduce hysteresis into the titration data. The hysteresis indicates that either the binding, or the release, of nitrite is slow on the time scale of the experiment. For 5, 50 μM and 1 mM nitrite, reduction of the high-spin heme occurs as a one electron process with a midpoint potential of $-300 \text{ mV} \pm 15 \text{ mV}$, Figure 4.8 and 4.11. The potential at which the high spin heme is reduced indicates that at each nitrite concentration the oxidised H264N NrfA is fully bound with nitrite. Reoxidation of the high-spin active site heme occurs at increasingly more positive potentials as the nitrite concentration is decreased, Figure 4.11. This indicates that the oxidation occurs at potentials reflecting an increasing population of Fe²⁺ to Fe³⁺, and of less Fe²⁺:NO₂⁻ to Fe³⁺:NO₂⁻, as the nitrite concentration is decreased. This is consistent with lower affinity of nitrite for the reduced as compared to the oxidised H264N NrfA, as concluded for the experiments described earlier in this chapter. The hysteresis indicates that either nitrite release from the Fe²⁺:NO₂⁻ or nitrite association to the Fe³⁺ is slow on the time scale of the experiment.

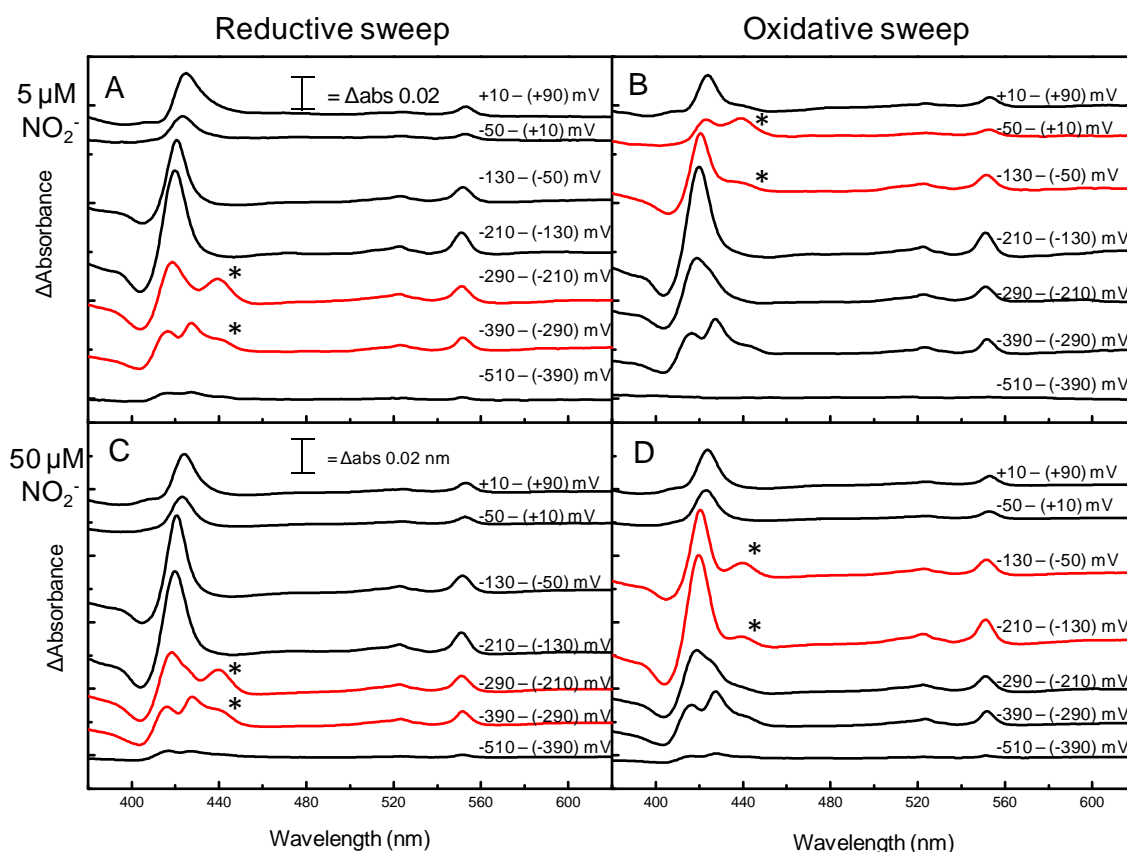


Figure 4.10- Spectropotentiometry of two independently prepared H264N NrfA protein films in the presence of 5 μ M and 50 μ M nitrite. Electronic absorbance difference spectra (reduced poised – oxidised poised at the potentials displayed) of H264N in the presence of 5 μ M nitrite, reductive (A) and oxidative titration (B) and in the presence of 50 μ M nitrite, reductive (C) and oxidative titrations (D) for the potentials stated. Absorbance spectra were recorded at sequential potentials. Buffer-electrolyte 1 mM NO_2^- , 2 mM CaCl_2 , 50 mM HEPES, pH7, 4°C

Further insight into the kinetics of the association and dissociation of nitrite from the H264N protein is difficult to gain from SnO_2 experiments. The precise concentration of nitrite in the mesoporous structure is not known as it does not appear to correspond to the concentration of the bulk solution. This is compounded by the fact that the rates of nitrite diffusion through the mesoporous structure are difficult to define. For this reason PFE on graphite electrodes were used to further explore nitrite interaction with H264N NrfA.

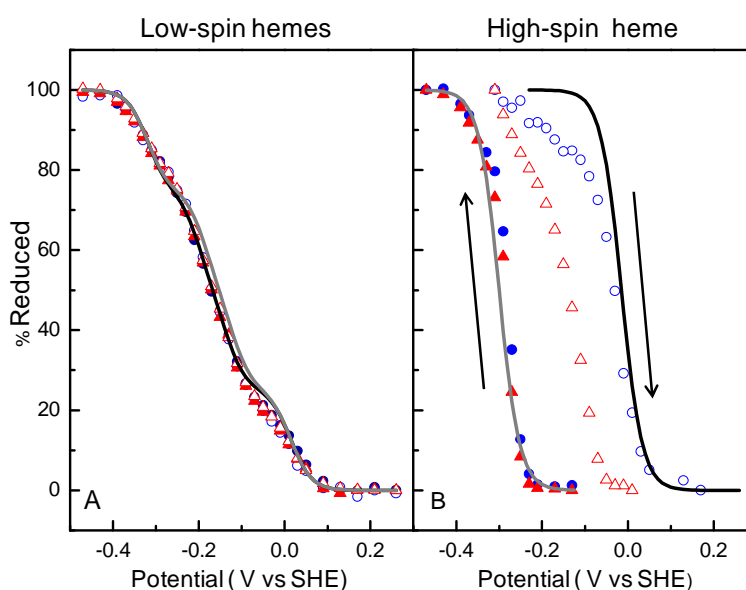


Figure 4.11- Nernst plots showing a redox cycle of H264N NrfA in the presence of 5 μM and 50 μM nitrite. (A) The redox profile of the four low-spin hemes (A₅₅₂ - A₅₈₂) showing the reductive (5 μM ●, 50 μM ▲) and oxidative (5 μM ○, 50 μM △) sweeps. The Nernstian fit for the low spin hemes of H264N NrfA in the absence (black line) and in the presence of 1 mM nitrite (grey line). (B) The redox profile of the high-spin heme (A₄₄₂ - A₄₅₂) showing the reductive (●, ▲) and oxidative (○, △) sweeps with the Nernstian fit for the high spin heme in the absence (black line) and presence of 1 mM nitrite.

4.3.2 PFE of hydroxylamine reduction by H264N NrfA in the presence of nitrite

4.3.2.1 Cyclic voltammetry revealing potential dependence of nitrite inhibition of hydroxylamine reduction

The redox driven binding and release of nitrite from H264N NrfA, as identified by experiments using SnO₂ electrodes, suggest an origin for the hysteresis in the cyclic voltammograms of hydroxylamine reduction by H264N NrfA, Figure 3.11. They may be explained by trace amounts of the nitrite inhibitor being driven on and off the enzyme dependent upon the oxidation state of the enzyme. To determine if this is indeed the case further cyclic voltammetry was performed.

Three consecutive cyclic voltammograms of H264N NrfA absorbed on a graphite electrode were recorded in the presence of 30 mM hydroxylamine with no added nitrite shown in Figure 4.12. In the first scan the observed hysteresis is more pronounced, with the second

and third overlaying and displaying less hysteresis. After switching off the potential control for a minute or two, the same behavior is observed on resuming cyclic voltammetry. Thus, greater inhibition is seen when the enzyme is allowed to spend a longer period of time at more positive, oxidizing potentials. All aspects of the hysteresis observed in the cyclic voltammograms are fully reversible consistent with non-covalent oxidation state dependent inhibition of H264N NrfA.

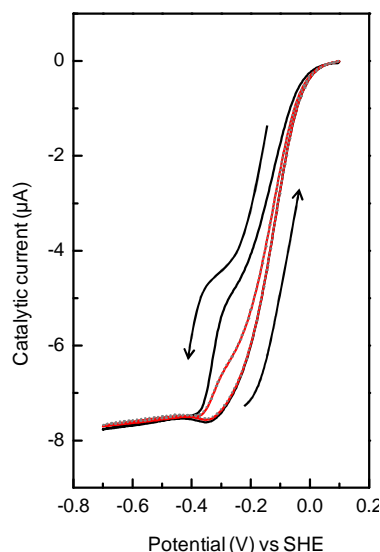


Figure 4.12- Protein film voltammetry of hydroxylamine reduction by H264N NrfA in the absence of added nitrite. The baseline subtracted and time corrected consecutive voltammograms of H264N NrfA absorbed onto PGE electrodes are shown. The experiment was carried out in 30 mM hydroxylamine 1st scan black line, 2nd scan red line, and 3rd scan grey dotted line. Arrows indicate the direction of the scan. Buffer-electrolyte 2 mM CaCl₂, 50 mM HEPES, pH 7, 20°C, scan rate 30 mVs⁻¹ and rotation rate of 3,000 rpm.

As nitrite is added to the electrochemical cell a decrease in the catalytic current at all potentials was observed, Figure 4.13. The decrease in the measured catalytic current was consistent with nitrite inhibiting the reduction of hydroxylamine in a dose dependent manner, as was previously seen in the chronoamperometry performed at -500 mV, Figure 4.4. At potentials more positive than -350 mV the addition of nitrite caused more pronounced inhibition in the reductive sweep than the oxidative sweep, i.e. greater hysteresis. The nitrite dependence of the catalytic cyclic voltammograms describing hydroxylamine reduction by H264N NrfA is then fully consistent with the hysteresis having its origin in the oxidation state dependent binding/release of nitrite from the enzyme. Tight binding of nitrite to the Fe³⁺ active site heme iron, was only relieved on the reduction of the enzyme and with relatively slow rebinding of nitrite to the oxidised enzyme can account for

the observations made on graphite and SnO₂ electrodes. On sweeping to negative potentials in the catalytic cyclic voltammetry has 'phases' in the increase of catalytic current can be noted. This is clearest in the derivative (di/dE) of the cyclic voltammograms, Figure 4.14. The first phase at high potentials corresponds to catalysis from uninhabited enzyme and decreases in magnitude with higher nitrite concentrations. The second phase, at low potential, corresponds to reduction of nitrite bound H264N centred on the potential of -300 mV, close to that of the nitrite bound active site heme, Figure 4.7. The magnitude of the second phase increases as the nitrite is added and dominates at nitrite concentrations of 1145 μM .

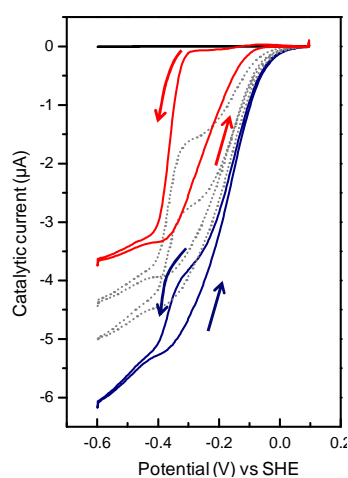


Figure 4.13- Protein film voltammetry of hydroxylamine reduction by H264N NrfA in the absence and presence of added nitrite. The baseline subtracted and time corrected voltammograms of H264N NrfA absorbed onto PGE electrodes are shown. The experiment was carried out in 30 mM hydroxylamine (blue line), with the addition of 80, 160 (grey dotted line) and 1145 μM nitrite (red solid line). Arrows indicate the direction of the scan. In each case the 2nd CV is shown baseline subtracted and time corrected. Buffer-electrolyte 2 mM CaCl₂, 50 mM HEPES, pH 7, 20°C, scan rate 30 mVs⁻¹ and rotation rate of 3,000 rpm.

The increase in inhibition in the reductive sweep would indicate that the H264N NrfA is more susceptible to nitrite inhibition when redox cycling from oxidised to reduced then reduced to oxidised states. The observed hysteresis shows that upon the reduction of the enzyme, inhibition caused by nitrite is driven off. This allows hydroxylamine reduction to proceed. On the re-oxidation of the enzyme nitrite can only be rebound slowly, causing the oxidative sweep to show greater catalytic activity than is observed in the reductive sweep. At 1145 μM nitrite the reductive sweep ceases being biphasic and catalysis is seen as a single sigmoidal wave starting as ca -300 mV. This is clearly illustrated in the first derivatives of the catalytic current with respect to potential, Figure 4.13. As the nitrite

concentration is increased the feature centred on -150 mV decreases as that of -350 mV increases. Sweeping to positive potentials a broad single feature is observed regardless of the nitrite concentration. This is consistent with the observations made of nitrite binding and release to the protein adsorbed on the SnO₂ electrode. The potential at which the affinity for nitrite switches in the cyclic voltammetry is ca -300 mV which agrees with the reduction potential of the active site heme with nitrite bound, indicating that the nitrite is driven off upon reduction of the active site heme.

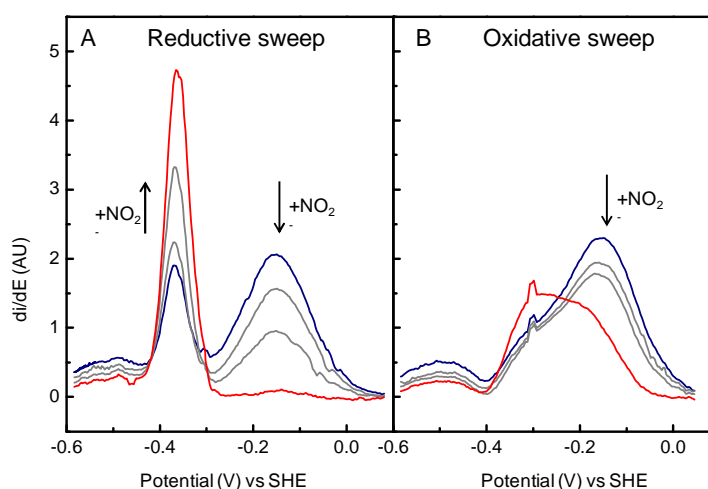


Figure 4.14- First derivatives of the catalytic current with respect to potential for H264N NrfA hydroxylamine reduction in the absence and presence of added nitrite. The first derivative plots for (A) the reductive and (B) the oxidative sweep in 30 mM hydroxylamine (blue line), with 80, 160 (grey lines) and 1145 μM (red line) added nitrite. Arrows indicate change upon increasing nitrite concentration. Experimental conditions are as Figure 4.13

In cyclic voltammetry variation of the potential and time are interlinked. Slower scan rates allow greater time for equilibration with applied potential. Variation of the scan rate allows the opportunity to check that the hysteresis is indeed due to the failure of the system to equilibrate on the time scale of the experiment. Scan rate dependence of cyclic voltammograms from H264N NrfA in 28 mM and 0.56 and 5.18 mM nitrite are shown in Figure 4.15. At slower scan rate (5 mV s^{-1}) both the first and second scans show much less hysteresis than those at 30 and 100 mV s^{-1} . For a given scan rate, hysteresis is less at higher nitrite concentrations due to the slower event being overcome, which is the binding of nitrite to the oxidised H264N active site heme. The rate of nitrite association (on) will be dependent on the concentration of H264N NrfA and nitrite, it will therefore be a second order reaction. The rate of nitrite dissociation (off) will only be dependent on the concentration of H264N:nitrite complex and will be first order.

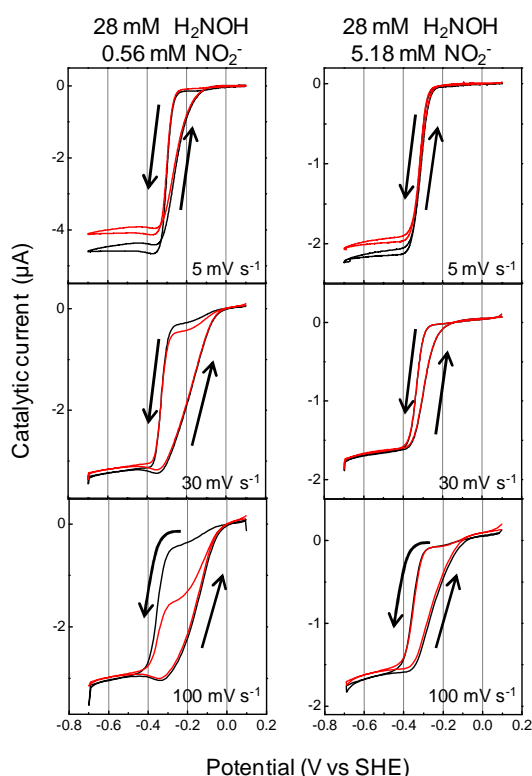


Figure 4.15- Scan rate dependence of nitrite inhibition of H264N NrfA hydroxylamine reduction. Baseline subtracted voltammograms of a single film of H264N NrfA in the presence of 28 mM hydroxylamine and either 0.56 mM or 5.18 mM nitrite, as indicated. First (black line) and second (red line) scans shown for each concentration and scan rate (5, 30, 100 mV s^{-1})

4.3.2.2 Kinetics of nitrite association and dissociation to H264N NrfA as derived by chronoamperometry

The variation of cyclic voltammetric scan rate revealed that both potential and time have an impact on the nitrite inhibition of H264N NrfA. To further characterise the time dependence of nitrite association and dissociation chronoamperometry was performed. This method is less convoluted as it removes the interdependence of the change of potential with time that is present in cyclic voltammetry.

Chronoamperometry was performed on a single protein film of H264N NrfA exposed to a 28 mM hydroxylamine solution containing 2 μM nitrite. Firstly the film was poised at -350 mV, a potential at which the active site heme should be fully reduced and allow the maximum catalytic current to be observed. The potential was then increased to +100 mV for 30 seconds to allow nitrite to bind to the oxidised heme. No catalysis should be detectable. The cell was then poised at the desired intermediate potential, Figure 4.16 A. At

the immediate potentials of -250 and -275 mV the H264N enzyme displayed an increase in catalysis with time revealing that nitrite was slowly dissociating from the H264N NrfA. The increase at -275 mV was faster indicative of a quicker rate of nitrite dissociation from the active site at more negative potentials.

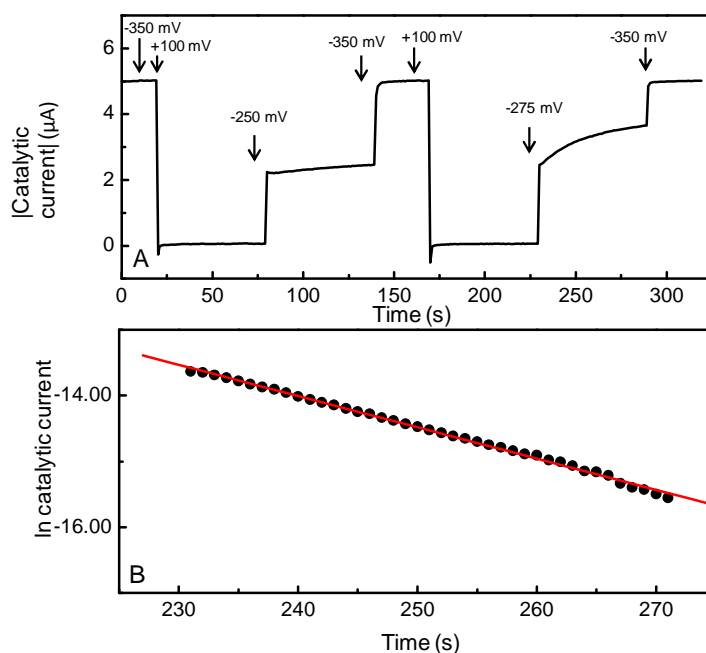


Figure 4.16- Potential dependence of nitrite binding to H264N NrfA. (A) Chronoamperometry performed on H265N NrfA in the presence of 28 mM hydroxylamine 2 µM nitrite. (B) Semi natural log plot of the change in catalytic current against time for the H264N film poised at -275 mV, to allow the first order rate constant for nitrite dissociation from H264N NrfA to be determined using, equation 4.8.

The increase in catalytic current upon poisoning at a defined potential is proportional to the increase in concentration of free H264N NrfA formed from the dissociation of the H264N:NO₂⁻ inhibitor complex. This can in turn be equated to the decrease in concentration of H264N:NO₂⁻ complex. Plotting the natural log of the current magnitude against time shows a straight line which indicates that the process is first order, Equation 4.8.

$$\ln|i| \propto \ln[\text{H264N:NO}_2^-] = -kt + \ln[\text{H264N:NO}_2^-]_{t=0}$$

Equation 4.8

Where (ln|i|) is the natural log of the current magnitude, ln[H264N:NO₂⁻] is the natural log of the concentration of the H264N nitrite complex at a defined time, here k is the rate

constant, t is time and $\ln[\text{H264N:NO}_2]_{t=0}$ is the concentration of the H264N nitrite complex at time zero. Plotting the natural log of the catalytic current against time yields a gradient equal to $-k$. The rate constant for nitrite dissociation at -275 mV was calculated to be 0.047 s^{-1} , Figure 4.16 B. This corresponds to a reaction half life of 14.7 s.

To determine the rate of nitrite dissociation from H264N NrfA over a range of potentials, the experiment was repeated for steps from $+100$ mV to a range of potentials to define the k_{app} vs. potentials, Figure 4.17. At the most positive potentials (-200 mV and -225 mV) there is an initial increase in the catalytic current but no change in catalytic current over time. This indicates that nitrite association and dissociation are at equilibrium therefore catalysis is occurring under steady state conditions for the uninhibited H264N NrfA. At more negative potentials (-250 , -275 and -300 mV) the initial catalytic current was followed by an increase in catalytic current with time indicating the population of nitrite bound H264N NrfA releasing bound nitrite. At -300 mV the increase in current reached a plateau after 30 s, as the enzyme reached a steady state for the association and release of nitrite from the reduced active site.

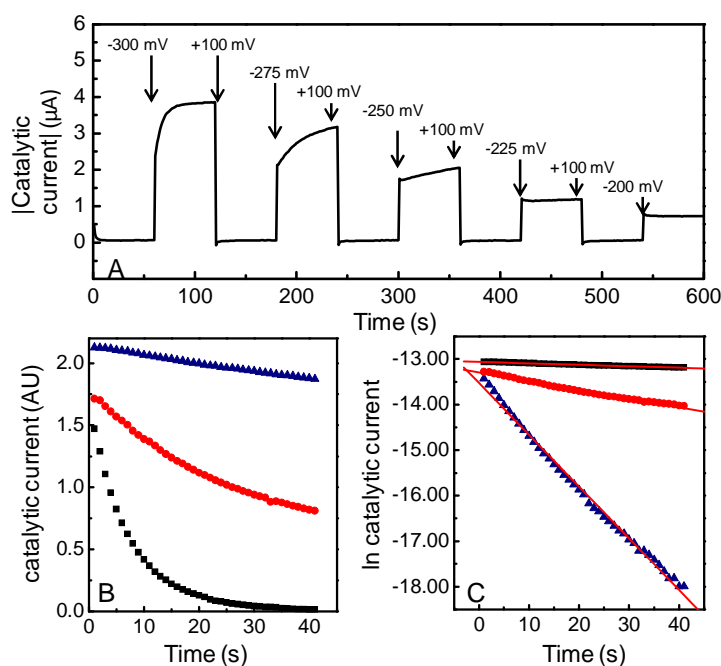


Figure 4.17 - Potential dependence of nitrite dissociation from H264N NrfA. (A) Chronoamperometry performed on H265N NrfA in the presence of 28 mM hydroxylamine 2 μM nitrite. (B) Change in the concentration of nitrite bound H264N over time when the protein is poised at -300 mV (black), -275 mV (red) and -250 mV (blue) as reported by the change in current after poisoning from (A). (C) Determining the first order rate constant for nitrite dissociation from H264N NrfA at -300 mV (black), -275 mV (red) and -250 mV (blue).

Fitting the data for a first order reaction using equation 4.8 yielded rate constants shown in Table 4.2. These reveal that the rate of nitrite dissociation is potential dependent with faster rates observed at more negative potentials Figure 4.17 A & B.

Potential (mV)	Rate constant (s^{-1})	Reaction half-life (s)
-300	0.1138 ± 0.0013	6
-275	0.0191 ± 0.0003	36
-250	0.0033 ± 0.0001	210

Table 4.2 - Rate constants for the dissociation of nitrite from H264N NrfA at various potentials after being poised at +100 mV for 60 seconds, (see Figure 4.16).

To assess nitrite association with H264N NrfA the enzyme was poised at -300 mV, where binding is weakest, then stepped to a more positive potential, Figure 4.18 A. the change in potential resulted in an initial drop in the current magnitude followed by a slow decrease over time. The decrease in current over time was slower than that for nitrite release, and with little evidence for potential dependence. This was confirmed by quantitative analysis, Figure 4.18 A and B. The rate of association is likely to be second order as it will be dependent of the concentration of nitrite and H264N NrfA. The lower concentration of enzyme compared to the nitrite means that the first order approximation can be made. This means that the rate is only dependent on enzyme concentration, as the effective nitrite concentration is unaltered because it is in a large excess. Making these assumptions, the semi log plot of change in catalytic current against time was well described as linear, with measured k values shown in Table 4.3.

The chronoamperometry experiments revealed that nitrite dissociation and association were described by different rate constants and potential dependent behavior. The rate of association appeared to be slow and independent of the potential, over the potential range examined. The kinetic constants determined by chronoamperometry are in agreement with the qualitative observations made of nitrite association and dissociation.

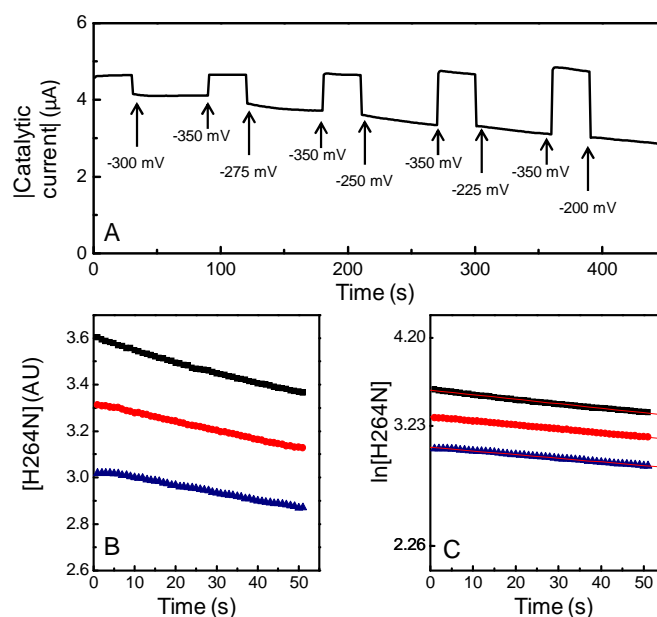


Figure 4.18- Nitrite association to H264N NrfA as a function of potential. (A) Chronoamperometry performed on H265N NrfA in the presence of 28 mM hydroxylamine $2 \pm 0.5 \mu\text{M}$ nitrite and poised at potentials indicated. (B) Change in the concentration free H264N over time when the protein is poised at -275 mV (black), -250 mV (red) and -225 mV (blue) as reported by the change in current after poising from (A). (C) Determining the Pseudo-first order rate constant for nitrite dissociation from H264N NrfA at -275 mV (black), -250 mV (red) and -225 mV (blue).

Potential (mV)	Rate constant ($\text{M}^{-1} \text{s}^{-1}$)	Reaction half-life (s)
-275	650 ± 64	769
-250	600 ± 27	833
-225	545 ± 41	917

Table 4.3- Rate constants for the dissociation of nitrite from H264N NrfA at various potentials after being poised at -350 mV for 60 seconds, (see Figure 4.17).

4.4 Discussion

The reduction of nitrite to ammonia by NrfA has been proposed to be initiated by the binding of nitrite to the distal position of the high-spin active site heme in which the iron is in its ferrous state [50, 73]. Due to the high specific activity of NrfA for nitrite, as soon as nitrite is bound to the ferrous active site the molecule is immediately reduced, forming ammonia. The speed of the reduction has prevented the characterisation of the interaction of the

reduced NrfA and nitrite, leaving only the interaction of the fully oxidized NrfA enzyme with nitrite bound to be studied as a model for the initial step of substrate reduction. The majority of the information about the interaction of nitrite with the oxidised and reduced active site of NrfA has come from crystallographic studies of oxidised NrfA and computer based methods utilising density function theory (DFT) which allowed the calculation of energies of potentials reaction intermediate complexes.

DFT calculation performed by Einsle et al suggested that the most stable form of nitrite binding was via the nitrogen atom in both the reduced and oxidised states. The DFT calculations were supported by the crystal structures of *W. succinogenes* NrfA with nitrite and hydroxylamine bound. The structures revealed that both molecules were bonded to the heme iron via the nitrogen atom. The characterisation of the interaction of nitrite with H264N NrfA has enabled further insight into the role active site His264 residue plays in nitrite binding and reduction. Chapter 3 of this thesis revealed the substitution of His264 for an asparagine residue removed the ability of the H264N NrfA variant to reduce nitrite and nitric oxide, while leaving the hydroxylamine reductase activity unaffected.

The work presented in this chapter shows that the loss of the stabilising hydrogen bond between the histidine and nitrite molecule in H264N NrfA does not affect nitrite binding in the oxidised state. The spectroscopically monitored titration of nitrite to air oxidised solutions of WT and H264N NrfA revealed nitrite was still able to bind to the active site hemes with comparable K_d^{ox} values for both proteins. The binding of nitrite to the reduced protein was confirmed by the observation that nitrite was a competitive inhibitor of hydroxylamine reduction. However for the H264N protein the K_d^{red} was much higher than the K_d^{ox} revealing the enzyme has a lower affinity for nitrite in the reduced state. When this is compared to WT the K_d^{red} which can be approximated to the K_M for nitrite reduction, the value is very similar to the WT K_d^{ox} value. This would indicate that the His264 residue is vital for high affinity binding of nitrite to reduced NrfA. Given that nitrite can bind to the H264N NrfA, although with a lower affinity than WT in the reduced state, it is not the lack of nitrite binding that causes the loss of nitrite reduction. Instead, it maybe that Histidine 264 is essential to enable the correct orientation of the nitrite to allow its reduction to ammonium. This ability to correctly orientate the nitrite molecule is lost when the H-bond donor is lost by the introduction of the asparagine residue at position 264.

For reduction of nitrite to occur it has been proposed the molecule must bind via the nitrogen atom (Fe-NOO⁻), Figure 4.1 A. In the H264N NrfA the loss of the hydrogen bond provided by the histidine residue could favour a different conformation. One possibility is

'end on' binding with an oxygen atom of the nitrite molecule coordinated to the heme iron (Fe-ONO⁻). Although this binding mode has not been observed in NrfA or *cd*₁ nitrite reductase, it has been documented in horse heart myoglobin, Figure 4.18 [8, 74]. Within the myoglobin the nitrite molecule has been shown to bind via a single oxygen in both the oxidized and photo reduced states. This orientation is stabilised by a hydrogen bond with an active site histidine residue. Myoglobin has been documented to reduce nitrite to nitric oxide. However, the mechanism for this reduction is not known so therefore the end on binding may not be relevant for substrate reduction.

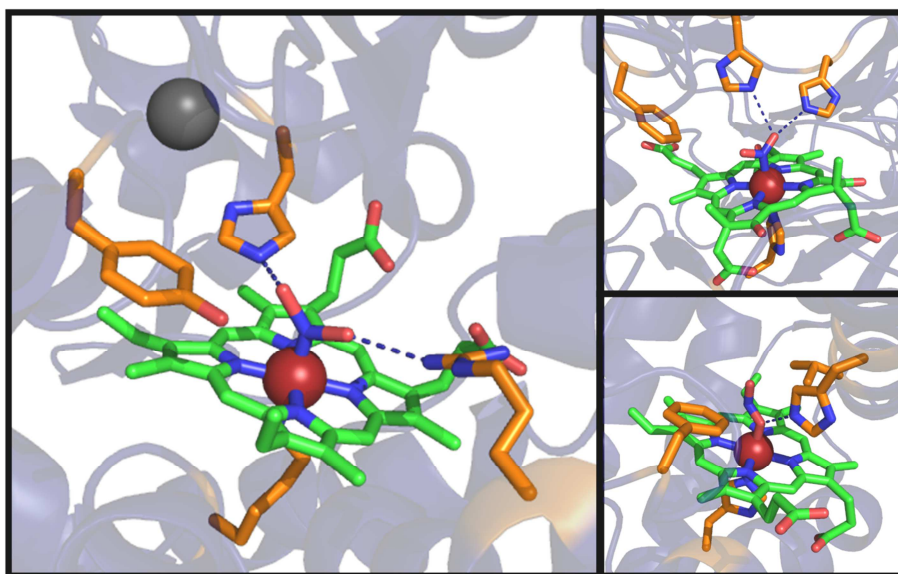
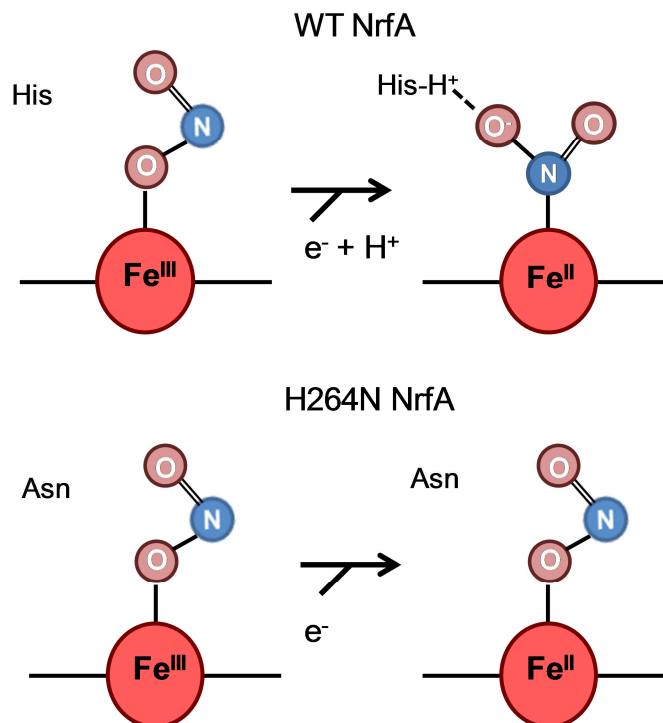


Figure 4.18- The crystal structure of nitrite bound heme adducts. (A) WT NrfA from *W. succinogenes* (PDB 2E80) (B) *cd*₁ nitrite reductase from *Paracoccus pantotrophus* (PDB 1AOM) (C) Horse heart myoglobin (PDB 3LR7). Heme represented as green sticks with iron atom depicted as a red sphere, bound the nitrite molecule shown as sticks, active site residues shown as orange sticks and protein backbone as transparent blue cartoon.

The hydrogen bonding between the His264 residue and nitrite as seen in the WT NrfA structure is dependent upon the protonation of the histidine residue. The pK_a of the imidazole group is around 7 meaning the protonation reaction is likely to occur at physiologically relevant pHs. The protonation of the histidine is likely to be favoured as the active site heme is reduced. This would mean that the reduction of the active site heme could cause the active site histidine to be protonated which in turn could be the switch that allows the nitrite molecule to adopt the nitrogen bonding mode, Scheme 4.3. In this model in the oxidised state with nitrite binding to WT and H264N enzymes is the same, reflecting the similar K_d^{ox} values. The higher K_d^{red} for H264N compared to WT NrfA is then due to the

inability of the asparagine residue at position 264 to be protonated, which would facilitate the correct orientation of the nitrite molecule to enable high affinity binding.



Scheme 4.3- Nitrite binding to the oxidised and reduced form of H264N NrfA.

It is also important to note that studies of H264N with nitrite bound revealed the active site heme had a midpoint potential of -300 mV, which would mean that if nitrite binds to the enzyme prior to reduction of the heme increased driving would be required for reduction, compared to if nitrite binds after reduction of the heme and protonation of the His264 residue. Such a mechanism would have physiological advantages such as when substrate was plentiful but the availability of electrons was limited catalysis would only commence at lower potentials, at which point more of the low-spin hemes would be reduced. This would increase the reservoir of electrons available prior to the onset of catalysis and prevent the possible release of reaction intermediates or the generation of low energy states that could create thermodynamic traps in the catalytic cycle. This would especially be important in the bacteria that use NrfB as the electron transfer partner to the NrfA, as the NrfA protein is more distant from the quinol dehydrogenase (NrfCD). This could cause a more sporadic supply of electrons compared the NrfHA system, which sees the catalytic subunit in direct contact with the quinol dehydrogenase (NrfH).

In closing this chapter PFE has shown that nitric oxide can be reduced by WT but not the H264N NrfA. Using nitric oxide as a substrate should circumvent the initial stages of nitrite reduction in which the first N-O bond is cleaved and therefore negate the need for the hydrogen bond provided by the histidine residue. The observation that nitric oxide reduction is not catalysed by the H264N would suggest that the histidine residue is also vital for additional stages of the NrfA nitrite reduction mechanism. The orientation of the nitric oxide molecule within the NO-bound intermediate is not known but the crystal structure of *W. succinogenes* NrfA with hydroxylamine bound shows that the oxygen atom of the hydroxylamine molecule interacts with the arginine residue and not the histidine residue. This would suggest that when the first N-O bond is broken the NO bound intermediate does not undergo a reorganisation in which the oxygen become stabilised by the histidine residue.

Histidine 264 is likely to act as a proton donor to the NO intermediate, allowing protonation of the nitrogen atom. The carboamide functional group of the asparagine is unable to accept a proton because its lone pair of electrons are delocalised over the carboamide functional group. The pK_a of the imidazole group is around 7, meaning the protonation reaction is likely to occur at physiologically relevant pHs. The inability of the asparagine to accept and donate protons could prevent the reduction of nitric oxide as the nitrogen atom of the NO-bound intermediate needs to be protonated to allow the reduction to continue. This protonation step will require a proton donor that has a suitable pK_a and orientation towards the nitrogen atom. Both of these requirements could be fulfilled by the native histidine but not the substitute asparagine residue in the H264N enzyme or conserved water molecules within the active site. The inability of the H264N enzyme to reduce nitric oxide therefore implies that the native histidine residue may be the only residue able to carry out the protonation of the nitrogen atom of the NO bound intermediate.

Chapter 5

**The importance of proximal
lysine ligation to the active
site heme in NrfA**

Chapter 5 - The importance of proximal lysine ligation to the active site heme in NrfA

5.1 Introduction

In c-type cytochromes, the heme group is normally covalently attached to two cysteine residues via thioether bonds. The cysteine residues are present within a CxxCH motif in which the histidine forms the proximal ligand to the heme iron. There are only 10 cysteine residues in the *E. coli* NrfA protein, eight of which are organized in four conventional heme binding motifs. The remaining two are found in a CxxCK motif in which the histidine residue has been replaced by a lysine residue. The novel CxxCK motif was confirmed to be a site of heme attachment with lysine forming the proximal heme ligand in the first structure published of NrfA [31]. There are however a number of ϵ -proteobacteria e.g. *C. jejuni*, which do not contain the novel CxxCK motif but instead maintain the conventional CxxCH motif. To date there are no structures of this class of NrfA protein. Therefore it is not possible to confirm if the active site heme is ligated by the histidine residue present within the CxxCH motif. The structure of octaheme tetrathionate reductase (OTR) from *Shewanella oneidensis* contains an active site heme that is attached via a CxxCH motif, but in the protein the histidine ligand is displaced by a lysine located on a nearby loop region [43]. An advantageous heme ligation such as this could enable the *C. jejuni* NrfA protein to have a CxxCH heme binding motif yet allow the active site heme to be ligated by a lysine residue. However, this could only be confirmed by obtaining a crystal structure.

The recognition of the CxxCK heme binding motif in the NrfA requires novel heme lyase proteins which adapt the CCM machinery to allow the heme to be attached to the protein. The heme lyase proteins are encoded by genes found within the Nrf operon. They are the *nrfEFG* genes in γ -proteobacteria and the *nrfIJ* genes in ϵ - and δ -proteobacteria [30]. The requirement for the expression of heme maturation proteins to allow the production of a functioning NrfA molecule represents an increased energy investment, compared to producing a NrfA molecule with five CxxCH motifs. This would suggest that the lysine ligated heme is vital for the activity of NrfA as it has been evolutionary conserved in the majority of *nrfA* gene sequences. To further explore the importance of the lysine ligation to the active site heme, the lysine 126 residue of *E. coli* NrfA has been substituted for a histidine residue. The aim of this work was to characterise the K126H NrfA protein, reveal if a histidine residue is able to coordinate the active site heme and examine how the NrfA characteristics depend upon the nature of the residue that immediately follows the CxxC

motif. While the work in this chapter begins to address these aims, it does not however lead to a clear conclusion and further work will be required to fully appreciate the role of the lysine 126 residue. In light of this, the data will be presented and discussed with further work suggested to address the questions that have been raised in the process of the initial characterisation of the K126H NrfA variant.

5.2 The 2.3 Å structure of K126H NrfA reveals a modified active site

The K126H NrfA variant crystallised under the same conditions as WT NrfA and formed crystals with a space group of $P2_1$. Molecular replacement generated an initial structure model containing four NrfA monomers within the asymmetric unit. The lysine 126 residue present within the initial model was substituted for a histidine residue and the structure was refined to a final resolution of 2.3 Å. Data and refinement statistics are displayed in Table 2.3. The substitution was confirmed by generating a composite simulated annealing omit density map, Figure 5.1. With a lysine residue modelled into the electron density of the active site heme ligand, the lysine side chain folds around on itself. The amine group is located away from the heme iron, an orientation that is not observed in WT NrfA. When a histidine residue is modelled in position 126 the density fits well to the imidazole ring of the histidine residue. These observations validate the substitution was successful.

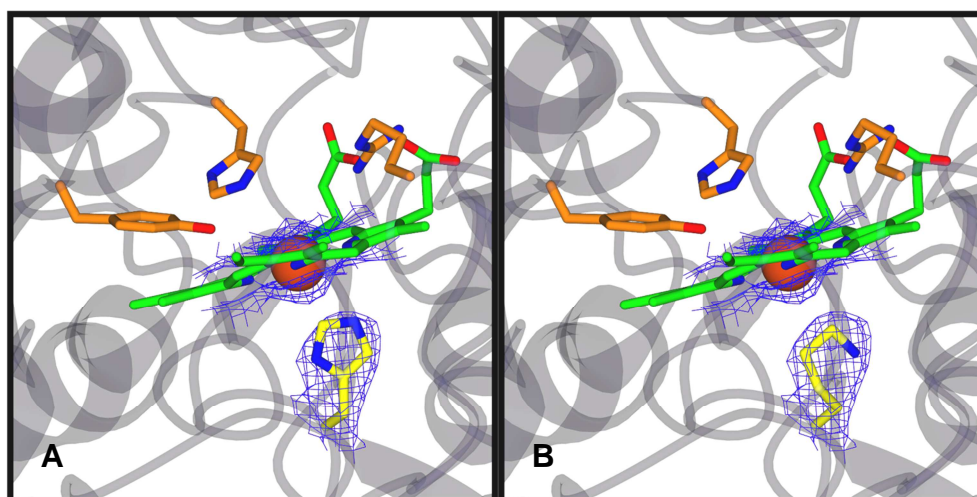


Figure 5.1 - Composite simulated annealing omit electron density map of K126H NrfA clipped around the histidine residue that forms the active site heme ligand and the heme iron (blue mesh) (σ 1.3). (A) The omit map is overlaid with the protein model in which the residue in position 126 is occupied by a histidine. (B) The Omit map is overlaid with a protein model in which a lysine residue occupies position 126. The active site histidine/lysine residue shown as

yellow sticks, residues of R106, Y216 and H264 shown as orange sticks and active site heme shown in green sticks with the iron represented as an orange sphere, the protein is shown in blue ribbon (transparent). Figures generated using ccp4mg.

The bis-His heme ligation of heme 3 of K126H NrfA contoured to σ 1.3, reveals how the electron density spans from the heme iron to both the proximal and distal histidine ligands indicating ligation of the heme iron, Figure 5.2 B. This behaviour is also seen in the ligation of the other three low-spin hemes in K126H NrfA and those in the WT protein. The position of the histidine residues allows the nitrogen atom of the imidazole ring to form the ligation of the heme iron with a Fe-N distance respectively of 2.04 ± 0.02 Å for the proximal and 2.06 ± 0.02 Å for the distal ligands, values are averages of the four bis-His hemes in the K126H monomer.

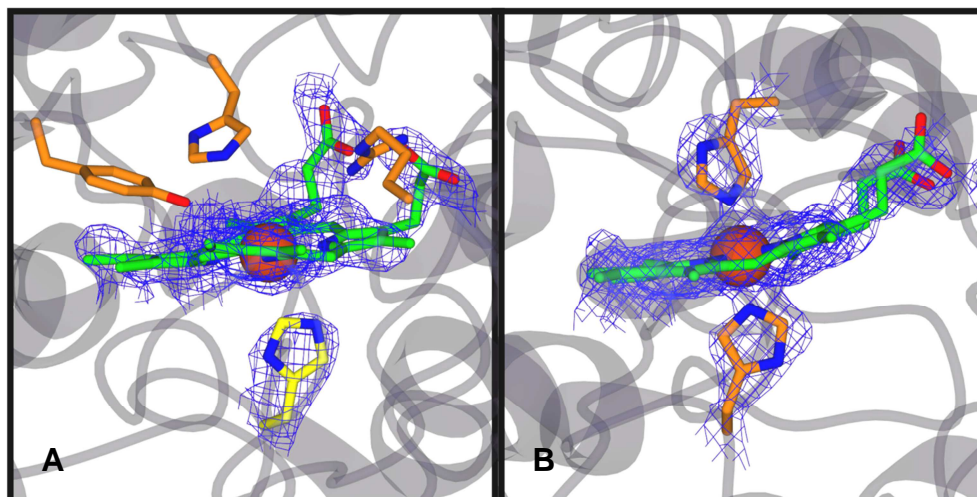


Figure 5.2 - Composite simulated annealing omit electron density map of K126H NrfA of the active site heme and heme 3 of K126H NrfA. (A) Omit electron density (blue mesh) clipped around the active site heme and ligand (σ 1.3), Orange sticks represent the NrfA catalytic triad, yellow sticks the substitute histidine residue and green sticks the heme cofactor. (B) Omit electron density (blue mesh) clipped around heme 3 of K126H NrfA and the proximal and distal histidine ligands (σ 1.3). Orange sticks represent the histidine ligands and green sticks the heme cofactor. The protein backbone is shown as blue ribbon (transparent) in both panels. Figures generated using ccp4mg.

The preferred orientation for the histidine 126 residue places a carbon atom closest to the heme iron at a distance of 2.66 ± 0.13 Å. The nearest nitrogen atom is located 3.32 ± 0.16 Å. Both distances are too great to form a bond to the heme iron. However, the imidazole ring has freedom to rotate and therefore the position of the carbon and nitrogen could be reversed. Even with rotation of the histidine residue the distance and the electron density

suggests the H126 is not a ligand to the heme iron. The increase in distance is caused by the histidine residue being slightly shorter and less flexible than a lysine residue.

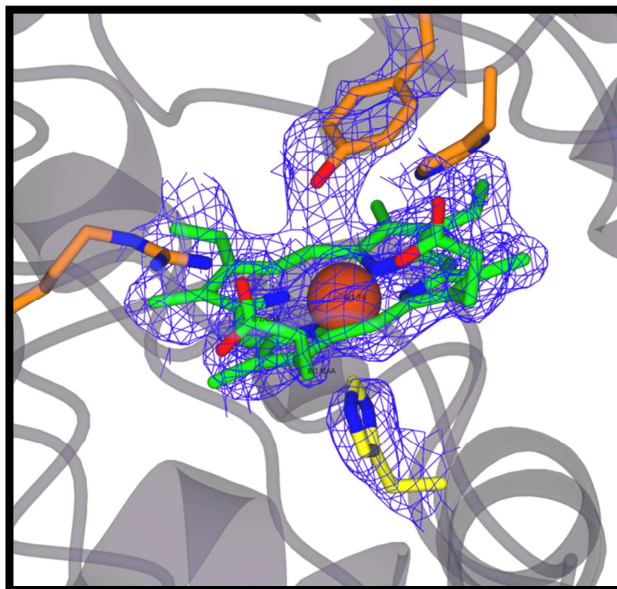


Figure 5.3 – The active site of K126H NrfA. Composite simulated annealing omit electron density (blue mesh) clipped around the heme cofactor and the H126 and Y216 residues and contoured to σ 1.3. Electron density propagates from the tyrosine residue to the 5' meso position of the porphyrin ring. Orange sticks represent the NrfA catalytic triad, yellow sticks the substitute histidine residue and green sticks the heme cofactor, with the protein backbone as transparent blue ribbon. Figures generated using ccp4mg.

The active site heme group is covalently bound to the protein via the two cysteine residues of the *c*-type heme-binding motif, Cys122 and Cys125. However, an unexpected feature of the active site of K126H NrfA is that there is evidence of a third covalent linkage to the porphyrin ring from the conserved Tyr216, Figure 5.3. The appearance of electron density propagating between the phenol oxygen of the tyrosine to the 5' meso position of the active site heme suggests a covalent bond is formed between the heme and tyrosine residue. The covalent attachment results in the tyrosine residue moving $\sim 1\text{\AA}$ closer to the heme plane than in the WT structure. The resultant (O-C) covalent bond length varies between monomers within the asymmetric unit. The lengths range from 1.92 to 2.18 \AA with the average length being $2.04 \pm 0.11 \text{\AA}$. The position of the bond out of the heme plane would suggest that the meso carbon has changed from sp^2 to sp^3 hybridised, which will disrupt the conjugation of the porphyrin pi system and convert the heme from a porphyrin into a phlorin. Such a covalent attachment has not been observed in WT NrfA structures that have been published previously, or any of the active site variants that have been discussed in this work.

5.3 Spectroscopy revealing the coordination environment of the active site heme of K126H NrfA

The presence of the covalent attachment within the crystal structure does not directly imply that the modified heme is present in solution. The process of collecting x-ray diffraction data exposes the protein crystal to large amounts of ionising radiation. This could cause the formation of radical species that could give rise to the features seen in the K126H protein. Radiation damage to metal containing protein has been documented previously [75]. The presence of varying bond lengths in the four NrfA monomers within the asymmetric would indicate that there is likely to be a mixed population of the covalently modified and unmodified heme during data collection.

The spectroscopic properties of K126H NrfA in solution are similar to those of WT NrfA with the Soret maximum occurring at 408 nm in the oxidised proteins. Upon reduction the maximum shifts to 420 nm, Figure 5.4. The alpha and beta bands appear with maxima at 524 and 552 nm in reduced forms of both proteins. The absorbance arising from the oxidised and reduced high-spin heme was not observed in the absorbance spectra or the first derivative of spectra of either WT or K126H NrfA presented in Figure 5.4. This has previously been discussed in relation to WT NrfA, in which the appearance of the reduced high-spin heme is likely to be prevented by the presence of sulphite introduced by the use of dithionite as a reductant. The presence of sulphite is likely to have the same effect in the K126H protein. Therefore any changes to the spectroscopic properties of the high-spin heme caused by the change in ligation or the potential presence of a covalent attachment may not be observed due to the binding of sulphite.

The crystal structure of K126H indicated that the histidine residue that forms the ligand to the heme iron adopted an unfavourable position to allow effective ligation. This will likely result in a weakened Fe-His bond. The weak ligation raises the possibility that a proportion of the population of the active site high-spin heme of the K126H protein is tetra-coordinated, caused by the loss of histidine ligation. The most well documented examples of hemes with no protein derived ligand are those of guanylate cyclase and cytochrome *c'*. When these proteins are exposed to nitric oxide the heme loses histidine coordination and forms a penta-coordinate NO heme complex [76, 77]. Under these circumstances the binding of nitric oxide causes a weakening of the distal bond by the trans effect of the nitric oxide molecule. A bis-NO complex is thought to form prior to the penta-coordinate species in which the nitric oxide molecule is located on the proximal face of the heme [70, 78].

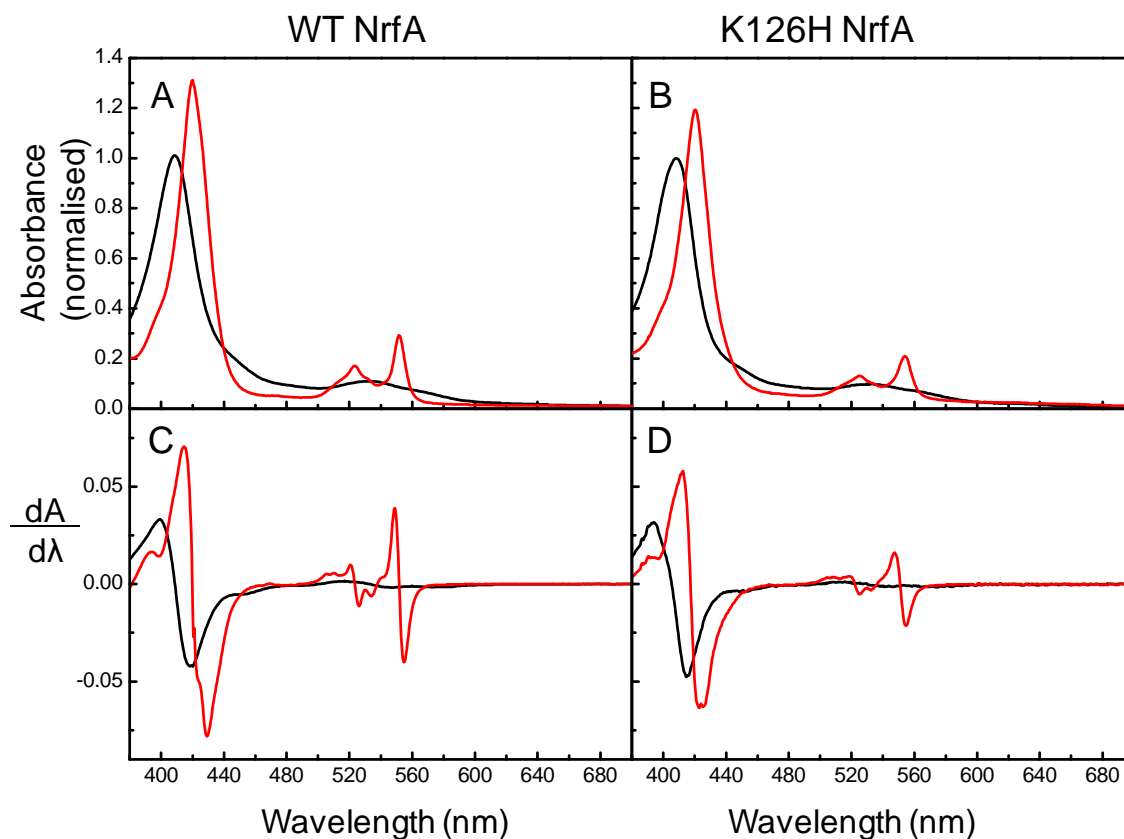


Figure 5.4- Electronic absorbance spectra of air-oxidised and dithionite reduced WT and K126H NrfA. A and B WT (3.5 μM) and K126H (2.7 μM) NrfA respectively with the spectra of the oxidised (black) and reduced (red) protein shown, normalised to the absorbance at 409 nm oxidised protein spectra. C and D show the first derivative of the data presented in A and B. Buffer 2 mM CaCl_2 , 50 mM HEPES, pH 7, 4 $^\circ\text{C}$.

To determine if the addition of nitric oxide to the K126H protein resulted in the generation of protein with a hexa- or a penta-coordinated active site heme, 75 μL of nitric oxide gas was bubbled through anaerobic solution of K126H NrfA (1.3 μM) within a sealed cuvette. The spectrum of the resulting solution can be seen in Figure 5.5. The addition of nitric oxide resulted in the change of the Soret peak from 408 to 415 nm and the appearance of the alpha and beta peaks at 531 and 564 nm. More information can be gained from the difference spectra of the nitric oxide bound – no nitrite oxide. The difference spectra reveals the greatest change in absorbance was at 400 to 419 nm, showing the ferric high-spin heme has an absorbance at 400 nm whilst the nitric oxide bound heme has an absorbance at 419 nm, Figure 5.5. Upon nitric oxide binding the heme is likely to have become auto reduced by the nitric oxide molecule. There is, however, some uncertainty on the position of the electrons and therefore the formal charge on the iron in the NO bound complexes is difficult to assign, especially in multi heme proteins [50].

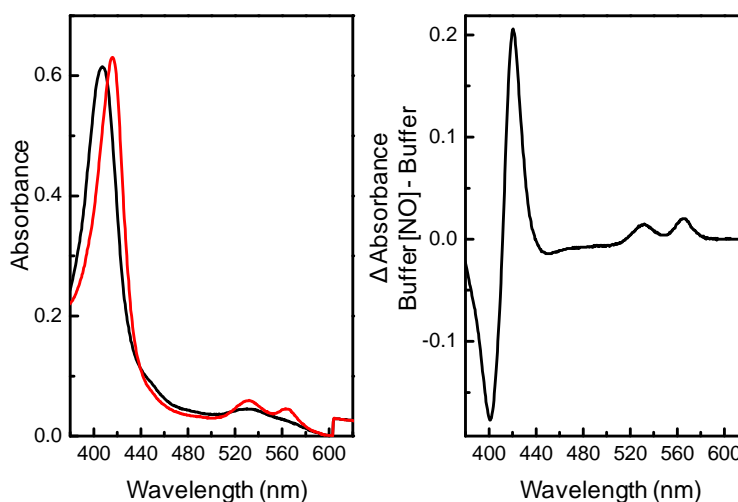


Figure 5.5- Nitric oxide binding to oxidised K126H NrfA. (A) Electronic absorbance spectra of K126H in an atmosphere of nitrogen (black) and exposed to 75 μ L of nitric oxide gas (red). (B) Difference absorbance spectra K1264:NO – K126H, change in absorbance indicating the formation of a nitric oxide bound hexa-coordinated active site heme. Buffer 2 mM CaCl_2 , 50 mM HEPES, pH 7, 21 $^\circ\text{C}$

The change in the absorbance of the active site heme K126H NrfA from 400 to 419 nm when exposed to nitric oxide can be reasonably assigned to changes in the high-spin heme and would suggest a hexa-coordinated heme iron is present, most likely with the substitute histidine residue as the proximal ligand and the nitric oxide binding at the distal position. This would suggest that in solution the histidine heme bond is stronger than is indicated by the crystal structure. The bound nitric oxide molecule should have a further weakening effect but the histidine ligation appears to be maintained.

The covalent modification of the porphyrin ring that was suggested in the crystal structure would affect the conjugated pi of the porphyrin ring. The conversion of a sp^2 hybridised carbon atom to a sp^3 would remove a double bond from the extended conjugated pi system, thus removing the macrocyclic properties of the porphyrin ring. Such a change is seen in hydroxylamine oxidoreductase which has a covalently modified active site heme with a maximum at 463 nm in the reduced protein. The spectrum of the reduced K126H protein has no indication of a 640 nm band making the presence of a tyrosine-heme crosslink unlikely. However, the high-spin heme is not clearly visible in the oxidised or reduced spectra.

5.4 Potential dependence of the redox cofactors in K126H

NrfA

The spectra of the fully oxidised and fully reduced WT and K126H NrfA adsorbed on to SnO₂ electrodes is presented in Figure 5.6. The four low-spin hemes of WT and K126H NrfA displayed the same features as they do in solution, with the appearance of well defined alpha and beta peaks at 523 nm and 552 nm and the Soret peak at 420 nm for the reduced protein. The high-spin heme contribution to the Soret region was observed as a shoulder on the Soret peak, with an absorbance at 435 nm in K126H NrfA compared to 442 nm in WT NrfA. The first derivative of the absorbance over wavelength of the reduced WT and K126H proteins clearly shows the high-spin heme features of both proteins compared to solution spectroscopy. The absorbance arising from the high-spin heme has blue shifted by 7 nm in the K126H protein compared to WT NrfA. The presence of the Soret band at 435 nm would suggest that the active site heme is likely to be present as a penta-coordinated high-spin with histidine 126 as the heme ligand. The absorbance 435 nm is in agreement with the Soret maximum of histidine ligated ferrous high-spin heme cytochrome *c'* from *Alcaligenes xylosoxidans*, which has a split Soret peak with absorbance maxima at 425 and 435 nm [79].

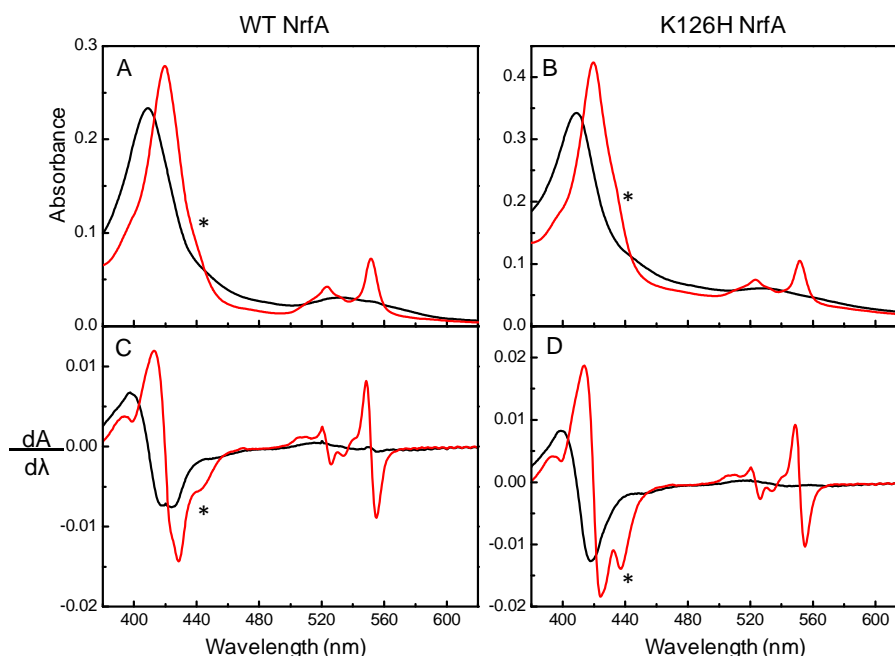


Figure 5.6- electronic absorbance spectra of WT and K126H NrfA adsorbed onto mesoporous SnO₂ electrodes. Electronic absorbance spectra of fully oxidised poised at +240 mV (black) and fully reduced poised at -600 mV for WT (A) and +241(black) and -559 mV (red) for K126H (B)

NrfA. First derivative of spectra presented in panels A and B, Black line fully oxidised and red line fully reduced protein for WT (C) and K126H (D) NrfA. * denotes the absorbance arising from high-spin heme. Buffer-electrolyte 2 mM CaCl₂, 50 mM HEPES, pH 7, 4 °C.

The midpoint potential for the hemes in K126H NrfA was determined by a spectroscopically monitored redox titration. The protein film was poised at increasingly negative potentials from +151 to -509 mV then was exposed to increasingly oxidising potentials, and at each potential absorbance spectrum was recorded, Figure 5.7 A and B. The spectra recorded on the reductive and oxidative titrations showed different characteristics. The oxidised spectra had increased absorbance in the 435 nm region at more oxidising potentials, compared to the reductive titration. This difference can be more readily observed in the adjacent difference absorbance spectra calculated for potential windows of 80 mV, Figure C and D. As the K126H protein is reduced positive features are observed at 420 nm and 552 nm that relate to the reduction of low-spin hemes. Another positive feature is also observed at 435 nm. This feature is only observed between +71 to -89 mV and relates to the reduction of the single high-spin heme within the K126H protein. The adjacent difference spectra of the oxidative titration contained the same features for the low-spin hemes that arise in the reductive titration.

However, the feature at 435 nm is different in the oxidative titration the feature is predominately confined to the potential window from +71 to -9 mV. The feature also has a greater magnitude, suggesting that the redox transition that occurred over a 160 mV range in the reductive sweep occurred over 80 mV window in the oxidative titration. The absorbance spectra indicate that the K126H protein has different behaviour in the reductive and oxidative titration, suggesting that the protein had not reached equilibrium during the experiment.

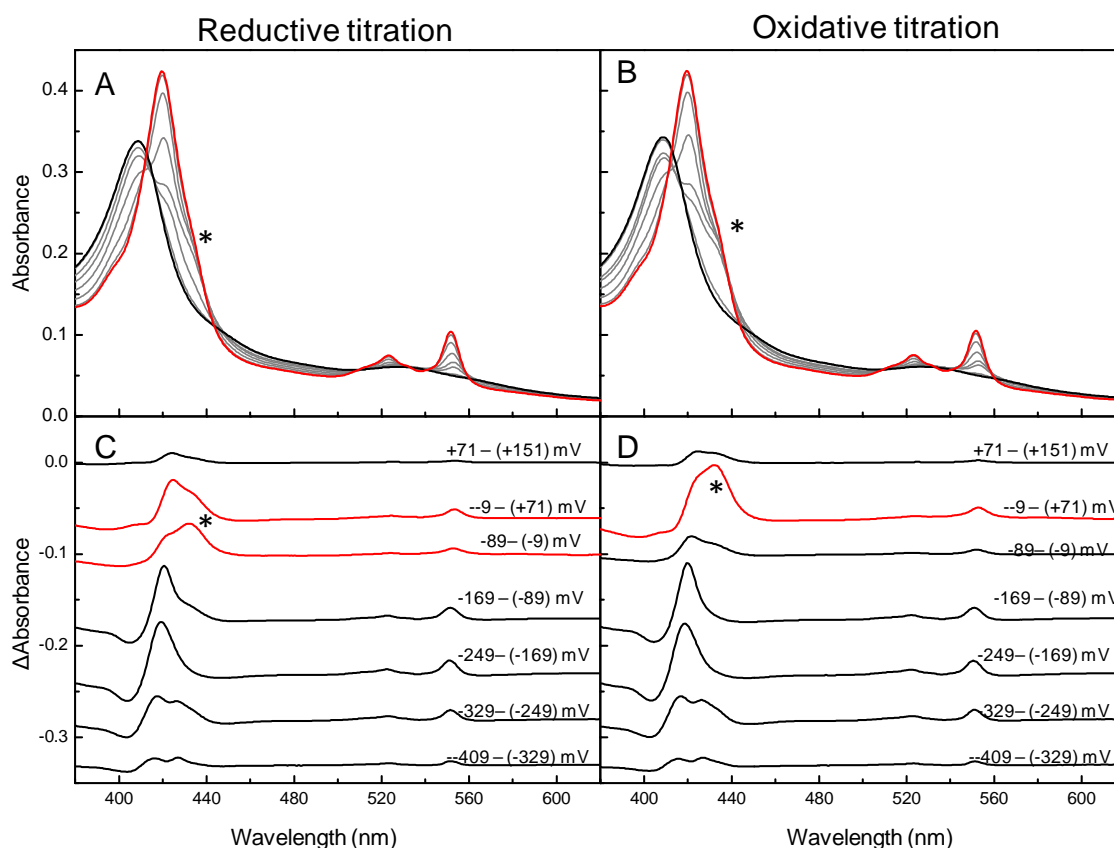


Figure 5.7- Spectropotentiometry of K126H NrfA immobilised on mesoporous tin oxide. Electronic absorbance spectra of the reductive (A) and oxidative (B) titration. Fully oxidised K126H NrfA poised at +151 mV (black), fully reduced poised at -559 mV (red) and intermediate potentials (grey). Spectra were recorded at sequential potentials. Difference spectra (reduced poised – oxidised poised at potentials indicated) of H264N reductive (C) and oxidative titration (D). Buffer-electrolyte, 2 mM CaCl₂, 50 mM HEPES, pH 7, 4°C

To further characterise the redox transitions of the hemes within K126H NrfA the mid-point potentials for the low- and high-spin hemes were resolved. Those for the four bis-His low-spin hemes were determined from the potential dependence of the absorbance intensity at 552 – 582 nm, Figure. 5.8. The reductive and oxidative titrations were overlaid and the data was well described as the sum of four independent one-electron processes that equally contribute to the total change in absorbance. This analysis generated mid-point potentials of +20, -125, -210, -310 mV (all ± 15 mV) for the low spin hemes in K126H NrfA at pH 7, compared to values for WT NrfA +15, -135, -200 and -320 mV (all ± 15 mV) under the same conditions.

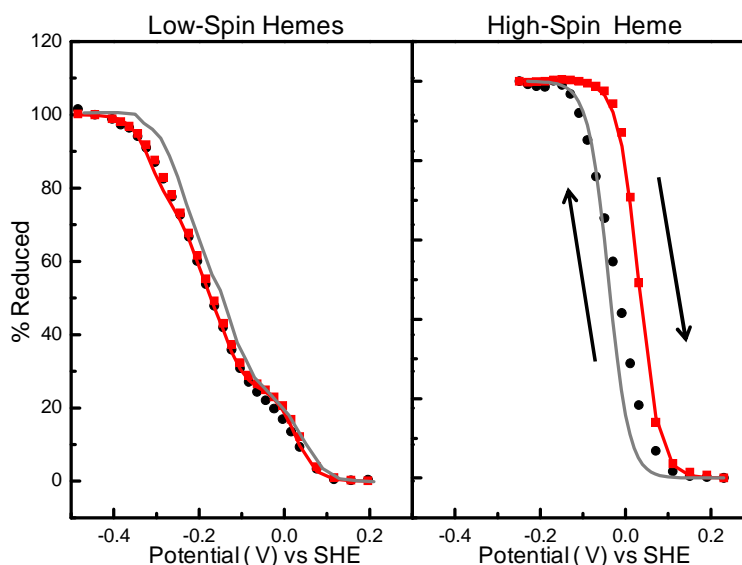


Figure 5.8- Nernst plots reductive (●) and oxidative (■) redox titrations for K126H NrfA adsorbed on SnO₂ electrodes, prepared from data in Figure 5.7. The extent of reduction of the low spin hemes in K126H NrfA as reported by the A₅₅₂ - A₅₈₂, red line the sum of four independent one electron (n =1) processes for redox centres with midpoint potential (E_m) values of +20, -125, -210, -310 mV (all ± 15 mV), Grey line, the low-spin heme mid-point potentials of WT NrfA +15, -135, -200 and -320 mV (all ± 15 mV. Extent of reduction of high-spin heme as reported by the A₄₃₅, red line represents a single one electron (n=1) Nernstian response for centres with E_m values of +30 mV (±15 mV) for K126H NrfA. Grey line represents the reduction of the high-spin heme of WT NrfA as reported by A₄₃₅ - A₄₅₂, grey line the single one electron (n=1) Nernstian response for centres with E_m values of -40 mV (±15 mV). Buffer-electrolyte 2 mM CaCl₂, 50 mM HEPES, pH 7, 4 °C

The midpoint potential of the high-spin heme was resolved by the change in absorbance at 435 nm plotted against potential, Figure 5.8. The data from the reductive and oxidative titrations did not overlay. The high-spin heme was reduced over a broader range of potentials than for its reoxidation. The oxidation of the high-spin heme was described by a single one electron (n=1) process with a midpoint potential of +30 mV (± 15 mV), significantly more positive than the mid-point potential of the high-spin of WT NrfA which was found to be -40 mV (± 15 mV), Chapter 3.2.4. However a single electron Nernstian fit was unable to be made to the data produced from the reductive titration. The inability to describe the reduction of the high-spin heme as a single one electron process could be due to the protein not being fully equilibrated at the poised potential when the absorbance spectra were recorded. If the K126H protein was not at equilibrium this would suggest that the reduction of the high-spin heme is slower than the oxidation. The slow rate of reduction was only seen in the high-spin heme as the reductive and oxidative titrations for the low-spin hemes were in agreement. This would indicate that the substitution has not only

impacted on the thermodynamics of the active site heme by increasing the mid-point potential by 70 mV, it has also affected the kinetics that describe the reduction of the active site heme.

The time dependence of the appearance of the 435 nm band, thought to indicate the generation of the reduced high-spin histidine coordinated active site heme in K126H NrfA, was further explored when the K126H NrfA was exposed to fully oxidising potentials (+151 mV) and then fully reducing potentials (-559 mV). Visible absorbance spectra of the fully reduced protein were recorded every 170 seconds (2.8 minutes) for 4200 seconds (70 minutes), Figure 5.9 A. When the protein was exposed to the fully reducing potentials the absorbance spectra displayed the features of reduced low-spin hemes with the shift in the Soret maxima and the appearance of the alpha/beta bands. Over time the position of the Soret maxima and the alpha/beta peaks did not change. However, an increase in absorbance intensity at 435 nm was observed. This is clearly seen in the difference spectrum of the K126H protein poised for 70 minutes minus initial spectrum recorded when the K126H protein was first poised at -559 mV, Figure 5.9 B. The increase in absorbance at 435 nm was accompanied with a broad decrease in absorbance with a maximum at 390 nm. The increase in absorbance at 435 nm appears to slow with time suggesting a plateau in absorbance will be reached if enough time was allowed, Figure 5.9 C.

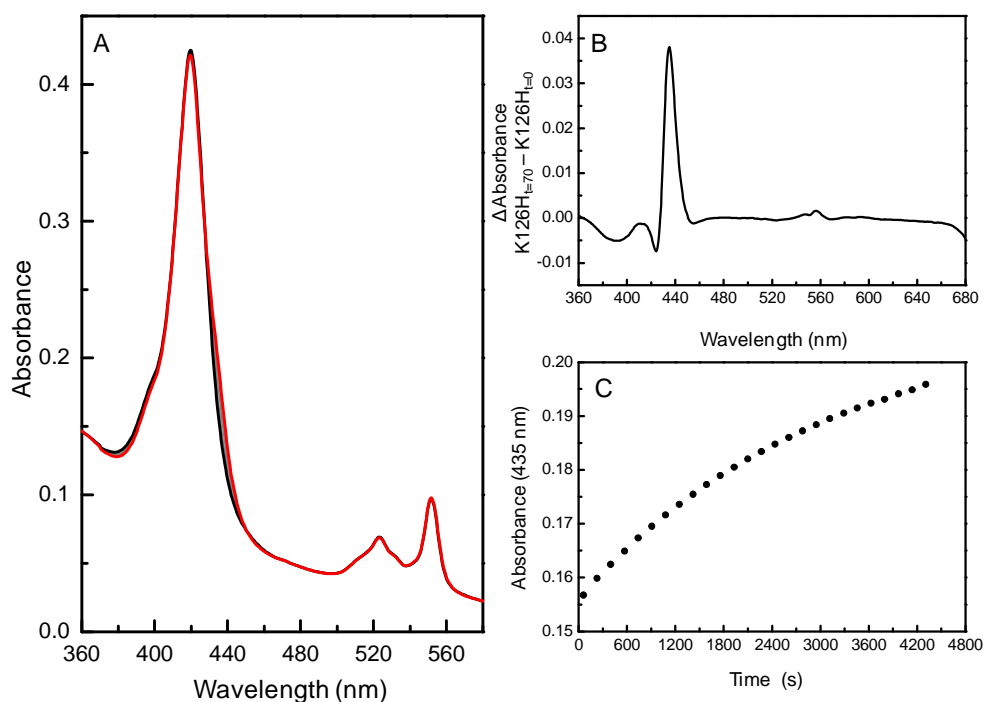


Figure 5.9- Time dependent changes in the electronic absorbance spectra of K126H NrfA adsorbed on an optically transparent SnO₂ electrode. (A) Electronic absorbance spectra of

K126H NrfA, poised at -559 mV for 60 (black line) 910, 1760, 2610, 3560 (grey lines), 4310 (red line) seconds. (C) Increase in absorbance at 435 nm with time. Buffer-electrolyte 2 mM CaCl₂, 50 mM HEPES, pH 7, 4 °C.

5.5 The catalytic properties of K126H NrfA

Spectroscopically monitored solution assays, in which dithionite reduced methyl viologen was used as electron donor to K126H NrfA, revealed the enzyme maintained both nitrite and hydroxylamine reductase activity, Figure 5.10. However, the substitution of the active site lysine ligand for a histidine severely compromised the rate of substrate reduction with the k_{cat} decreasing more than ten-fold for the reduction of nitrite and hydroxylamine substrates compared to the WT enzyme. The K_M for nitrite reduction increased from $46 \pm 5 \mu\text{M}$ in WT NrfA to $788 \pm 221 \mu\text{M}$ indicating the K126H NrfA has a lower affinity for nitrite. The affinity of hydroxylamine was unaffected as the determined K_M value for hydroxylamine reduction by K126H NrfA is similar to that observed value for WT NrfA, Table 3.3. The observed decrease in nitrite affinity indicates that the substitution of the lysine ligand must impact on the heme iron. This in turn, causes the binding of nitrite to be less favourable.

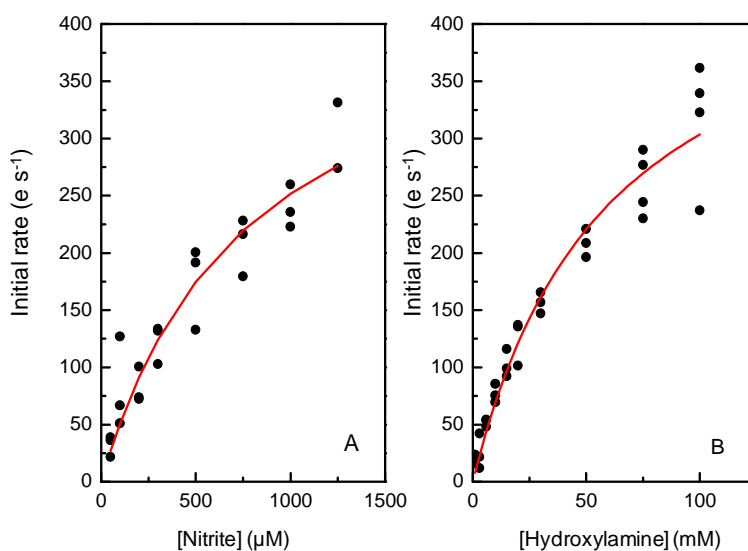


Figure 5.10- Nitrite and hydroxylamine reduction by K126H NrfA as determined by colorimetric solution assay. Initial rate of nitrite (A) and hydroxylamine (B) reduction plotted against substrate concentration, line shows the fit to the Michaelis-Menten equation fitted using non-linear regression yielding a k_{cat} of $450 \pm 66 \text{ e}^- \text{ s}^{-1}$, K_M of $788 \pm 221 \mu\text{M}$ for nitrite reduction and k_{cat} of $486 \pm 43 \text{ e}^- \text{ s}^{-1}$ and K_M of $60 \text{ mM} \pm 11$ for hydroxylamine reduction.

The reduction of nitrite by K126H NrfA was further explored by PFE of the protein adsorbed on graphite electrodes. The addition of nitrite resulted in the generation of a negative current in agreement with nitrite reduction catalysed by K126H NrfA, Figure 5.11 A. The sequential addition of nitrite caused an increase in the generated current. A plot of the catalytic current magnitude against the nitrite concentration could be described by the Michaelis-Menten equation with kinetic parameters for the K_M of 17.2 ± 4.4 mM and i_{max} of 0.71 ± 0.12 μ A. The observed parameters reveal that under the conditions of the PFE experiment the K126H enzyme displays a significantly increased K_M compared to the value obtained from the solution assay. The i_{max} observed for nitrite reduction is also very low compared to PFE performed on WT NrfA. Although direct comparison of the i_{max} values cannot be made as the amount of protein present within the film is unknown, the WT and K126H films were prepared under similar conditions with the same protein concentration so it is reasonable to presume the amount of protein present in a film is unlikely to be significantly different. The crystal structure also confirms that the overall protein structure is unaffected by the substitution of the active site residue. This suggests that the binding of the K126H protein to the electrode should not be compromised compared to the WT enzyme. Therefore the PFE would support the solution assays in describing a lower rate of nitrite turnover by the K126H enzyme.

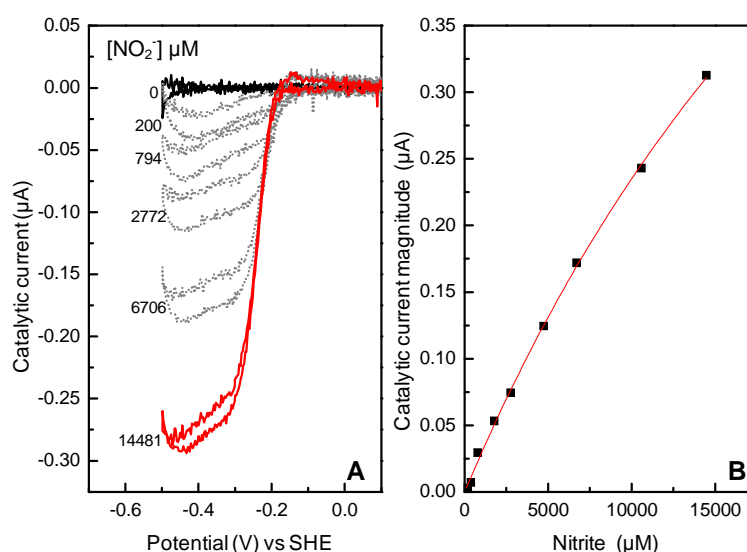


Figure 5.11- Nitrite reduction by K126H NrfA as determined by PFE. (A) Cyclic voltammograms of nitrite reduction (nitrite concentrations stated, μ M). (B) Michaelis-Menten fit to the catalytic current at -450 mV in panel A. Line shows the fit to the Michaelis-Menten equation with a K_M of 17.2 ± 4.4 mM and an i_{max} of 0.71 ± 0.12 μ A. Buffer-electrolyte 2 mM CaCl_2 , 50 mM HEPES, pH 7, scan rate 30 mVs^{-1} , rotation rate of 3,000 rpm, 20°C .

The PFE of K126H NrfA absorbed on PGE electrodes also allowed the rate of nitrite reduction to be quantified as a function of potential (+0.2 to -0.5 V). This revealed that the catalysis occurs

at more negative potentials than the WT enzyme with a single sigmoidal feature commencing at -200 mV compared to catalysis commencing at -100 mV in WT NrfA. The potential at which catalysis occurs often corresponds to the midpoint potential of the active site cofactor. This, however, is not observed in the K126H protein, as nitrite reduction occurs at potentials over 200 mV more negative than the active site heme midpoint potential. This would suggest that either the reduction of the high-spin heme is not the switch that governs nitrite reduction, the reduction potential changes upon substrate binding, or another change occurs in the protein at more negative potentials that enables K126H NrfA to adopt a catalytically active form.

Chronoamperometry performed on K126H NrfA in the presence of 14,500 μM nitrite allowed the protein to be poised at a defined potential and the change in current to be monitored as a function of time alone, Figure 5.12. The K126H protein film was poised at +297 mV for 10 seconds before being stepped to a reducing potential (-3, -103, -203, -303, -403 mV) for 300 seconds. No nitrite reduction was observed when the protein was poised at -3 and -103 mV in agreement with cyclic voltammetry experiments presented in Figure 5.11. When the potential was stepped to -203 mV a constant catalytic current was observed. On stepping to -303 and -403 mV the catalytic current generated increased with time, indicating that the enzyme was becoming activated when poised at reducing potentials. The increase in catalysis is temporary, once the protein is oxidised and then reduced the gain in activity is lost.

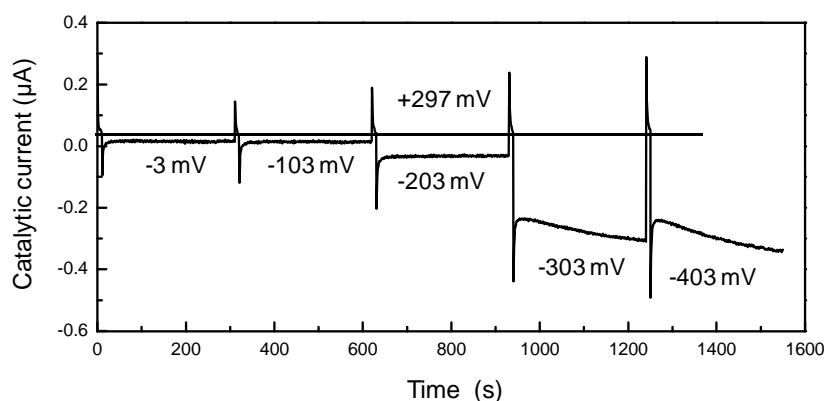


Figure 5.12- Potential dependence of nitrite reduction by K126H NrfA. Chronoamperometry performed on K124H NrfA in the presence of nitrite at 14,500 μM . Protein film is poised at +297 mV for 10 seconds before being stepped to a reducing potential (-3, -103, -203, -303, -403 mV) for 300 seconds. Buffer-electrolyte 2 mM CaCl_2 , 50 mM HEPES, pH 7, 20 $^\circ\text{C}$, electrode rotation at 2,000 RPM.

5.6 Discussion

The substitution of the active site lysine for a histidine residue in *E. coli* NrfA provided an opportunity to investigate the role the lysine ligand plays in the reduction mechanism. The substitution generated the conventional CxxCH c-type cytochrome binding motif and allowed the active site heme to be successfully incorporated into the K126H protein. The crystal structure of K126H NrfA revealed that the substitution of the lysine for a histidine residue was not sufficient to allow histidine ligation of the heme iron as seen in other c-type cytochromes. The structure revealed two novel features of this protein. The first was that the substituted histidine residue was only weakly associated with the heme iron and the second that a potential tyrosine heme cross link was present. Complexities in the structure are reflected in complex spectroscopy and electrochemistry for this NrfA variant causing the effects of the lysine to histidine substitution to be harder to reconcile than those of the NrfA distal pocket variants discussed in the previous chapters.

The mechanism of nitrite reduction proposed by Einsle et al indicates that to facilitate high affinity nitrite binding to the ferrous heme a back bonding interaction is present between the heme iron and the nitrite molecule [50]. This interaction allows charge to be transferred from the heme iron into the pi anti-bonding orbital of the nitrite molecule. This has the effect of strengthening the Fe-NO₂⁻ bond while weakening the N-O double bond of the nitrite molecule. With the active site lysine ligand substituted for a histidine residue in the K126H, NrfA variant the characteristics of the heme iron will be altered. The change in the heme ligation caused a decrease in the V_{max} and an increase in the K_M . The increased K_M reveals that the K126H NrfA has a lower affinity for nitrite compared to WT NrfA, suggesting that the iron ligand is able to alter the characteristics of the iron-NO₂ bond. The observed decrease in the V_{max} would suggest that the nitrite reduction occurs at a slower rate in the K126H NrfA than in WT NrfA. A slower rate of reduction could be caused by a slower rate of electron transfer to the active site of NrfA or a slower activation of the nitrite molecule. The presence of a histidine ligand to the active heme could reduce the ability of the heme iron to transfer charge to the nitrite molecule. Without this charge transfer the N-O double bond of the nitrite molecule will not be weakened and therefore require an increased amount of energy to break.

The nitrite reductase activity of K126H NrfA is observed to increase with time; this behaviour is very different to that observed for the WT enzyme. The increasing level of nitrite reduction with time is in agreement with the spectroelectrochemical observations that revealed the slow appearance of a 435 nm feature. The appearance of a 435 nm feature is

thought to reflect a slow change in the active site of K126H NrfA when the protein is poised at potentials in which the protein is fully reduced. It has not been possible to identify the precise change that occurs within the active site of K126H NrfA that gives rise to the slow transition. However it is most likely reflecting a change in the heme coordination, the crystallography of this NrfA variant revealed an active site heme that was not ligated by the H126 residue. The possibility that under certain conditions the active site heme of K126H can change from a penta-coordinated to a tetra coordinated would explain such an observation. Tetra-coordinated hemes have been documented previously in variants of myoglobin and cytochrome c peroxidases with the native proximal histidine ligand substituted by smaller residues such as glycine [80]. The substitution of the histidine residue for a glycine in sperm whale myoglobin resulted in subtle changes in the absorbance spectra of the ferric protein with the Soret maximum shifting from 408 to 405 nm at pH 7 [81, 82]. The spectra of oxidised K126H NrfA revealed no changes to Soret maximum. However, such a subtle change could easily be masked by the presence of the 4 low-spin hemes. The spectroscopic and crystallographic characterisation of K126H NrfA certainly would suggest that the substitution has impacted on the heme ligation, but the full extent still needs to be determined.

The novel tyrosine link in K126H NrfA was observed between the 5' meso position of the carbon ring and the phenol oxygen of the tyrosine 216 residue. This attachment has not been identified in any WT or variant NrfA structure presented to date. However there are two examples of c-type heme proteins that contain a heme modified at a meso position of the porphyrin ring. These proteins are hydroxylamine oxidoreductase (HAO) and cytochrome P460. Both are found in the *Nitrosomonas europaea*, an ammonia oxidising bacteria. The HAO enzyme is able to catalyse the oxidation of hydroxylamine to ammonia which liberates four electrons. These are passed from the active site P460 heme to electron acceptor proteins. The HAO enzyme and ammonia mono-oxygenase which produces the hydroxylamine are of fundamental importance to the nitrogen cycle as they are responsible for the majority of ammonia oxidation within the biosphere [3, 21]. The function of periplasmic cytochrome P460 in *Nitrosomonas europaea* has not been established although it does show low levels of hydroxylamine oxidation as well as the ability to bind small molecules such as nitric oxide and carbon monoxide [83].

The crystal structures of HAO and cytochrome P460 revealed that the heme modifications are at different positions in both proteins [44, 84]. The only structure of HAO to be solved to date revealed a heme that was covalently modified by linkage to a tyrosine residue from a neighbouring HAO monomer. The tyrosine residue is attached via a meso carbon of the

tyrosine ring to the 5' carbon of the porphyrin ring, Figure 5.13 [44]. The linkage occurs at the same position in the HAO and K126H NrfA proteins. However in the K126H protein the tyrosine attaches via a C-C bond and not the C-O bond. The proposed bonding in HAO causes the phenol oxygen of the tyrosine residue to come into close contact with the heme at a distance of 1.2 Å. This orientation would likely cause a steric clash. The HAO structure was resolved to a lower resolution (2.8 Å) compared to the K126H (2.3 Å) structure, and it has been suggested that the phenol oxygen and not a carbon atom could be bonding to the porphyrin ring in HAO [84]. The 1.8 Å structure of cytochrome P460 revealed a heme modification at the meso 15' position. The attachment is formed between the porphyrin ring and the amine group lysine of the side chain, revealing that heme modifications can be made at other meso positions of the porphyrin ring [84]. The process of heme modification in HAO and cytochrome P460 is thought to be autocatalytic. It has been proposed it could progress through either nucleophilic attack by a lone pair of electrons or by the formation of radical species that can attack the porphyrin ring. However, the exact mechanism is still unknown.

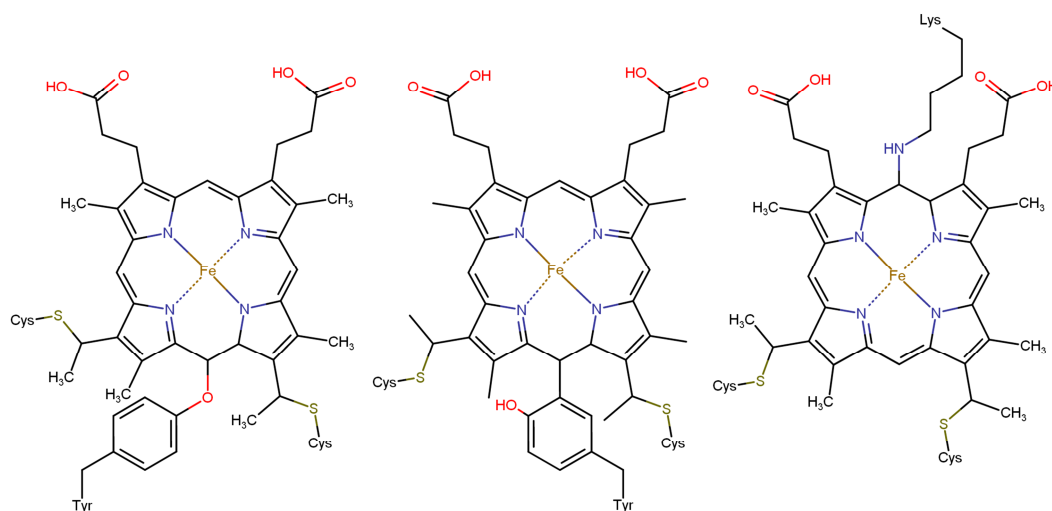


Figure 5.13- Schematic of the heme covalently modified hemes in (A) K126H NrfA, (B) P460 structure in HAO and (C) P460 structure in cytochrome P460 from *N. europaea*.

Although the HAO and cytochrome P460 enzymes are modified at opposite meso positions of the porphyrin ring they give rise to similar electronic absorbance spectra. The defining feature of the spectra of the ferrous proteins is an intense absorption peak around 460 nm. The shift in the Soret peak to longer wavelengths is a result of the modification of the porphyrin ring to generate a phlorin. The presence of the sp^3 hybridized carbon atom at the meso position has a profound effect on the properties of phlorins as it disrupts the

conjugation of the macrocycle which enables longer wavelengths of light to be absorbed. The midpoint potentials of the P460 hemes in HAO and cytochrome P460 have been measured to be -260 mV and at -402 mV, respectively, at pH 7.0 both significantly lower than that of the active site heme of K126H NrfA, which has a midpoint potential of +30 mV (± 15 mV) [85]. While the crystal structure of K126H suggested the presence of a P460 heme, the spectroscopy of K126H both in solution and absorbed on the SnO₂ electrode did not show any absorbance at 460 nm region indicative of a P460 heme. The spectra of the ferrous K126H enzyme absorbed on the SnO₂ electrode did have a shoulder on the main Sort peak at a 435 nm which is thought to reflect the high spin active site heme. A ferrous heme absorbing at 435 nm is likely to reflect a histidine ligated high spin heme and not the presence of a covalently modified heme.

The absence of spectroscopic evidence of a covalently modified heme would suggest that the modification is an artefact of data collection. To obtain the X-ray data the protein crystal is exposed to radiation that is able to ionise the protein. This could generate a radical which could result in the covalent modification being formed whilst the crystal is in the beam [86]. This is supported by the observed variation in the bond distance suggesting that there are mixed population, with some proteins within the crystal forming the covalent attachment while others do not. Whilst the data obtained so far suggests the covalent attachment is unlikely to be present in solution it is still an important observation as a similar modification has not been observed to occur in the WT protein when exposed to X-ray radiation. This indicates the active site K126H protein is responding differently to x-ray radiation than the WT protein.

Covalent modification of the active site tyrosine is not observed in any WT NrfA characterised to date, but it has been documented in TvNir. In the structures of TvNir active site the tyrosine is covalently attached to a neighbouring cysteine residue. The modification is thought to be present within solution and causes the reduction of the pK_a of the phenol proton [22, 87, 88]. The Tyr-Cys modification is not able to form in NrfA, as no NrfA protein sequence has a cysteine residue in the correct position. The presence of a covalent modification reveals that the active site of TvNir is able to undergo autocatalytic reactions. As well as acting to change the pK_a of the tyrosine residue, the Tyr-Cys modification might be important in preventing the formation of tyrosine radicals during the catalytic cycle or side reactions. If a radical did form the cysteine linkage could prevent the tyrosine from attacking the porphyrin ring by physically limiting its movement, however the function of the Tyr-Cys bond is still uncertain.

The insights gained in to the K126H NrfA variant reveal very interesting structural and spectroscopic features arising from the substitution. Further study of the K126H NrfA protein will hopefully allow for greater clarity on the effect the presence of a histidine ligand has on the NrfA protein. Future experiments would include more in-depth crystallography to determine if the covalent attachment is generated during data collection. This could be carried out using a micro-spectrophotometer to measure the absorbance spectrum of the K126H protein crystal, at defined time points during data collection, to determine if a P460 heme is formed. Multiple data sets could be collected from a single crystal to determine if the density that is accounted for by the covalent attachment becomes stronger the longer the crystal is exposed to radiation. The nature of the heme ligation could be explored using further solution spectroscopic techniques, such as magnetic circular dichroism of the oxidised protein to determine if the K126H protein is penta- or tetra-coordinated.

Chapter 6

Summary and Future Perspectives

Chapter 6 - Summary and Future Perspectives

The enzyme catalysed reduction of nitrite to ammonia by NrfA is a complicated process, requiring multiple electron and multiple proton transfer steps [50]. The process occurs at the distal position of a heme within a cavity formed by highly conserved residues found in NrfA and TvNir proteins [21]. The research in this thesis has explored the active site of *E. coli* NrfA and has added to knowledge of the role that the first sphere amino acids play in the reduction of nitrite within this group of enzymes. The lysine ligation to the active site heme iron has also been investigated, as well as those residues forming the distal cavity. The substitution of these key residues resulted in proteins with different characteristics to the WT enzyme and each other, suggesting that each residue plays a different role in nitrite reduction.

For NrfA to efficiently reduce nitrite it must be able to bind nitrite and provide electrons and protons when required. NrfA has a high affinity for nitrite with a K_M value of 25 μM [32]. The residues that are thought to be important for nitrite binding are the arginine and histidine residues that are located within the active site pocket. They have been shown by crystallography to directly interact with the nitrite molecule. And indeed when the active site arginine residue is substituted for a lysine residue, as in the R106K variant, there is a six fold increase in the K_M . This would suggest that the native residue is likely to play a role in nitrite recognition and binding. However, the change is rather modest. A more dramatic change is observed in the H264N NrfA variant which has completely lost the ability to reduce nitrite. Further characterisation of the H264N variant in Chapter 4 revealed that nitrite is still able to bind to the active site heme without the histidine residue being present. The observation that nitrite is binding but not being reduced suggested the nitrite molecule is positioned in the incorrect orientation for reduction. The cause of this is likely to be that the nitrite molecule in the H264N enzyme binds 'end on' via an oxygen atom, an orientation that is seen in myoglobin [74]. This is in agreement with the suggested reaction mechanism that requires the nitrite molecule to bind via the nitrogen atom for catalysis to commence.

It is not only the arginine and histidine residues that affect nitrite binding to the active site heme. The substitution of the lysine ligand to a histidine resulted in a large increase in the K_M . The K126H K_M is more than 17 times larger than that of the WT enzyme, as measured by spectroscopically monitored solution assays in which dithionite reduced MV was the electron donor to the protein. The K_M was even larger when measured using cyclic voltammetry, Table 3.1. This large increase in K_M indicates that the proximal ligand to the active site heme iron plays an important role in defining the properties of the Fe-NO₂ bond.

The crystallography and spectroelectrochemistry of the K126H variant were inconclusive in confirming the nature of the active site heme ligation in the K126H enzyme. Ambiguity remains to whether the histidine residue is the active site heme ligand or not. It would also be possible that the active site heme is present as a mixed population of both tetra- and penta-coordinated states. To resolve these discrepancies MCD spectroscopy of the solution protein could be carried out, to ascertain if the active site heme is ligated by a histidine residue. In MCD visible and infra red MCD a high-spin heme with a histidine or lysine present typically gives rise to two charge transfer bands, one in the 600-670 nm region and the second above 800 nm. If the charge band is present it would confirm that the histidine is forming a ligand to the active site heme. If the histidine residue is a ligand, the MCD can also report what is the likely sixth ligand to the active site [32]. The temperature can also be varied to see if the ligation is temperature dependent.

Even with this ambiguity over the ligation of the K125H active site heme it is clear that changes in the iron coordination sphere impact the binding of substrate dramatically, even when the histidine and arginine residues are present. With the information gained from the R106K, H264N and K126H mutants it is clear that high affinity binding of nitrite to the NrfA is most dependent on the proximal lysine ligand. However, the distal residues are also vital in the orientation of the nitrite molecule. The H264N protein shows that even with substrate binding it is the orientation of the substrate that is fundamental for nitrite reduction, Scheme 4.3. Conformation of nitrite binding via an oxygen atom would validate the role of the histidine. This information would be gained from the crystal structure of the H264N protein with nitrite bound in the active site. Attempts have been made to obtain such a structure during the course of this work but to date it has not been possible to obtain a crystal that diffracts to a resolution allowing confirmation of nitrite binding or orientation to the active site of H264N NrfA.

Of the four NrfA variants characterised in this work, only the H264N variant reported a complete loss of detectable nitrite reduction. For those variants maintaining nitrite reductase activity the potential dependence of the reduction was revealed by PFE carried out at pH 7. The substitution of the distal pocket arginine for a lysine residue resulted in the smallest change to the characteristics of the NrfA enzyme with V_{max} unaltered and K_M increasing. The PFE of R106K in the presence of nitrite revealed that the attenuation feature that is associated with nitrite reduction by NrfA was maintained. The attenuation feature was prominent at higher concentrations in the R106K NrfA than the WT. However, this is likely to be a reflection of the higher K_M experienced by the R106K protein, This was also observed in the Q253E variant of NrfA [11]. The presence of the attenuation and the

same V_{\max} would indicate that the R106K enzyme is still active as a nitrite reductase and is also likely to be reducing nitrite the same way as the WT protein. The similarity between the WT and R106K variant could partly be due to the lysine residue compensating for the native arginine residue. To see if this is the case, further mutagenesis studies could be conducted, generating NrfA proteins in which the arginine residue is substituted for an uncharged amino acid, such as leucine. As an uncharged amino acid would be unable to form hydrogen bonds with bound substrate. Such mutations may reveal that the role of the arginine is more important than the current investigation has revealed.

The tyrosine residue located in the active site of NrfA is not thought to interact directly with the nitrite or the reaction intermediates, as inferred from the crystal structure [45]. It was therefore unexpected that the Y216F variant would have a more prominent effect on nitrite reduction than the R106K substitution. The Y216F substitution, which removes the hydroxyl group of the tyrosine residue, gave rise to substrate inhibition and shifted the catalytic wave to more negative potentials compared to that observed in the WT enzyme. The presence of substrate inhibition in NrfA has been observed previously. However, it does not become apparent until high nitrite concentrations (greater than 5 mM) whereas Y216F is observed in the μM range (Thomas Lowe, unpublished). Whilst substrate inhibition is the simplest explanation for the observed behaviour, the crystal structure of the same mutation in the *W. succinogenes* NrfA with nitrite bound did not report a second nitrite molecule binding near the active site heme. Therefore the analysis of the observed inhibition resulting from a second nitrite binding site may be too simplistic and inaccurate. As suggested in the Chapter 3, the CuNir nitrite reductase may offer an alternative analysis, with substrate binding to either the oxidised or reduced active site heme and causing a change in the rate of catalysis, generating two pathways with different kinetics, Scheme 3.2. The idea that nitrite binding prior to reduction causes a slow rate of electron transfers is supported by the observation made of the H264N enzyme. The presence of nitrite caused the reduction potential of the active site heme to decrease from -15 mV to -300 mV. A more negative reduction potential for the active site heme would cause a slower rate of electron transfer to the active site. The reason why this may occur in the Y216F NrfA variant is likely to relate to changes in the conserved water network within the active site of the protein, which will impact on the proton transfer into the active site. Disruption to the proton transfer could generate a proton deficit in the active site, which will likely result in the active site histidine being present in its deprotonated state. In the deprotonated state the histidine residue will be unable to stabilise the nitrite molecule via hydrogen bond formation, thus allowing it to bind end on and increasing the reduction potential of the heme. Further work on characterising the Y216F and WT enzyme at varying pHs will allow a greater insight to the

role the proton transfer has on the activity of the NrfA protein. It is also interesting to observe in Y216F NrfA that nitrite reduction occurs over the same potential range as the attenuation feature which is present in the WT enzyme at low nitrite concentrations and the catalytic boost is observed at high nitrite concentration [65]. While the cause of the attenuation/boost feature is unknown, the observation could be an indication that the feature is due to the sequence of heme reduction, protonation of active site residues and substrate binding. Further work characterizing the Y216F mutation will help to explore the cause of the attenuation/boost feature. The creation of His/Met substitutions of the distal ligands of the low-spin hemes may also allow an insight into the attenuation/boost feature as they will cause a change in the reduction potential of the ligated heme and therefore likely impact on the electron transfer rate.

All NrfA variants maintained hydroxylamine reductase activity. This is not surprising as many reduced penta-coordinated hemes can reduce hydroxylamine [89-92]. The most surprising feature, when comparing all variants, was how similar the enzymatic constants for hydroxylamine reduction are while those describing nitrite reduction vary greatly. This would indicate that the characteristics of hydroxylamine reduction by *E. coli* NrfA are not limited by the active site residues. Instead other features of the NrfA enzyme have a more dominant effect on the reduction of hydroxylamine. The likely cause of the low affinity of NrfA for hydroxylamine is likely to reflect the ability of the ingress and egress channels to deliver hydroxylamine to the active site. The ingress and egress channels of *E. coli* NrfA are positively and negatively charged, respectively, to allow the negative nitrite and positive ammonium ions to efficiently enter and leave the active site. The hydroxylamine molecule has no charge and therefore is unable to interact with either channel [49]. It is therefore likely the active site affinity for hydroxylamine is much higher than is represented by the observed K_M . This would agree with the observation that hydroxylamine intermediates are not seen to leak from the active site during nitrite reduction.

The work in this thesis has also identified that studying the properties of the active site heme in isolation is not possible as it is affected by the oxidation state of the other hemes. This was highlighted in Chapter 4 which characterised the association of nitrite with the oxidised and reduced active site of H264N NrfA, Figure 4.9. The association of nitrite to H264N NrfA could not be described by a single square scheme, Figure 4.9. This would suggest the overall redox state of the protein affects the active site. This could be mediated through changes in the protein conformation in the electron transfer hemes. The subtle changes in the protein that are mediated by the other hemes in NrfA are likely to result in the efficient reduction of nitrite. A model based upon the active site heme and the first

sphere amino acids is therefore an over-simplification as it does not take into account the other redox centre of the protein or changes that the protein may undergo when bound to electrons transfer proteins (NrfB or NrfH). To further explore the role of the other hemes further mutational studies could be carried out to change the redox characteristics of these hemes. The most effective way to do this would be to change the distal heme ligand from histidine to methionine, which can increase the heme reduction potential by around 200 mV and therefore reveal the role of that heme in the reduction process [93]. It would also be of interest to carry out studies of NrfA in the presence of NrfB to determine if the presence of the electron transfer proteins impacts on the activity of the NrfA enzyme.

New advances in technology have increased high throughput whole genome-sequencing efforts, many of which have included prokaryotes that facilitate fundamental processes in many of the biogeochemical cycles [21]. The analyses of these genomes along with robust biochemical and physiological experimentation has allowed for those biogeochemical cycles to be re-evaluated. This is evident in the nitrogen cycle with the relatively recent discovery of the anaerobic ammonium oxidation (anammox) pathway which allows the oxidation of ammonia by nitrite forming dinitrogen. This reaction is catalysed by a number of enzyme complexes that are still being identified and have yet to be fully characterised. The anammox pathway introduces a new reaction intermediate, hydrazine, which is formed by the reaction of nitric oxide and ammonia. The anammox bacteria contain a larger number of c-type cytochromes with many being similar to enzymes already present in the nitrogen cycle, such as NrfA and HAO [94]. While work continues to characterise these new proteins it will be important to understand how they are evolutionarily linked to the other enzymes in the nitrogen cycle and how they gain specificity for the reactions they catalyse. In light of this it would be interesting to screen the NrfA variants discussed in this work with a wider range of substrates including nitric oxide and hydrazine to determine if WT NrfA or any of the active site variants can also perform these reactions.

References

- 1 Berks, B. C., Ferguson, S. J., Moir, J. W. B. and Richardson, D. J. (1995) Enzymes and associated electron transport systems that catalyse the respiratory reduction of nitrogen oxides and oxyanions. *Biochimica et Biophysica Acta - Bioenergetics* **1232**, 97-173
- 2 Simon, J., van Spanning, R. J. M. and Richardson, D. J. (2008) The organisation of proton motive and non-proton motive redox loops in prokaryotic respiratory systems. *Biochimica et Biophysica Acta - Bioenergetics* **1777**, 1480-1490
- 3 Klotz, M. G. and Stein, L. Y. (2008) Nitrifier genomics and evolution of the nitrogen cycle. *FEMS Microbiology Letters* **278**, 146-156
- 4 Igarashi, N., Moriyama, H., Fujiwara, T., Fukumori, Y. and Tanaka, N. (1997) The 2.8 Å structure of hydroxylamine oxidoreductase from a nitrifying chemoautotrophic bacterium, *Nitrosomonas europaea*. *Nature Structural Biology* **4**, 276-284
- 5 Bertero, M. G., Rothery, R. A., Palak, M., Hou, C., Lim, D., Blasco, F., Weiner, J. H. and Strynadka, N. C. J. (2003) Insights into the respiratory electron transfer pathway from the structure of nitrate reductase A. *Nature Structural Biology* **10**, 681-687
- 6 Najmudin, S., Gonzalez, P. J., Trincao, J., Coelho, C., Mukhopadhyay, A., Cerqueira, N. M. F. S. A., Romao, C. C., Moura, I., Moura, J. J. G., Brondino, C. D. and Romao, M. J. (2008) Periplasmic nitrate reductase revisited: A sulfur atom completes the sixth coordination of the catalytic molybdenum. *Journal of Biological Inorganic Chemistry* **13**, 737-753
- 7 Tocheva, E. I., Rosell, F. I., Mauk, A. G. and Murphy, M. E. P. (2007) Stable copper-nitrosyl formation by nitrite reductase in either oxidation state. *Biochemistry* **46**, 12366-12374
- 8 Williams, P. A., Fülöp, V., Carman, E. F., Saunders, N. F. W., Ferguson, S. J. and Hajdu, J. (1997) Haem-ligand switching during catalysis in crystals of a nitrogen-cycle enzyme. *Nature* **389**, 406-412
- 9 Hino, T., Matsumoto, Y., Nagano, S., Sugimoto, H., Fukumori, Y., Murata, T., Iwata, S. and Shiro, Y. (2010) Structural basis of biological N₂O generation by bacterial nitric oxide reductase. *Science* **330**, 1666-1670
- 10 Brown, K., Djinic-Carugo, K., Haltia, T., Cabrito, I., Saraste, M., Moura, J. J. G., Moura, I., Tegoni, M. and Cambillau, C. (2000) Revisiting the catalytic CuZ cluster of nitrous oxide (N₂O) reductase: Evidence of a bridging inorganic sulfur. *Journal of Biological Chemistry* **275**, 41133-41136

- 11 Clarke, T. A., Kemp, G. L., Van Wonderen, J. H., Doyle, R. M. A. S., Cole, J. A., Tovell, N., Cheesman, M. R., Butt, J. N., Richardson, D. J. and Hemmings, A. M. (2008) Role of a conserved glutamine residue in tuning the catalytic activity of *Escherichia coli* cytochrome *c* nitrite reductase. *Biochemistry* **47**, 3789-3799
- 12 Simon, J. (2002) Enzymology and bioenergetics of respiratory nitrite ammonification. *FEMS Microbiology Reviews* **26**, 285-309
- 13 Rodrigues, M. L., Oliveira, T. F., Pereira, I. A. C. and Archer, M. (2006) X-ray structure of the membrane-bound cytochrome *c* quinol dehydrogenase NrfH reveals novel haem coordination. *EMBO Journal* **25**, 5951-5960
- 14 KrÄ¶lger, A., Biel, S., Simon, J., Gross, R., Uden, G. and Lancaster, C. R. D. (2002) Fumarate respiration of *Wolinella succinogenes*: Enzymology, energetics and coupling mechanism. *Biochimica et Biophysica Acta - Bioenergetics* **1553**, 23-38
- 15 Jormakka, M., Yokoyama, K., Yano, T., Tamakoshi, M., Akimoto, S., Shimamura, T., Curmi, P. and Iwata, S. (2008) Molecular mechanism of energy conservation in polysulfide respiration. *Nature Structural and Molecular Biology* **15**, 730-737
- 16 Clarke, T. A., Cole, J. A., Richardson, D. J. and Hemmings, A. M. (2007) The crystal structure of the pentahaem *c*-type cytochrome NrfB and characterization of its solution-state interaction with the pentahaem nitrite reductase NrfA. *Biochemical Journal* **406**, 19-30
- 17 Simon, J., Gross, R., Einsle, O., Kroneck, P. M. H., Kroger, A. and Klimmek, O. (2000) A NapC/NirT-type cytochrome *c* (NrfH) is the mediator between the quinone pool and the cytochrome *c* nitrite reductase of *Wolinella succinogenes*. *Molecular Microbiology* **35**, 686-696
- 18 Kemp, G. L., Clarke, T. A., Marritt, S. J., Lockwood, C., Pooch, S. R., Hemmings, A. M., Richardson, D. J., Cheesman, M. R. and Butt, J. N. (2010) Kinetic and thermodynamic resolution of the interactions between sulfite and the pentahaem cytochrome NrfA from *Escherichia coli*. *Biochemical Journal* **431**, 73-80
- 19 Kern, M., Volz, J. and Simon, J. (2011) The oxidative and nitrosative stress defence network of *Wolinella succinogenes*: Cytochrome *c* nitrite reductase mediates the stress response to nitrite, nitric oxide, hydroxylamine and hydrogen peroxide. *Environmental Microbiology* **13**, 2478-2494
- 20 Pereira, I. C., Abreu, I. A., Xavier, A. V., LeGall, J. and Teixeira, M. (1996) Nitrite Reductase from *Desulfovibrio desulfuricans* (ATCC 27774) A Heterooligomer Heme Protein with Sulfite Reductase Activity. *Biochemical and Biophysical Research Communications* **224**, 611-618
- 21 Klotz, M. G., Schmid, M. C., Strous, M., Op Den Camp, H. J. M., Jetten, M. S. M. and Hooper, A. B. (2008) Evolution of an octahaem cytochrome *c* protein family that is key

- to aerobic and anaerobic ammonia oxidation by bacteria. *Environmental Microbiology* **10**, 3150-3163
- 22 Trofimov, A. A., Polyakov, K. M., Boyko, K. M., Tikhonova, T. V., Safonova, T. N., Tikhonov, A. V., Popov, A. N. and Popov, V. O. (2010) Structures of complexes of octahaem cytochrome *c* nitrite reductase from *Thioalkalivibrio nitratireducens* with sulfite and cyanide. *Acta Crystallographica Section D: Biological Crystallography* **66**, 1043-1047
- 23 Cole, J. A. (1968) Cytochrome *c*₅₅₂ and nitrite reduction in *Escherichia coli*. *BBA - Bioenergetics* **162**, 356-368
- 24 Liu, M. C. and Peck Jr, H. D. (1981) The isolation of a hexaheme cytochrome from *Desulfovibrio desulfuricans* and its identification as a new type of nitrite reductase. *Journal of Biological Chemistry* **256**, 13159-13164
- 25 De Vries, W., Neikus, H. G. D., Van Berchum, H. and Stouthamer, A. H. (1982) Electron transport-linked proton translocation at nitrite reduction in *Campylobacter sputorum* subspecies *bubulus*. *Archives of Microbiology* **131**, 132-139
- 26 Liu, M. C., Liu, M. Y. and Payne, W. J. (1983) *Wolinella succinogenes* nitrite reductase: Purification and properties. *FEMS Microbiology Letters* **19**, 201-206
- 27 Schumacher, W. and Kroneck, P. M. H. (1991) Dissimilatory hexaheme *c* nitrite reductase of 'Spirillum' strain 5175: Purification and properties. *Archives of Microbiology* **156**, 70-74
- 28 Pereira, I. A. C., Legall, J., Xavier, A. V. and Teixeira, M. (2000) Characterization of a heme *c* nitrite reductase from a non-ammonifying microorganism, *Desulfovibrio vulgaris* Hildenborough. *Biochimica et Biophysica Acta - Protein Structure and Molecular Enzymology* **1481**, 119-130
- 29 Darwin, A., Hussain, H., Griffiths, L., Grove, J., Sambongi, Y., Busby, S. and Cole, J. (1993) Regulation and sequence of the structural gene for cytochrome *c*₅₅₂ from *Escherichia coli*: Not a hexahaem but a 50 kDa tetrahaem nitrite reductase. *Molecular Microbiology* **9**, 1255-1265
- 30 Eaves, D. J., Grove, J., Staudenmann, W., James, P., Poole, R. K., White, S. A., Griffiths, I. and Cole, J. A. (1998) Involvement of products of the *nrfEFG* genes in the covalent attachment of haem *c* to a novel cysteine-lysine motif in the cytochrome *c*₅₅₂ nitrite reductase from *Escherichia coli*. *Molecular Microbiology* **28**, 205-216
- 31 Einsle, O., Messerschmidt, A., Stach, P., Bourenkov, G. P., Bartunik, H. D., Huber, R. and Kroneck, P. M. H. (1999) Structure of cytochrome *c* nitrite reductase. *Nature* **400**, 476-480

- 32 Bamford, V. A., Angove, H. C., Seward, H. E., Thomson, A. J., Cole, J. A., Butt, J. N., Hemmings, A. M. and Richardson, D. J. (2002) Structure and spectroscopy of the periplasmic cytochrome *c* nitrite reductase from *Escherichia coli*. *Biochemistry* **41**, 2921-2931
- 33 Einsle, O., Stach, P., Messerschmidt, A., Simon, J., Kroger, A., Huber, R. and Kroneck, P. M. H. (2000) Cytochrome *c* nitrite reductase from *Wolinella succinogenes*: Structure at 1.6 Å resolution, inhibitor binding, and heme-packing motifs. *Journal of Biological Chemistry* **275**, 39608-39616
- 34 Cunha, C. A., Macieira, S., Dias, J. M., Almeida, G., Goncalves, L. L., Costa, C., Lampreia, J., Huber, R., Moura, J. J. G., Moura, I. and Romao, M. J. (2003) Cytochrome *c* nitrite reductase from *Desulfovibrio desulfuricans* ATCC 27774. The relevance of the two calcium sites in the structure of the catalytic subunit (NrfA). *Journal of Biological Chemistry* **278**, 17455-17465
- 35 Youngblut, M., Judd, E. T., Srajer, V., Sayyed, B., Goelzer, T., Elliott, S. J., Schmidt, M. and Pacheco, A. A. (2012) Laue crystal structure of *Shewanella oneidensis* cytochrome *c* nitrite reductase from a high-yield expression system. *Journal of Biological Inorganic Chemistry* **17**, 647-662
- 36 Lockwood, C., Butt, J. N., Clarke, T. A. and Richardson, D. J. (2011) Molecular interactions between multihaem cytochromes: Probing the protein-protein interactions between pentahaem cytochromes of a nitrite reductase complex. *Biochemical Society Transactions* **39**, 263-268
- 37 Stephenson, K. (2005) Sec-dependent protein translocation across biological membranes: Evolutionary conservation of an essential protein transport pathway. *Molecular Membrane Biology* **22**, 17-28
- 38 Natale, P., Bruser, T. and Driessen, A. J. M. (2008) Sec- and Tat-mediated protein secretion across the bacterial cytoplasmic membrane-Distinct translocases and mechanisms. *Biochimica et Biophysica Acta - Biomembranes* **1778**, 1735-1756
- 39 Thony-Meyer, L. (1997) Biogenesis of respiratory cytochromes in bacteria. *Microbiology and Molecular Biology Reviews* **61**, 337-376
- 40 Stevens, J. M., Mavridou, D. A. I., Hamer, R., Kritsiligkou, P., Goddard, A. D. and Ferguson, S. J. (2011) Cytochrome *c* biogenesis System i. *FEBS Journal* **278**, 4170-4178
- 41 Pisa, R., Stein, T., Eichler, R., Gross, R. and Simon, J. (2002) The *nrfi* gene is essential for the attachment of the active site haem group of *Wolinella succinogenes* cytochrome *c* nitrite reductase. *Molecular Microbiology* **43**, 763-770
- 42 Pittman, M. S., Elvers, K. T., Lee, L., Jones, M. A., Poole, R. K., Park, S. F. and Kelly, D. J. (2007) Growth of *Campylobacter jejuni* on nitrate and nitrite: Electron transport to

- NapA and NrfA via NrfH and distinct roles for NrfA and the globin Cgb in protection against nitrosative stress. *Molecular Microbiology* **63**, 575-590
- 43 Mowat, C. G., Rothery, E., Miles, C. S., Mclver, L., Doherty, M. K., Drewette, K., Taylor, P., Walkinshaw, M. D., Chapman, S. K. and Reid, G. A. (2004) Octaheme tetrathionate reductase is a respiratory enzyme with novel heme ligation. *Nature Structural and Molecular Biology* **11**, 1023-1024
- 44 Igarashi, N., Moriyama, H., Fujiwara, T., Fukumori, Y. and Tanaka, N. (1997) The 2.8 Å... structure of hydroxylamine oxidoreductase from a nitrifying chemoautotrophic bacterium, *Nitrosomonas europaea*. *Nature Structural Biology* **4**, 276-284
- 45 Lukat, P., Rudolf, M., Stach, P., Messerschmidt, A., Kroneck, P. M. H., Simon, J. and Einsle, O. (2008) Binding and reduction of sulfite by cytochrome c nitrite reductase. *Biochemistry* **47**, 2080-2086
- 46 Clarke, T. A., Mills, P. C., Pooock, S. R., Butt, J. N., Cheesman, M. R., Cole, J. A., Hinton, J. C. D., Hemmings, A. M., Kemp, G., Söderberg, C. A. G., Spiro, S., Van Wonderen, J. and Richardson, D. J. (2008) *Escherichia coli* Cytochrome c Nitrite Reductase NrfA. In *Methods in Enzymology* (Poole, R. K., ed.), pp. 63-77
- 47 Dolla, A., Blanchard, L., Guerlesquin, F. and Bruschi, M. (1994) The protein moiety modulates the redox potential in cytochromes c. *Biochimie* **76**, 471-479
- 48 Marritt, S. J., Kemp, G. L., Xiaoe, L., Durrant, J. R., Cheesman, M. R. and Butt, J. N. (2008) Spectroelectrochemical characterization of a pentaheme cytochrome in solution and as electrocatalytically active films on nanocrystalline metal-oxide electrodes. *Journal of the American Chemical Society* **130**, 8588-8589
- 49 Clarke, T. A., Hemmings, A. M., Burlat, B., Butt, J. N., Cole, J. A. and Richardson, D. J. (2006) Comparison of the structural and kinetic properties of the cytochrome c nitrite reductases from *Escherichia coli*, *Wolinella succinogenes*, *Sulfurospirillum deleyianum* and *Desulfovibrio desulfuricans*. *Biochemical Society Transactions* **34**, 143-145
- 50 Einsle, O., Messerschmidt, A., Huber, R., Kroneck, P. M. H. and Neese, F. (2002) Mechanism of the six-electron reduction of nitrite to ammonia by cytochrome c nitrite reductase. *Journal of the American Chemical Society* **124**, 11737-11745
- 51 Burlat, B., Gwyer, J. D., Pooock, S., Clarke, T., Cole, J. A., Hemmings, A. M., Cheesman, M. R., Butt, J. N. and Richardson, D. J. (2005) Cytochrome c nitrite reductase: From structural to physicochemical analysis. *Biochemical Society Transactions* **33**, 137-140
- 52 Van Wonderen, J. H., Burlat, B., Richardson, D. J., Cheesman, M. R. and Butt, J. N. (2008) The nitric oxide reductase activity of cytochrome c nitrite reductase from *Escherichia coli*. *Journal of Biological Chemistry* **283**, 9587-9594

- 53 Stach, P., Einsle, O., Schumacher, W., Kurun, E. and M.h. Kroneck, P. (2000) Bacterial cytochrome *c* nitrite reductase: New structural and functional aspects. *Journal of Inorganic Biochemistry* **79**, 381-385
- 54 Schumacher, W., Hole, U. and Kroneck, P. M. H. (1994) Ammonia-forming cytochrome *c* nitrite reductase from *Sulfurospirillum deleyianum* is a tetraheme protein: New aspects of the molecular composition and spectroscopic properties. *Biochemical and Biophysical Research Communications* **205**, 911-916
- 55 Wijma, H. J., Jeuken, L. J. C., Verbeet, M. P., Armstrong, F. A. and Canters, G. W. (2006) A random-sequential mechanism for nitrite binding and active site reduction in copper-containing nitrite reductase. *Journal of Biological Chemistry* **281**, 16340-16346
- 56 Gwyer, J. D., Angove, H. C., Richardson, D. J. and Butt, J. N. (2004) Redox-triggered events in cytochrome *c* nitrite reductase. *Bioelectrochemistry* **63**, 43-47
- 57 Potter, L. C. and Cole, J. A. (1999) Essential roles for the products of the *napABCD* genes, but not *napFGH*, in periplasmic nitrate reduction by *Escherichia coli* K-12. *Biochemical Journal* **344**, 69-76
- 58 Winter, G. (2009) Xia2: An expert system for macromolecular crystallography data reduction. *Journal of Applied Crystallography* **43**, 186-190
- 59 McCoy, A. J., Grosse-Kunstleve, R. W., Adams, P. D., Winn, M. D., Storoni, L. C. and Read, R. J. (2007) Phaser crystallographic software. *Journal of Applied Crystallography* **40**, 658-674
- 60 Vagin, A. A., Steiner, R. A., Lebedev, A. A., Potterton, L., McNicholas, S., Long, F. and Murshudov, G. N. (2004) REFMAC5 dictionary: Organization of prior chemical knowledge and guidelines for its use. *Acta Crystallographica Section D: Biological Crystallography* **60**, 2184-2195
- 61 Murshudov, G. N., Skubak, P., Lebedev, A. A., Pannu, N. S., Steiner, R. A., Nicholls, R. A., Winn, M. D., Long, F. and Vagin, A. A. (2011) REFMAC5 for the refinement of macromolecular crystal structures. *Acta Crystallographica Section D: Biological Crystallography* **67**, 355-367
- 62 Langer, G., Cohen, S. X., Lamzin, V. S. and Perrakis, A. (2008) Automated macromolecular model building for X-ray crystallography using ARP/wARP version 7. *Nature Protocols* **3**, 1171-1179
- 63 Chen, V. B., Arendall Iii, W. B., Headd, J. J., Keedy, D. A., Immormino, R. M., Kapral, G. J., Murray, L. W., Richardson, J. S. and Richardson, D. C. (2010) MolProbity: All-atom structure validation for macromolecular crystallography. *Acta Crystallographica Section D: Biological Crystallography* **66**, 12-21

- 64 Mayhew, S. G. (1978) The Redox Potential of Dithionite and SO_2^- from Equilibrium Reactions with Flavodoxins, Methyl Viologen and Hydrogen plus Hydrogenase. *European Journal of Biochemistry* **85**, 535-547
- 65 Angove, H. C., Cole, J. A., Richardson, D. J. and Butt, J. N. (2002) Protein film voltammetry reveals distinctive fingerprints of nitrite and hydroxylamine reduction by a cytochrome c nitrite reductase. *Journal of Biological Chemistry* **277**, 23374-23381
- 66 Krissinel, E. and Henrick, K. (2004) Secondary-structure matching (SSM), a new tool for fast protein structure alignment in three dimensions. *Acta Crystallographica Section D: Biological Crystallography* **60**, 2256-2268
- 67 Ghiladi, R. A., Medzihradszky, K. F., Rusnak, F. M. and Ortiz De Montellano, P. R. (2005) Correlation between isoniazid resistance and superoxide reactivity in *Mycobacterium tuberculosis* KatG. *Journal of the American Chemical Society* **127**, 13428-13442
- 68 Blanc, B., Mayfield, J. A., McDonald, C. A., Lukat-Rodgers, G. S., Rodgers, K. R. and Dubois, J. L. (2012) Understanding how the distal environment directs reactivity in chlorite dismutase: Spectroscopy and reactivity of Arg183 Mutants. *Biochemistry* **51**, 1895-1910
- 69 Bamford, V., Dobbin, P. S., Richardson, D. J. and Hemmings, A. M. (1999) Open conformation of a flavocytochrome c_3 fumarate reductase. *Nature Structural Biology* **6**, 1104-1107
- 70 Marti, M. A., Capece, L., Crespo, A., Doctorovich, F. and Estrin, D. A. (2005) Nitric oxide interaction with cytochrome c' and its relevance to guanylate cyclase. Why does the iron histidine bond break? *Journal of the American Chemical Society* **127**, 7721-7728
- 71 Moura, I. and Moura, J. J. G. (2001) Structural aspects of denitrifying enzymes. *Current Opinion in Chemical Biology* **5**, 168-175
- 72 Renault, C., Andrieux, C. P., Tucker, R. T., Brett, M. J., Balland, V. and Limoges, B. Unraveling the mechanism of catalytic reduction of O_2 by microperoxidase-11 adsorbed within a transparent 3D-nanoporous ITO film. *Journal of the American Chemical Society* **134**, 6834-6845
- 73 Martins, G., Rodrigues, L., Cunha, F. M., Matos, D., Hildebrandt, P., Murgida, D. H., Pereira, I. A. C. and Todorovic, S. (2010) Substrate binding to a nitrite reductase induces a spin transition. *Journal of Physical Chemistry B* **114**, 5563-5566
- 74 Yi, J., Orville, A. M., Skinner, J. M., Skinner, M. J. and Richter-Addo, G. B. (2010) Synchrotron X-ray-induced photoreduction of ferric myoglobin nitrite crystals gives the ferrous derivative with retention of the O-bonded nitrite ligand. *Biochemistry* **49**, 5969-5971

- 75 Carman, E. F. and McSweeney, S. M. (2007) Progress in research into radiation damage in cryo-cooled macromolecular crystals. *Journal of Synchrotron Radiation* **14**, 1-3
- 76 Vogel, K. M., Hu, S., Spiro, T. G., Dierks, E. A., Yu, A. E. and Burstyn, J. N. (1999) Variable forms of soluble guanylyl cyclase: Protein-ligand interactions and the issue of activation by carbon monoxide. *Journal of Biological Inorganic Chemistry* **4**, 804-813
- 77 Derbyshire, E. R. and Marletta, M. A. (2012) Structure and regulation of soluble guanylate cyclase. In *Annual Review of Biochemistry*, pp. 533-559
- 78 Lawson, D. M., Stevenson, C. E. M., Andrew, C. R. and Eady, R. R. (2000) Unprecedented proximal binding of nitric oxide to heme: Implications for guanylate cyclase. *EMBO Journal* **19**, 5661-5671
- 79 Barbieri, S., Murphy, L. M., Sawers, R. G., Eady, R. R. and Hasnain, S. S. (2008) Modulation of NO binding to cytochrome c' by distal and proximal haem pocket residues. *Journal of Biological Inorganic Chemistry* **13**, 531-540
- 80 Barrick, D. (1994) Replacement of the proximal ligand of sperm whale myoglobin with free imidazole in the mutant His-93 to Gly. *Biochemistry*, 6546-6554
- 81 Pond, A. E., Roach, M. P., Sono, M., Rux, A. H., Franzen, S., Hu, R., Thomas, M. R., Wilks, A., Dou, Y., Ikeda-Saito, M., Ortiz De Montellano, P. R., Woodruff, W. H., Boxer, S. G. and Dawson, J. H. (1999) Assignment of the heme axial ligand(s) for the ferric myoglobin (H93G) and heme oxygenase (H25A) cavity mutants as oxygen donors using magnetic circular dichroism. *Biochemistry* **38**, 7601-7608
- 82 Pond, A. E., Roach, M. P., Thomas, M. R., Boxer, S. G. and Dawson, J. H. (2000) The H93G Myoglobin Cavity Mutant as a Versatile Template for Modeling Heme Proteins: Ferrous, Ferric, and Ferryl Mixed-Ligand Complexes with Imidazole in the Cavity. *Inorganic Chemistry* **39**, 6061-6066
- 83 Bergmann, D. J. and Hooper, A. B. (2003) Cytochrome P460 of *Nitrosomonas europaea*: Formation of the heme-lysine cross-link in a heterologous host and mutagenic conversion to a non-cross-linked cytochrome c'. *European Journal of Biochemistry* **270**, 1935-1941
- 84 Pearson, A. R., Elmore, B. O., Yang, C., Ferrara, J. D., Hooper, A. B. and Wilmot, C. M. (2007) The crystal structure of cytochrome P460 of *Nitrosomonas europaea* reveals a novel cytochrome fold and heme - Protein cross-link. *Biochemistry* **46**, 8340-8349
- 85 Collins, M. J., Arciero, D. M. and Hooper, A. B. (1993) Optical spectropotentiometric resolution of the hemes of hydroxylamine oxidoreductase: Heme quantitation and pH dependence of Em. *Journal of Biological Chemistry* **268**, 14655-14662

- 86 Burmeister, W. P. (2000) Structural changes in a cryo-cooled protein crystal owing to radiation damage. *Acta Crystallographica Section D: Biological Crystallography* **56**, 328-341
- 87 Polyakov, K. M., Boyko, K. M., Tikhonova, T. V., Slutsky, A., Antipov, A. N., Zvyagilskaya, R. A., Popov, A. N., Bourenkov, G. P., Lamzin, V. S. and Popov, V. O. (2009) High-Resolution Structural Analysis of a Novel Octaheme Cytochrome *c* Nitrite Reductase from the Haloalkaliphilic Bacterium *Thioalkalivibrio nitratireducens*. *Journal of Molecular Biology* **389**, 846-862
- 88 Tikhonova, T. V., Slutsky, A., Antipov, A. N., Boyko, K. M., Polyakov, K. M., Sorokin, D. Y., Zvyagilskaya, R. A. and Popov, V. O. (2006) Molecular and catalytic properties of a novel cytochrome *c* nitrite reductase from nitrate-reducing haloalkaliphilic sulfur-oxidizing bacterium *Thioalkalivibrio nitratireducens*. *Biochimica et Biophysica Acta - Proteins and Proteomics* **1764**, 715-723
- 89 Richter, C. D., Allen, J. W. A., Higham, C. W., Koppenhofer, A., Zajicek, R. S., Watmough, N. J. and Ferguson, S. J. (2002) Cytochrome *cd*₁, reductive activation and kinetic analysis of a multifunctional respiratory enzyme. *Journal of Biological Chemistry* **277**, 3093-3100
- 90 Kostera, J., McGarry, J. and Pacheco, A. A. (2010) Enzymatic interconversion of ammonia and nitrite: The right tool for the job. *Biochemistry* **49**, 8546-8553
- 91 Sturms, R., DiSpirito, A. A., Fulton, D. B. and Hargrove, M. S. (2011) Hydroxylamine reduction to ammonium by plant and cyanobacterial hemoglobins. *Biochemistry* **50**, 10829-10835
- 92 Atkinson, S. J., Mowat, C. G., Reid, G. A. and Chapman, S. K. (2007) An octaheme *c*-type cytochrome from *Shewanella oneidensis* can reduce nitrite and hydroxylamine. *FEBS Letters* **581**, 3805-3808
- 93 Takayama, Y., Werbeck, N. D., Komori, H., Morita, K., Ozawa, K., Higuchi, Y. and Akutsu, H. (2008) Strategic roles of axial histidines in structure formation and redox regulation of tetraheme cytochrome *c*₃. *Biochemistry* **47**, 9405-9415
- 94 Kartal, B., De Almeida, N. M., Maalcke, W. J., Op den Camp, H. J. M., Jetten, M. S. M. and Keltjens, J. T. How to make a living from anaerobic ammonium oxidation. *FEMS Microbiology Reviews* **37**, 428-461